The Dissertation Committee for Ryan Cotter Ewing Certifies that this is the approved version of the following dissertation:

AEOLIAN DUNE-FIELD BOUNDARY CONDITIONS AND DUNE INTERACTIONS RELATED TO DUNE-FIELD PATTERN FORMATION ON EARTH AND MARS

Committee:

Gary Kocurek, Supervisor

David Mohrig

Wonsuck Kim

Lesli Wood

Andreas Baas

AEOLIAN DUNE-FIELD BOUNDARY CONDITIONS AND DUNE INTERACTIONS RELATED TO DUNE-FIELD PATTERN FORMATION ON EARTH AND MARS

BY

RYAN COTTER EWING, BA, MS

DISSERTATION

Presented to the Faculty of the Graduate School of

The University of Texas at Austin

in Partial Fulfillment

of the Requirements

for the Degree of

Doctor of Philosophy

The University of Texas at Austin

December 2009

DEDICATION

Ken, RuAnn and Jay

Acknowledgements

My family provided unfailing support. I have made generations of great friends during my more than overnight stay at the hotel. I certainly have forgotten some names, but all are a part of me… Christian and Eric kept me light, Shane believed in me, Sam kept me Sam-wise, Richard…I'm still laughing, Anna knows, Brandon and Jeff opened my science eyes, Philip was always there, Ben-spiration, Mac, Brian, Dennis, Ted, Brooke, Danuska - Queen of Liliovka, Carrie - Miss Desierto, Erin, Ania, Nysha, Aymeric. Dominique reminded me life is as free as you want it to be. Matt, Billy and Elizabeth reminded me there is life outside of school.

As an advisor and friend Gary provided a bouquet of experiences that I will have with me forever. The semester in Prague, daily readings from The Thornbirds, the summer in Nadslav at The Academy, shooting a wild boar at his castle, the Gran Desierto, too many journeys to White Sands, daily encouragement, daily discouragement, spontaneous emails of life perspective. I have learned to appreciate detail, but to keep my eyes ahead. Each paper matters. Through pain and glory, I can now write.

David Morhig provided scientific and moral support and advice. Lesli Wood gave me the opportunity to present my work to industry and provided financial and scientific support. Larry Lake provided scientific advice. Funding for this dissertation was provided by The Jackson School of Geosciences, National Science Foundation through the National Center for Airborne Laser Mapping (NCALM), the National Park Service

as part of the Chihuahuan Desert Network Inventory and Monitoring Program, NASA MDAP NNX07AV36G, and The University of Texas at Austin Continuing Fellowship. White Sands National Monument provided the 1963 and 1985 aerial photographs. I am especially grateful to Hildy Reiser and David Bustos of the National Park Service in facilitating this study.

AEOLIAN DUNE-FIELD BOUNDARY CONDITIONS AND DUNE INTERACTIONS RELATED TO DUNE-FIELD PATTERN FORMATION ON EARTH AND MARS

Publication No._____

Ryan Cotter Ewing, PhD

The University of Texas at Austin, 2009

Supervisor: Gary Kocurek

Aeolian dune fields form some of the most striking patterns on Earth and Mars. These patterns reflect the internal dune dynamics of self-organization within boundary conditions, which are the unique set of environmental variables within which each dune field evolves. Dune-field pattern self-organization occurs because of interactions between the dunes themselves and the rich diversity of dune-field patterns arises because boundary conditions alter the type and frequency of dune interactions. These hypotheses are explored in three parts. First, source-area geometry and areal limits are two newly recognized boundary conditions. Measurements of crest length and spacing from satellite images of dune patterns with point and line source-area geometries show an increase in crest length and spacing over distance, whereas crest length and spacing in plane-sourced patterns emerge equally across the dune field. The areal limit boundary condition is the size and shape of the dune field itself. Empirical measurements from ten dune fields ranging over four orders of magnitude in area show that spacing increases and defect density decreases as the area of the dune field increases. A simple analytical model indicates that dune fields that are five times longer in the dune migration direction can achieve the greatest spacing for a given area. Second, time-series aerial photographs and airborne LiDAR show that fully developed, crescentic aeolian dunes at White Sands, New Mexico, interact and the dune pattern organizes in systematically similar ways as wind ripples and subaqueous dunes and ripples. Interaction type, classified as

constructive, regenerative or neutral in terms of pattern development, changes spatially with the pattern because of the imposition of the line-source area and sediment-availability boundary conditions. Upwind dominance by constructive interactions at the field line-source yields to neutral and regenerative interactions in the sediment availability-limited field center. Third, the dune-field pattern in the Olympia Undae Dune Field on Mars is comprised of two generations of dunes. This scenario of pattern reformation with a new wind regime shows that the emergence of the younger pattern is controlled by the boundary condition of the antecedent dune topography imposed upon the interaction between the younger and older patterns.

Table of Contents

List of Figures

List of Tables

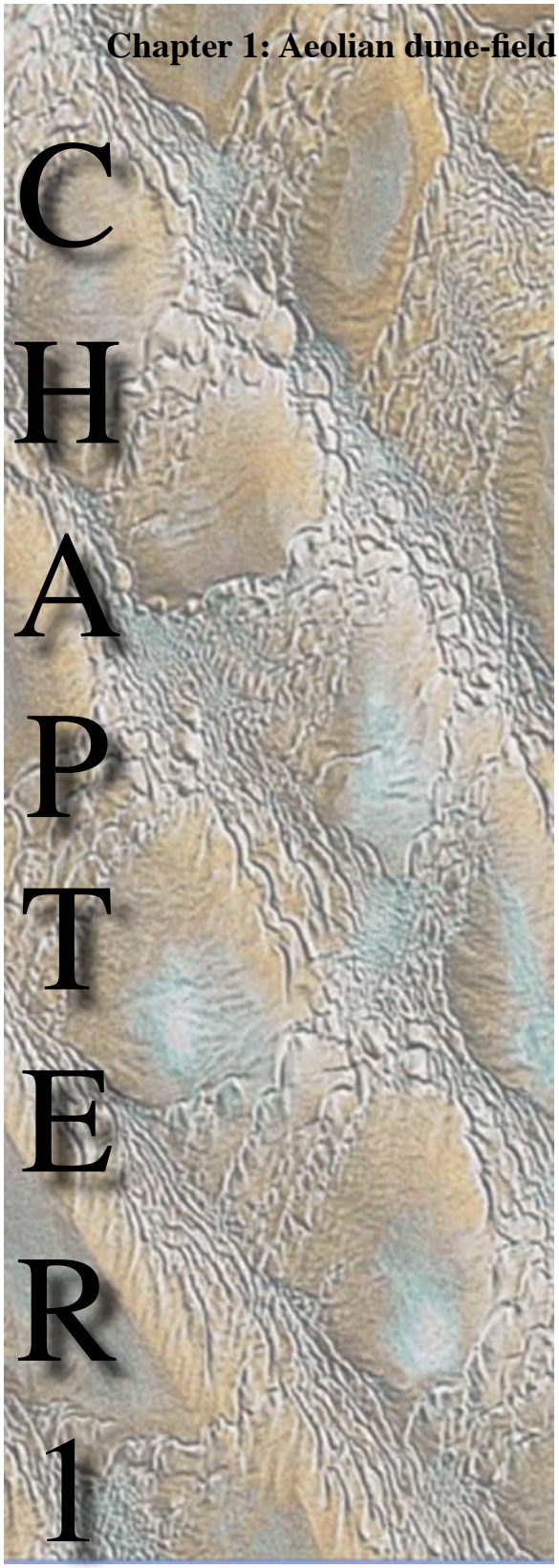

Chapter 1: Aeolian dune-field pattern boundary conditions

ABSTRACT

Aeolian dune-field patterns reflect the complex external environment within which the pattern evolves. These external environmental controls are the boundary conditions on aeolian dune-field pattern formation. The influences of boundary conditions such as wind regime and sediment supply are well-known, however, boundary conditions represent a relatively unexplored area of dune-field pattern formation. Source-area geometry and areal limits are two newly recognized boundary conditions. Measurements of crest spacing and crest length from satellite images of dune-field patterns with point and line source-area geometries show an increase in spacing and crest length over distance, whereas spacing and crest length in plane-sourced patterns emerge equally across the dune field. The impact of the size and shape of a dune field on crest spacing is tested using a previously established analytical model. Model results indicate that the area of a dune field limits the maximum spacing that can occur within a given area, and that dune fields that are five times longer in the direction of dune migration than in the crest-parallel direction can achieve the greatest spacing within a given area. Empirical measurements of spacing, defect density and dune-field area from ten different dune fields, ranging over four-orders of magnitude in size, show that spacing increases and defect density decreases as dune-field area increases. Because the formation of all dune fields involves a wind regime and sediment supply, there must be interplay of boundary conditions within the same dune field. At different stages of pattern development one boundary condition may dominate over others, and with changing climatic, eustatic or tectonic parameters, boundary conditions may change to modify an existing pattern. Recognizing boundary condition controls on aeolian dune-field pattern formation provides a framework for recognizing the signature of the external environment in which a pattern developed and can be used for reconstructing past dune constructional events and climatic change.

Introduction

Aeolian dune-field patterns are now widely interpreted as self-organizing phenomena arising within the complex system of sediment transport (e.g., Hallet, 1990; Werner, 1995, 1999; Bishop et al., 2002; Baas, 2007). A common attribute of self-organizing, complex systems is that pattern ordering occurs as an emergent behavior or autogenic process not determined by any template created within the external environment (Werner, 2003). The emergence of a pattern of bedforms with sediment transport is evident across a wide range of scales (ripples to dunes), environments (aeolian or subaqueous) and even planets (Earth and Mars). At some yet more fundamental level, this reflects the robust nature of pattern emergence in complex systems.

For aeolian dune systems, pattern ordering is thought to occur through a variety of dune-dune interactions (e.g., merging, lateral linking and defect dynamics). If only these dune-dune interactions are considered, a now familiar dune-field pattern emerges, best exemplified through cellular automaton models (Werner, 1995; Momiji et al., 2002; Baas, 2002; Bishop et al., 2002). For aeolian systems, pattern development is characterized by increasing dune size, crest spacing and crest length, and a decrease in defect density with time (Werner and Kocurek, 1997, 1999; Ewing et al., 2006).

Patterns emergent through dune-dune interactions, as in model simulations, however, do not begin to mimic the richness of dune patterns seen within and between aeolian dune fields in nature. In natural systems, dune-dune interactions operate within a much more complex external environment. It is the external environment that is the driving force for much diversity (Werner, 2003). The boundary conditions within which the dune-dune interactions operate is the external environment. As with other systems, these boundary conditions impact on pattern development.

In other systems the impact of boundary conditions on pattern development is well known (Murray, 1990; Cross and Hohenberg, 1993; Ball, 1999). In aeolian systems,

although some boundary conditions are already well known, the overall impact of boundary conditions upon dune-field pattern development has been thus far largely unexplored.

This paper addresses the impact of boundary conditions upon pattern evolution in aeolian dune-fields. First, we present the role of boundary conditions within the concept of complex systems, noting some already well-known external parameters that alter the pattern development in dune fields. Second, we explore newly recognized boundary conditions of source-area geometry and areal limits. Third, we discuss the interplay of boundary conditions, the changing role of boundary conditions through pattern development, and changing boundary conditions through time. We conclude that many of the complexities observed in natural dune-field patterns arise from the imposition of environmental boundary conditions upon dune-field pattern development.

Boundary conditions

Within the context of self-organization of aeolian dune systems, dune-field patterns are thought to represent an attractor or state to which the system evolves through its phase space (Werner, 1995; 1999). Whereas variables characterizing the system state define the axes of the phase space, the external environmental parameters govern its structure and determine the trajectory of the system over time (Werner, 2003; Werner and McNamara, 2007) (Fig. 1A). Where changes in the external environment arise, distortion of the phase-space structure may occur, resulting in the modification of the attractor or emergent pattern (Fig. 1B).

The role of boundary conditions in bedform self-organization is evident from the cellular automaton models used to envision bedform-bedform interactions. These models essentially represent "neutral" bedforms until rules (e.g., slab jump length, angle of repose) are imposed that determine whether the bedforms are aeolian or subaqueous and ripples or dunes (e.g., Forrest and Haff, 1992; Landry and Werner, 1994; Werner, 1995;

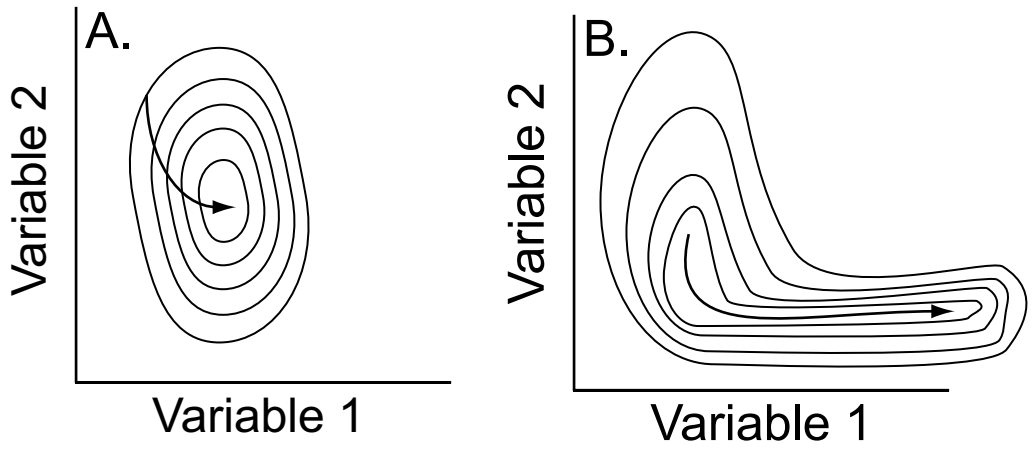

Figure 1. (A) Schematic showing the phase space of Variables 1 and 2 around an attractor. The contours show the structure of the phase space and arrow indicates the trajectory of the system through its phase space toward the attractor defined by the external environment. (B) As the external environment changes, the structure of the phase space and the trajectory of the system toward the attractor are modified. Modified from Werner (2003) Fig. 5.

Bishop et al., 2002). Subsequent additional parameters, such as periodicity and intensity of the transport directions (Werner, 1995) that give rise to different crestline morphologies (i.e., crescentic, linear or star forms), reflect aspects of the external environment and are boundary conditions. Within the model, boundary conditions have been used to strongly alter the emergent patterns. For example, the boundary condition of sediment supply accounts for the transition from barchan to crescentic dunes (Werner, 1995; Bishop et al., 2002). Ultimately, boundary conditions impose a strong influence upon the type and frequency of bedform-bedform interactions that occur within a dune-field, which, in turn, strongly influence the resulting pattern.

Source area geometry

Point, line, and plane source areas

Does the shape of a sediment source area influence the formation of a dune-field pattern? Dune-field source areas are not all the same, but rather, can be defined by a point, line or plane geometry. Point and line sources are end-member geometries of an

external sediment supply to a dune field. Point sources arise where sand is supplied to a dune field from a narrow upwind area, such as a wind gap. Line sources occur where the sand source originates along a linear geomorphic feature such as a beach. Plane sources

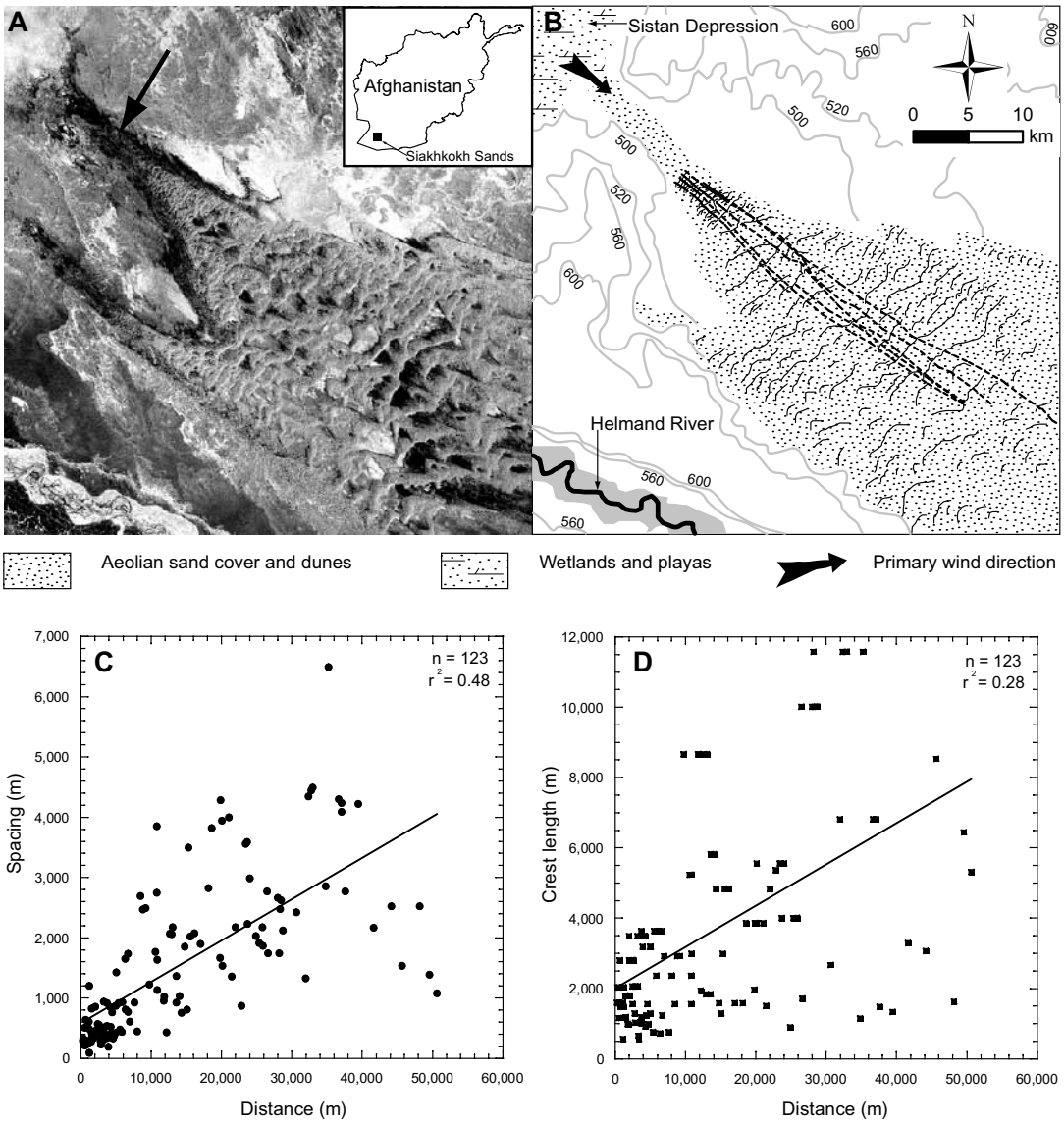

Figure 2. (A) Landsat ETM+ mosaic satellite image (14.5 m/pixel spatial resolution) showing the Siakhkokh Sands Dune Field in the Helmand Basin in Afghanistan. (B) Geomorphic map of the Siakhkokh Sands with digitized crestlines (solid black lines) and spacing transect (dashed black line) along the distance of the dune field. Gray lines indicate contours with corresponding elevations in meters above sea level determined from an SRTM 90 digital elevation model. Arrow indicates primary dune migration direction to the southeast. (C) Plot showing spacing vs. distance along transect indicated in (2B). (D) Plot showing crest length vs. distance along transect indicated in (2B).

refer to sediment supplied to the dune internally by aeolian reworking of the sediment base upon which the dune-field pattern is developing. The designation of a point, line and plane source as a boundary condition provides a geomorphic context for the nature of the sediment source.

The effect of this boundary condition is tested here by considering three dune-field patterns that result from each source-area type: (1) the Siakhkokh Sands Dune Field, southern Afghanistan, originates from a point source; (2) the Guerrero Negro Dune Field, Baja, Mexico, originates from a line source; and (3) the Taklimakan Desert dune field derives from a plane source in northwestern China.

The Siakhkokh Sands are situated near the terminus of the Helmand River in the Sistan Depression in the lower Helmand Basin of Afghanistan (Lee, 2003; Whitney, 2006). The dune field lies in a low-relief catchment that ephemerally drains to wetlands and playas in the Sistan Depression to the northwest (Fig. 2A-B). Sand comprising the dune field derives from deflation of the playas by strong northwesterly '120 Day' winds (Whitney, 2006). The dune field initiates at a wind gap in the local topography and terminates against the Helmand River to the southwest. Compound crescentic dunes, transverse to the dominant northwesterly winds, characterize the overall dune type. Sediment moved through the wind gap at the upwind margin of the dune field creates the point source.

The Guerrero Negro Dune Field is located on a tidally-flooded barrier island on the Pacific coast of the Baja Peninsula, Mexico (Fig. 3A-B; Fryberger et al., 1990). Sand comprising the dune field originates from the beach to the northwest of the dune field and is transported inland by onshore northwesterly winds. The dune field is characterized by simple crescentic dunes, transverse to the onshore winds. The beach serves as the line-source for the dune-field sediment.

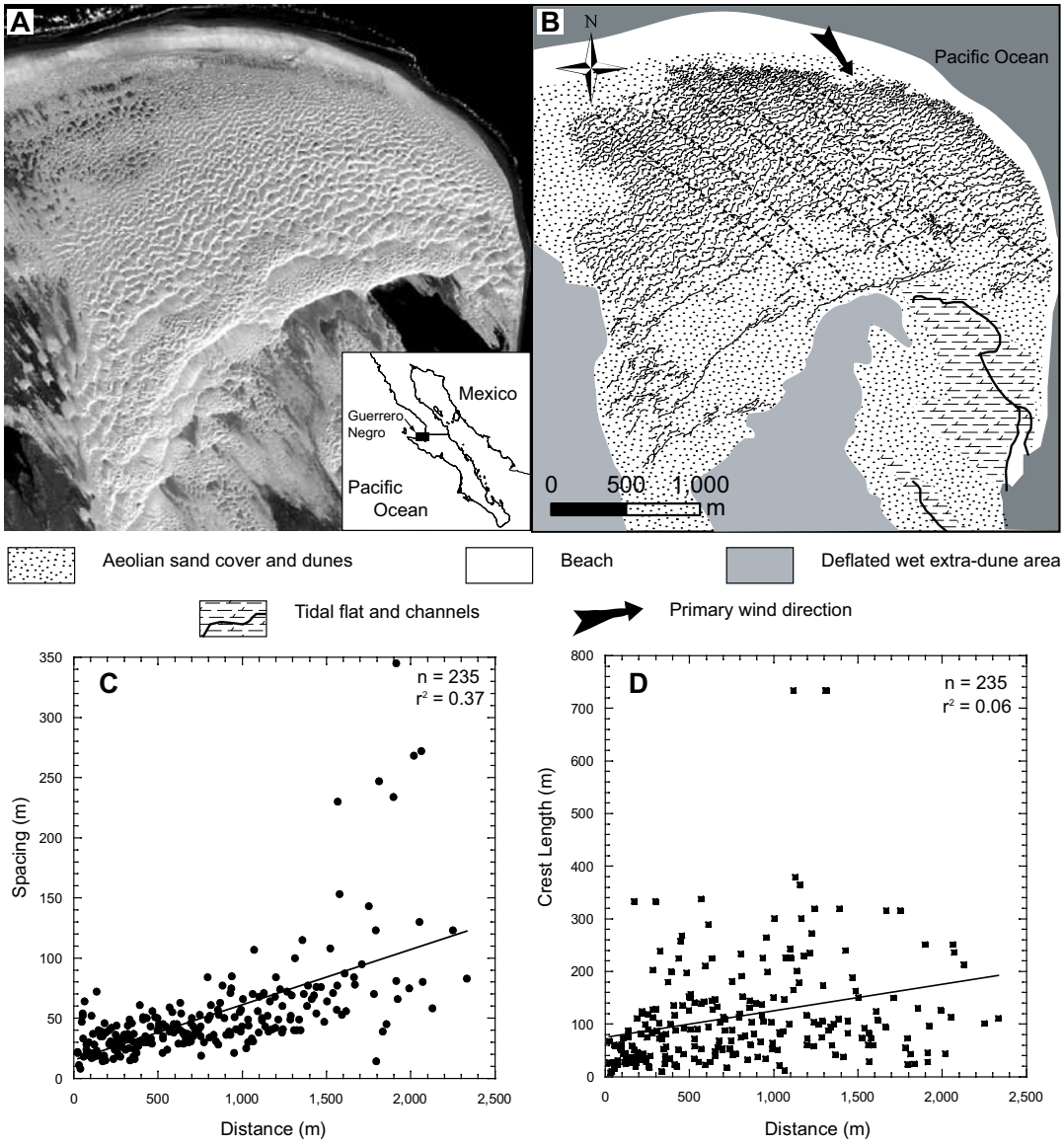

Figure 3. (A) Quickbird satellite image (60 cm/pixel spatial resolution) of the Guerrero Negro Dune Field in Baja, Mexico. (B) Geomorphic map of the Guerrero Negro with digitized crestlines (solid black lines) and spacing transect (dashed black line) along the distance of the dune field. Arrow indicates primary dune migration direction to the southeast. (C) Plot showing spacing vs. distance along transect indicated in (3B). (D) Plot showing crest length vs. distance along transect indicated in (3B).

The Taklimakan Desert extends across the enclosed Tarim Basin in northwestern China (Fig. 4A-B). Stratigraphic evidence suggests aeolian activity and accumulation in the basin initiated by at least the late Miocene (~ 5.3 Ma) and has persisted in some form since this time (Sun and Liu, 2006). However, the age of the modern field in this region of

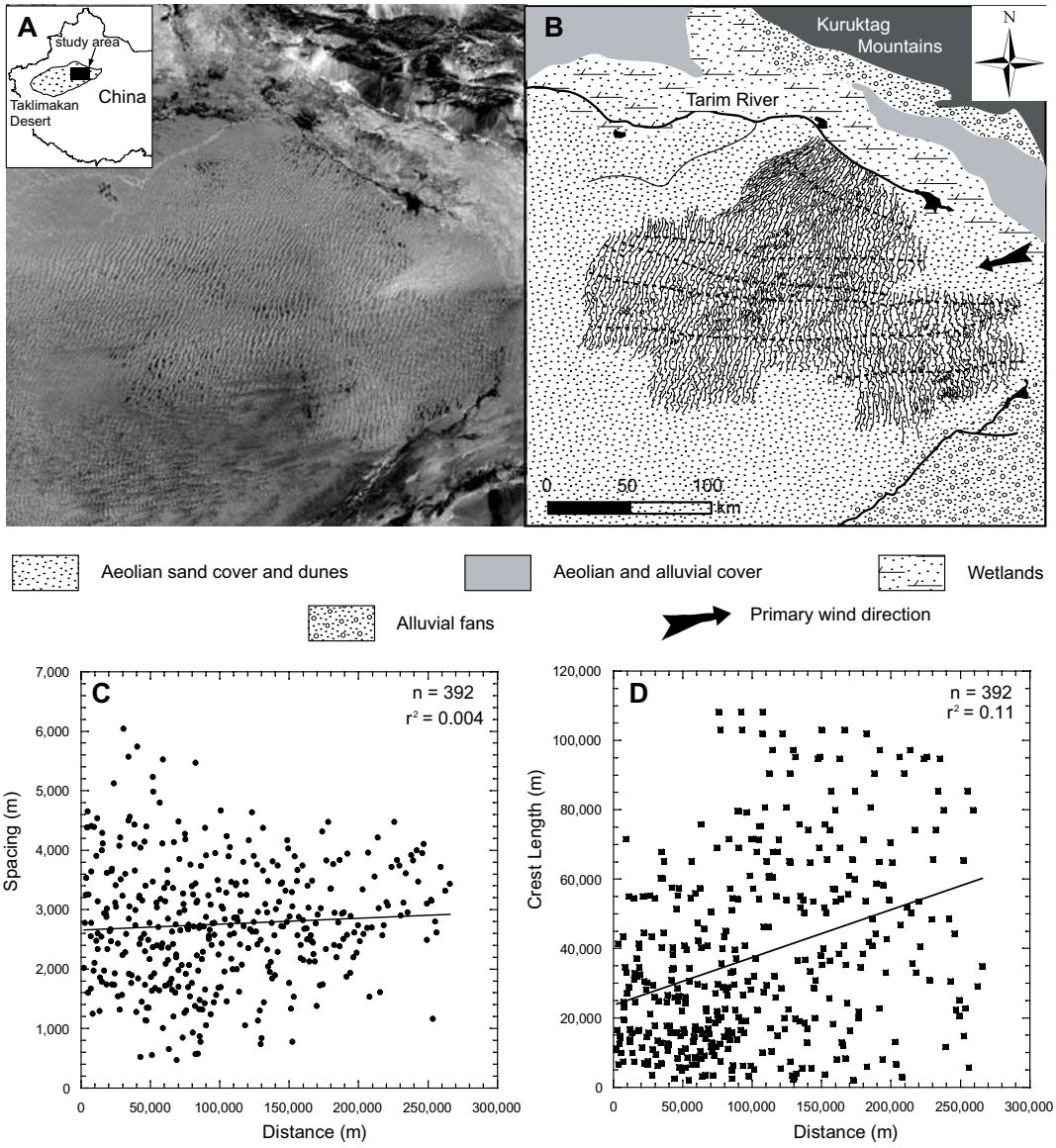

Figure 4. (A) Landsat ETM+ mosaic satellite image (14.5 meter/pixel spatial resolution) showing the eastern margin of the Taklimakan Sand Sea in the Tarim Basin in northwestern China. (B) Geomorphic map of the eastern Taklimakan Sand Sea with digitized crestlines (solid black lines) and spacing transect (dashed black line) along the distance of the dune field. Arrow indicates primary dune migration direction to the west. (C) Plot showing spacing vs. distance along transect indicated in (4B). (D) Plot showing crest length vs. distance along transect indicated in (4B).

the Taklimakan is poorly constrained. Modern winds blow from the east-northeast (Wang et al., 2005; Zu et al., 2008). Although dunes in the study area at the eastern, upwind margin of the dune field have been interpreted as mostly linear forms (Wang et al., 2002, 2005), the ubiquitous westward-facing slipfaces suggest instead that the dunes are compound/

complex crescentic ridges oriented transverse to the modern winds.

Infilling of the Tarim Basin occurs from all sides, with influx from bordering alluvial fans and fluvial systems. Low rates of sediment influx at the upwind margin of the dune field suggest that the bulk of the sand comprising the modern dunes derives from basin fill (Wang et al., 2002). The basin fill creates a blanket of available sand or an in situ sediment source with equal potential for aeolian transport across the basin floor that is the plane source.

Spatial trends from point, line and plane source areas

In order to characterize the dune pattern associated with each source-area type, spatial trends in the crest spacing and crest length were evaluated. These variables were used because they represent basic geometrical properties of a pattern (Werner, 1999, 2003) and have been used previously in dune-field pattern analysis studies (Ewing et al., 2006; Derickson et al., 2008). Although defect density is also a well-recognized pattern variable, it is a field-scale variable represented by a single value, and not appropriate for this study because the interest is in trends within the field. For each dune field, crestlines were manually digitized and measured from satellite imagery using geographic information system (GIS) software following the methods of Ewing et al. (2006). Crest spacing and crestline lengths were measured in series along transects parallel to the dune migration direction to preserve the position of the measurement within the dune field. The data were plotted against distance in the dune migration direction. A simple linear regression was applied to each data set to highlight the presence or absence of a trend in spacing and crest length over distance.

In both the Siakhkokh Sands and Guerrero Negro dune fields, the data show an increasing trend in spacing over distance (Fig. 2C, 3C). A weak correlation is observed with the increase in crest length over distance in the Siakhkokh Sands (Fig. 2D) and no

trend is observed in the Guerrero Negro (Fig. 3D). The high variability in crest length at the Guerrero Negro may reflect a greater frequency of dune-interactions, which cause defects, and which arise from new dunes being injected into the field along the upwind line-sourced margin. The greater degree of variability in crest length over spacing is consistent with other studies that have shown crest length to be a less representative pattern variable (Ewing et al., 2006; Derickson et al., 2008). Distinct from a point or line source of sediment, the plane source of the Taklimakan Sand Sea imparts a spatial signature in which no trend in crest spacing occurs in the dune migration direction (Fig. 4C). Similar to the Guerrero Negro, no trend is observed with crest length over distance in the Taklimakan Dune Field (Fig. 4D).

Emergent patterns from point, line, and plane source areas

An explanation as to why distinct patterns emerge from point, line and plane source areas arises from the role of time and distance in pattern formation. First, models (Landry and Werner, 1994; Werner, 1995; Werner and Kocurek, 1999) and empirical studies (Kocurek et al., 1992; Ewing et al., 2006) indicate that dune spacing and crest length evolve as a function of time. Second, the trends observed for point and line source patterns indicate that spacing and crest length also evolve as a function of distance. This suggests that under the influence of these boundary conditions the distance over which a pattern evolves is proportional to the pattern constructional time (i.e., distance is time). In effect, the point or line source geometry imposes a pattern signature that represents the ontogeny of the dune field from the source. In contrast, plane source dune-field patterns reveal only a single snapshot of their developmental history, with pattern evolution occurring equally across the entire field. For plane source patterns the constructional time is reflected by the average crest spacing (c.f., Ewing et al., 2006).

Dynamically, point and line source dune-field patterns initiate with the emergence

of small dunes at the upwind sediment source, rather than across the entire dune field as with a plane source. Pattern evolution occurs as the dunes migrate away from the point or line source in a manner similar to how patterns evolve with time (i.e., bedform-bedform interactions give rise to an increase in spacing over both time and distance). Recent cellular automaton models of point, line and plane sources for dune fields (Eastwood et al., in review) support both the interpretation of the system dynamics and the resulting pattern evolution as presented here.

Recognizing the pattern signature of the source-area boundary condition increases the ability to make better geomorphic and paleoclimatic interpretations based upon dune-field pattern analysis. Determining the type of sand source has application especially where there is no longer an obvious connection between a dune field and its sand source, such as with relict patterns or with the rock record (e.g., Beveridge et al., 2006). Line sources typically originate from relative or absolute falling lake or sea level, driven by climate or other causes, in which shoreline sands become available for aeolian transport (Kocurek et al., 1991). Plane source patterns emerge following the loss of vegetation and the accompanying increase in sand availability occurring with the onset of desertification or with the development of a new dune-field pattern on an older generation of dunes (i.e., the older generation is the plane source).

AREAL LIMITS

The geomorphic container

Does the spatial extent of a dune field influence dune-field pattern evolution? Areal limits at the aeolian dune-field scale can be thought of as the geomorphic container within which the pattern develops. Typically, the spatial extent of a dune field is defined by some antecedent condition. At the larger scale, the antecedent condition may be the basin within which the dune field is housed; at the smaller scale the antecedent condition may be a

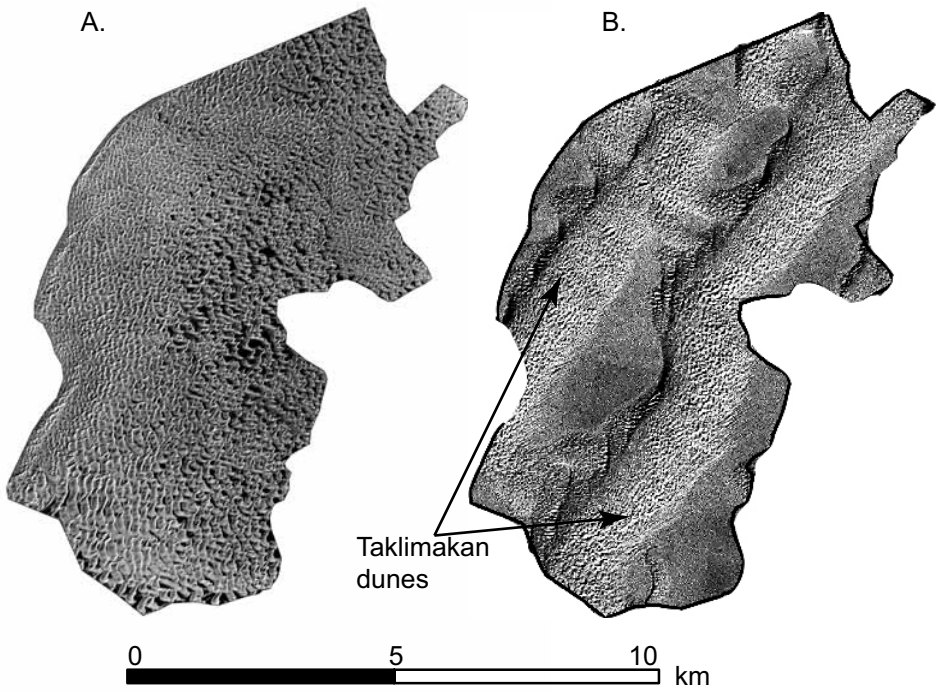

Figure 5. (A) Digital orthophoto (1 meter/pixel spatial resolution) of the White Sands dune field in New Mexico, USA cropped to the core area of the dune field following the definition of dune-field area defined in the text. (B) Landsat ETM+ satellite image of the Taklimakan Sand Sea cropped to show the equivalent area as in Fig. 5A. Note the scale is the same for both images.

host dune or relict dune topography. The impact of the size and shape of this geomorphic container on pattern evolution is of interest here.

The areal limit boundary condition can be intuitively understood by considering the implausible occurrence of dunes the size of those in the Taklimakan Desert (~3 km in spacing and ~120 m in height, Fig. 5B) within the area of a modestly-sized dune field such as White Sands, New Mexico (58 km2, Fig. 5A). It is proposed that the control of areal limits as a boundary condition that impacts pattern development is the limitation on the frequency of dune-dune interactions. Because there are initially fewer dunes and defects in smaller fields, the frequency of interactions in a smaller area decays more quickly as proportionally more defects are removed from a smaller field than a larger field. Essentially the areal limit constrains the number of bedform interactions that can occur before a steady

state is approached.

An example of how areal limits impact pattern formation in nature is the development of superimposed dunes hosted on the stoss slope of larger bedforms. Where superimposed dunes are confined to the stoss slope of the host bedform, the length of the stoss slope defines the areal limit for the superimposed pattern. Limitations in the dune-migration direction constrain the number of dune-dune interactions and limit the maturity of the pattern, thus accounting for capped values of spacing, defect density, and crest length (Fig. 6; Derickson et al., 2008).

Analytical approach

During the evolution of a dune field when does the field size become an areal limit boundary condition? How does the shape of the geomorphic container affect the

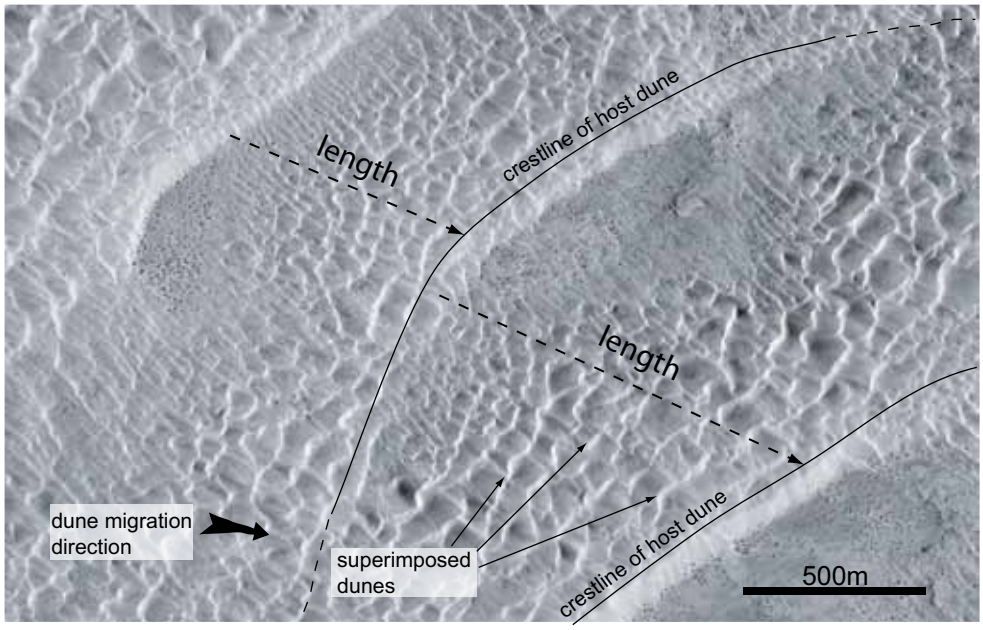

Figure 6. Digital orthophoto (1 meter/pixel spatial resolution) showing two dune crestlines (solid black lines) within the core of the Algodones Dune Field, California. The dashed arrows indicate the length of the stoss slopes of the two dunes over which the superimposed dunes migrate. This length defines the areal limit boundary condition for the superimposed dunes. The dune migration direction of the superimposed dunes to the east-southeast is indicated by the arrow.

evolution of crestline spacing? These questions can be explored using a model relating defect dynamics to the evolution of spacing and defect density of transverse dunes (Werner and Kocurek, 1999).

Within the Werner and Kocurek (1999) model, dune spacing evolves through defect interactions. Dunes are abstracted as uniformly spaced crestlines represented by line segments. The terminations of the line segments are defects, which migrate through the field faster than the primary crestlines. The spacing and defect density of the pattern evolve through the loss of crestline defects and crestline length (L) as defects merge with a downwind crestline and are lost at the downwind margin of the dune field. Crest spacing (λ) is related to the geometrical relationship $\lambda = A/L$, where A is the area of the dune field defined by the dune-field length (Y) times the width (X). As defects internal to the field are removed, pattern evolution slows and defects at the edge of the field, which migrate at the same rate as the primary crestlines, dominate the pattern evolution. At this transition, bedform spacing exponentially approaches an asymptotic limit and defect density is 1/X.

Although the model represents sand volume exchange between dunes during the loss of crestline length, there are limited empirical data that constrain the modeled values in well-developed transverse dunes. Data from Hersen and Douady (2005) indicate that during mergers among barchan dunes significant sand loss may occur through calving of new bedforms at the defects (i.e., horns), whereas bedform volume is conserved through mergers and defect migration within the Werner and Kocurek (1999) model. In addition, other dune-dune interactions are recognized that are not explicitly treated in the model and that promote sediment exchange between bedforms, pattern growth, and pattern destruction (see review in Kocurek and Ewing, 2005). To that end, the model is used here to illustrate the areal limit concept that the size and shape of a dune field impacts the development of dune spacing and not as a predictive tool.

Utilizing the same initial conditions as in Werner and Kocurek (1999), crest spacing

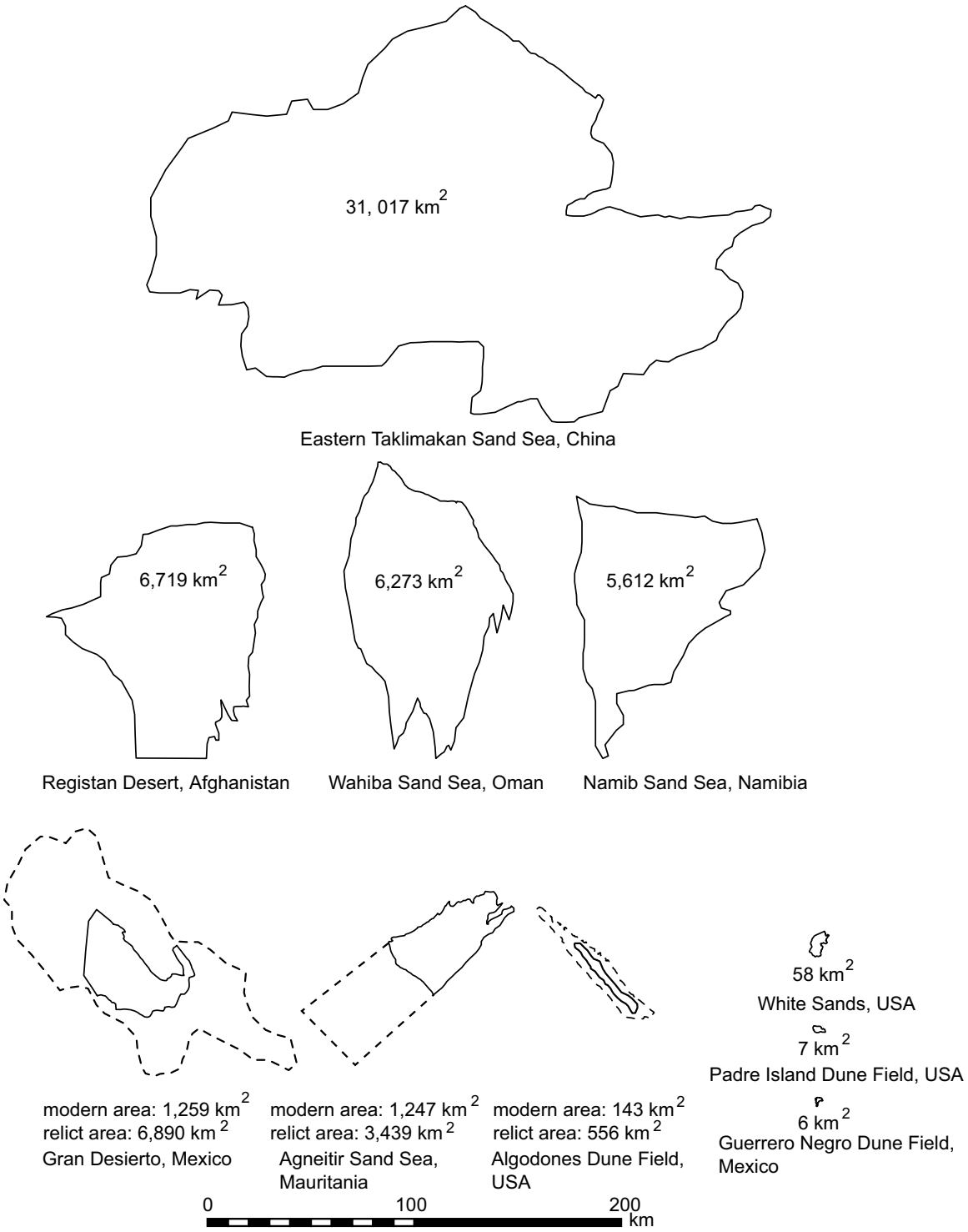

Figure 7. Dune-field area, as defined in text, for ten dune fields used in this study. Area is given in km2. Solid black lines represent the modern dune-field areas. Dashed lines around the Gran Desierto, Agneitir Sand Sea and Algodones Dune Field indicate relict dune-field areas (see Section 4.3 in text for discussion). Note scale is the same for all areas.

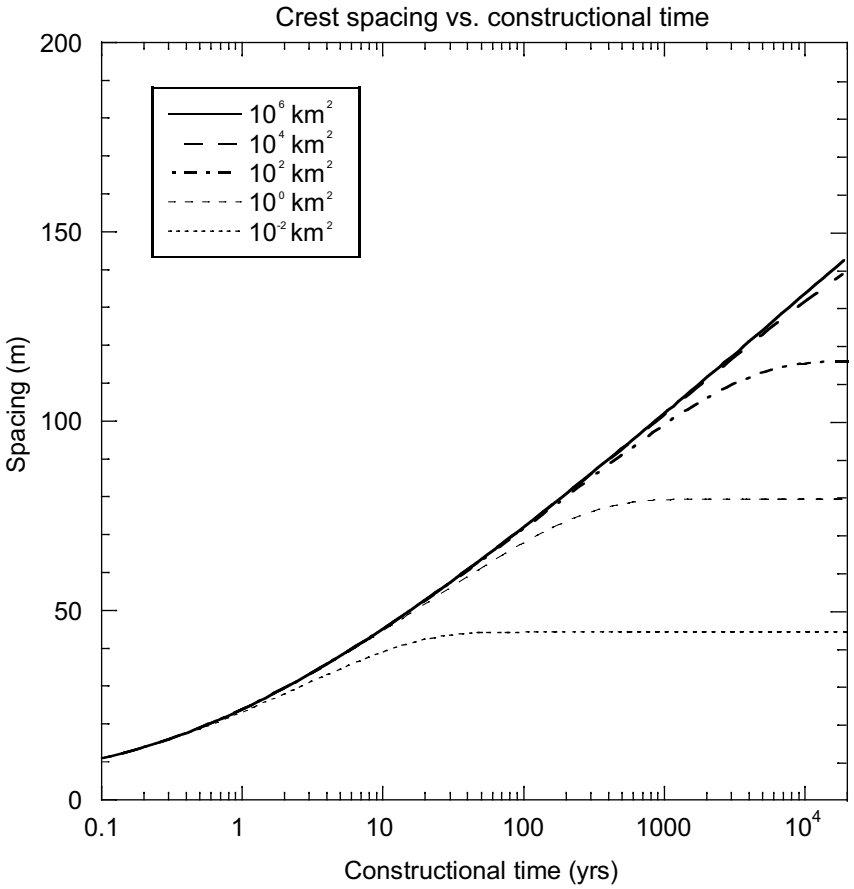

Figure 8. Plot showing the change in crest spacing over time for dune fields of different sizes. Note that for small dune-field areas the change in spacing decreases rapidly, achieving a near steady state scenario, whereas the impact of the dune-field area is minimal in large dune fields. Model is based on Werner and Kocurek (1999).

is allowed to evolve for 20,000 years within different dune-field areas ranging from 10-2 km^2 to 106 km^2. The 20,000 year time frame represents an orbital, precession-forced global climate cycle and the time since the Late Glacial Maximum over which many modern dune-field patterns have developed (Lancaster, 1995; Ewing et al., 2006). The span of areas captures dune-field sizes ranging from small, coastal dune fields to large, regional sand seas (Fig. 7). The ratio of dune-field width to length is maintained at 1:1.

Figure 8 shows that smaller dune fields are most profoundly affected by the areal limit boundary condition, whereas larger fields (>104 km^2) are minimally influenced by spatial boundaries. In smaller areas, the rate of change in spacing decreases early in pattern

development and spacing quickly approaches an asymptotic limit constrained by the areal limit boundary condition.

The effect of dune-field shape on the evolution of spacing was explored by changing the ratio of across dune-field width to streamwise dune-field length and measuring the maximum spacing over a 20,000 year constructional time interval for dune-field areas ranging from 10-2 km^2 to 106 km^2. Width/length ratios varied from 1/100 to 100/1. Fig. 9 shows that the maximum dune spacing for all dune-field areas occurs where the dune-field length is ~5x greater than the dune-field width. Within the tested width to length ratios, dune spacing declines to lower values where the length is limited. These observations suggest that the streamwise dune-field length is a stronger controlling parameter in pattern evolution than across dune-field width. Consistent with Fig. 8, Fig. 9 also indicates that as dune-field area increases the impact of the areal limit boundary condition decreases.

Area limits in natural dune fields

The areal limit boundary condition in natural dune fields was explored by measuring the empirical relationships between dune-field area and dune spacing and defect density over a broad range of dune-field sizes as shown in Fig. 7. Dune crestlines, crest spacing, and area were measured manually measured from these 10 dune fields using GIS software. Measurements of spacing and crest length were taken following the methods of Ewing et al. (2006). Dune-field area was defined and measured as an area that contains dunes, has no geomorphic interruptions, and within which no significant changes in dune-pattern type occurs. The largest dune pattern within the dune-field area was measured (i.e., not superimposed patterns). Spacing and defect density are plotted against dune-field area (Figs. 10,11).

Figure 10 shows an increase in average dune spacing as dune-field area increases. Although the dune fields are at different stages of development, the strong correlation

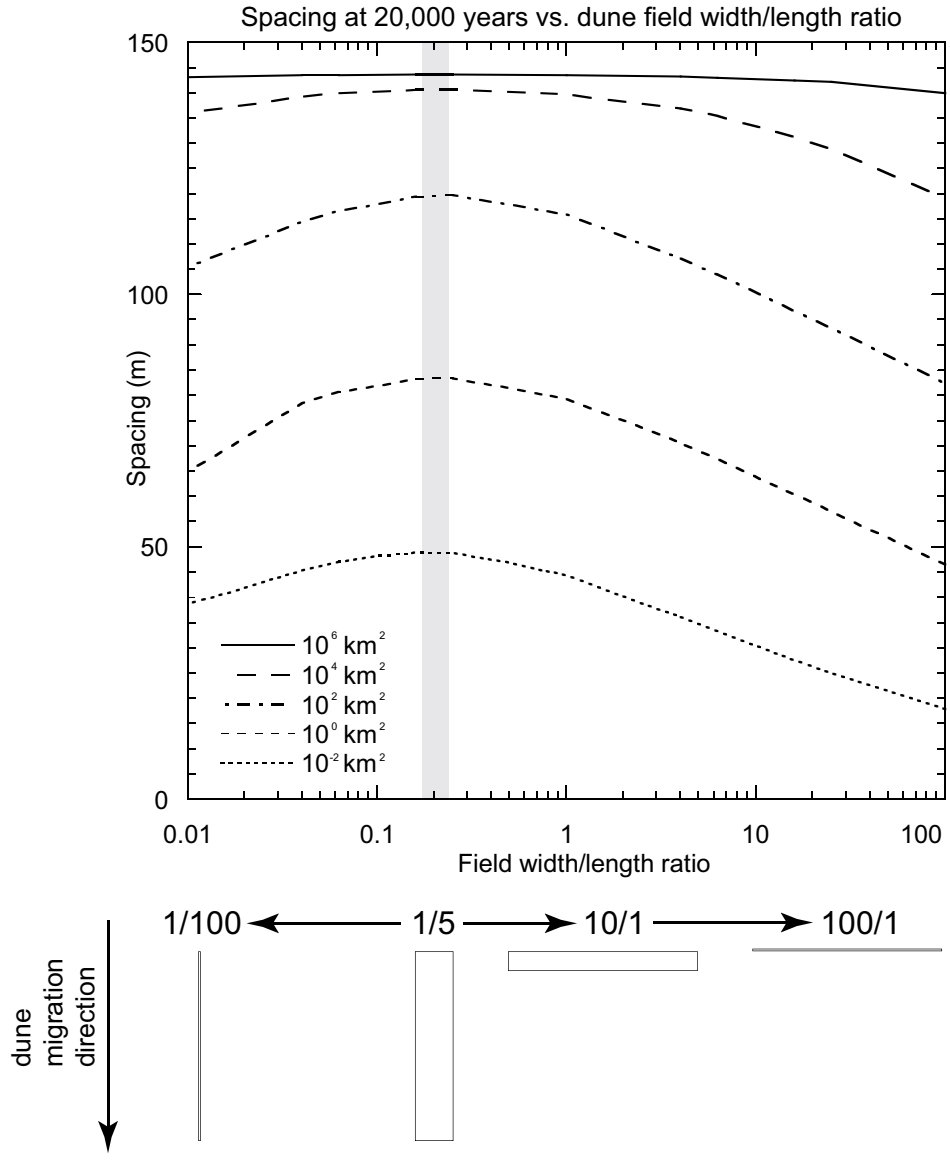

Figure 9. Plot showing maximum crest spacing at 20,000 years for different dune-field width to length ratios. The gray bar on the plot indicates the maximum spacing for each area considered and corresponds to a width/length ratio of 1/5. The schematic below the plot shows the areas plotted in the above figure. Note the implied dune migration direction is denoted by the arrow. Model is based on Werner and Kocurek (1999).

between spacing and area indicates that dunes developing within large areas can attain a greater spacing than dunes confined to small areas. This relationship agrees with the model results presented in Fig. 8.

The solid line in Fig. 10 represents the best-fit line to the data points. The Padre

Island Dune Field, Namib Sand Sea, and Registan Desert lay near the line. The Guerrero Negro Dune Field, White Sands Dune Field, the Wahiba Sand Sea, and the Taklimakan Sand Sea lie below the line. The Algodones Dune Field, the Agneitir Sand Sea and the Gran Desierto lie above the line and most significantly depart from the trend of the data. A consideration of the stage of pattern development, the geomorphic history, and the boundary conditions of these dune fields can account for their departure from the overall data trend.

Geomorphic reconstructions of the Algodones Dune Field (Derickson et al., 2008), the Agneitir Sand Sea (Lancaster et al., 2002) and the Gran Desierto (Beveridge et al.,

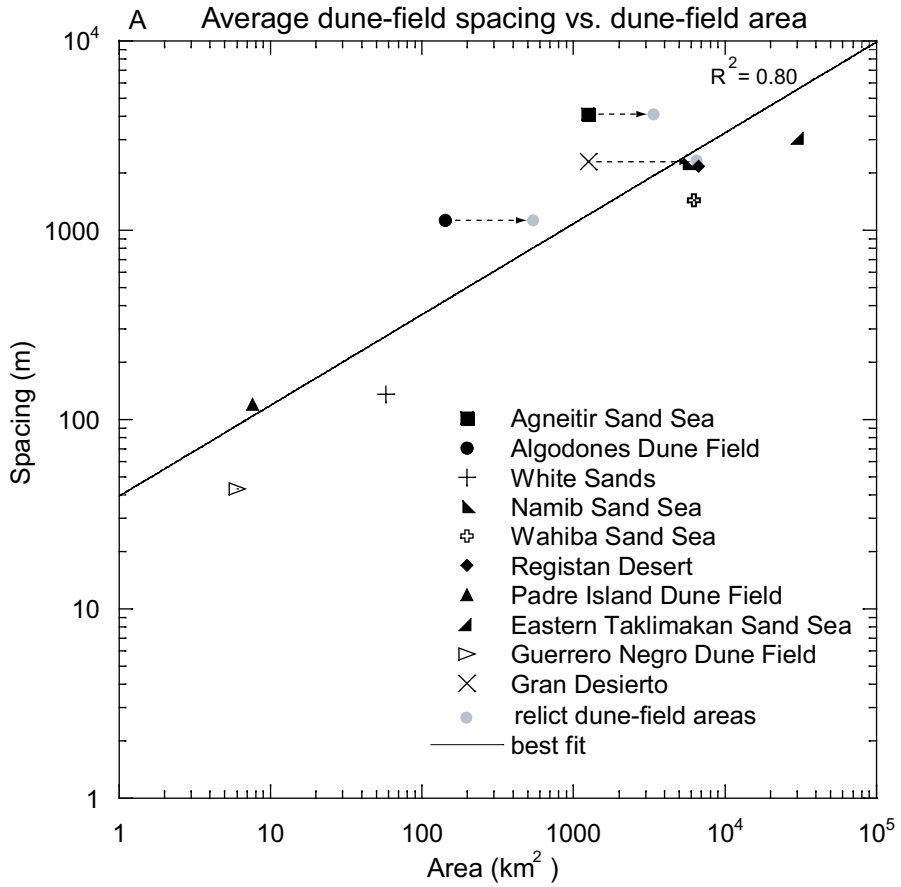

Figure 10. Plot showing measured average crest spacing vs. dune-field area for the ten dune fields shown in Fig. 7. The solid line shows the best fit to the data (black symbols). The gray dots show the spacing to relict dune-field area relationship for the Algodones Dune Field, Gran Desierto and Agneitir Sand Sea. Dashed arrows correspond to the modern areas of these dune fields.

2006) indicate that the largest spaced dune patterns within these fields are relict features that developed under different climatic and geomorphic conditions. Accounting for the geomorphic history of these dune fields, it is reasonable to suggest that the modern area of each field is smaller than the dune-field area during the constructive phase of the largest pattern. During the Pleistocene glacial period, when the largest pattern in the Agneitir Sand Sea developed (Lancaster et al., 2002), sea-level was lower by ~120 m and the Agneitir linear dunes extended ~ 50 km from the modern shoreline to the continental shelf (Sarnthein and Diester-Haas, 1977). Subsequent sea-level rise has truncated much of the original dune-field area and the modern, measured dune-field area is smaller. Relict crestlines in the Algodones Dune Field extend eastward of the dune field and the westward flanks of the largest-scale dunes are being reworked by a younger generation of dunes (see Fig. 11, Derickson et al., 2008), suggesting that the area of the dune field has been reduced. Relict linear dunes in Gran Desierto extend into sand sheets to the southeast and northwest of the modern, active dune-field area (see Fig. 4, Beveridge et al., 2006), suggesting that area of the dune field during the formation of the linear dunes was once larger. In Fig. 10, the gray dots, connected by dashed arrows from the data points representing these dune fields, indicate the best approximation of the relict dune-field areas (dashed areas in Fig. 7) based on the geomorphic evidence given above. Each data point shifts toward the best fit line and results in a better overall correlation between spacing and area.

Figure 11 shows an overall decrease in dune-field defect density as dune-field area increases. The open squares represent the minimum defect density for the area of each dune field calculated as 1/X, where X represents the maximum distance in the across dune-field width in the along-crest orientation within the measured dune-field area (i.e., one crestline extending the width of the dune-field area). For the Algodones Dune Field, the Gran Desierto and the Agneitir Sand Sea the minimum defect density is calculated from the relict dune-field areas and plotted against the relict areas denoted in Fig. 7. Arrows relate

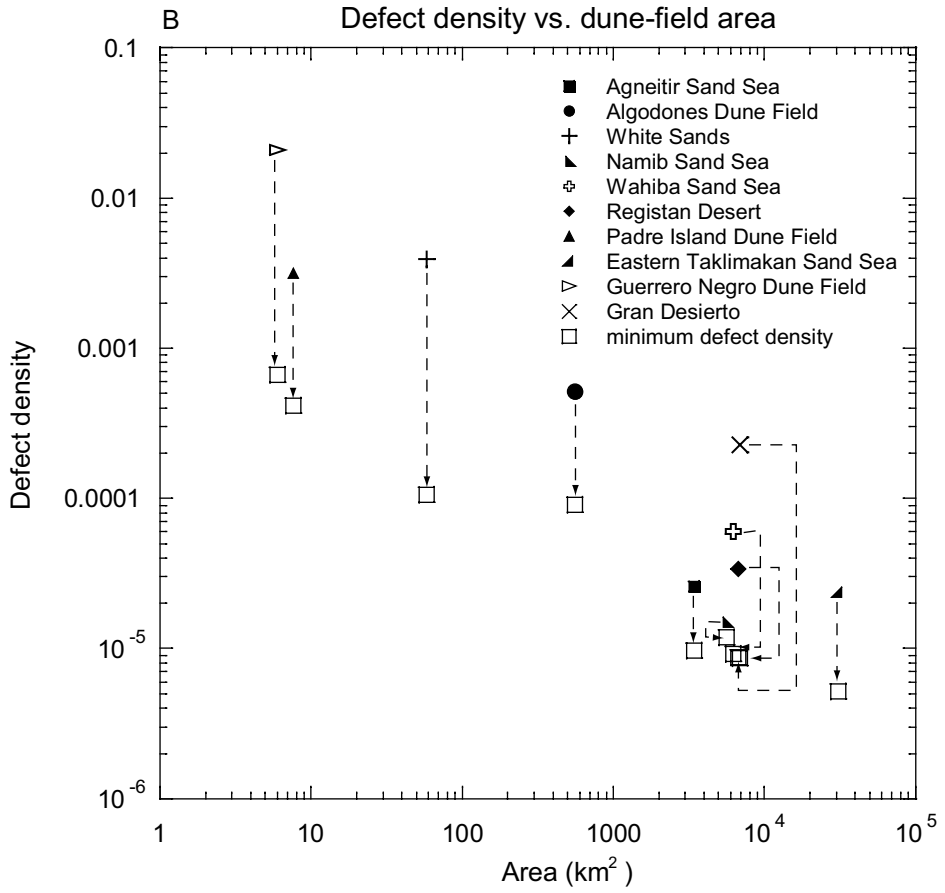

Figure 11. Plot showing the measured defect density vs. dune-field area for the ten dune fields shown in Fig. 7. The open squares show the minimum defect density determined by a measured value of 1/X where X is the maximum dune-field width. Dashed arrows correlate each measured defect density value to the respective minimum defect density value.

the measured defect density values (symbols) to the minimum defect density values (open squares) calculated for each corresponding dune field. In Fig. 11 the Namib Sand Sea lies near its calculated minimum defect density and all other dune fields have defect density values greater than their minimum.

A dune-field pattern having achieved a minimum defect density state would consist of crestlines that extend the width of the dune field without any internal defects and represent a highly organized pattern. This state does not occur in any of the dune-field patterns measured here and, in general, such a "perfect" minimal defect density state

probably never occurs in natural dune fields because dune-field pattern formation is a dynamic process in which some bedform interactions, such as crestline splitting, create new defects. Spacing, however, should continue to increase because of a host of other bedform interactions, such as merging and lateral linking, which increase dune size and contribute to an overall increase in pattern organization.

The defect density of the Namib Sand Sea, which closely approaches its minimum defect density, probably represents a pattern that has evolved to a highly ordered state. The current activity of the dune field (Bristow et al., 2007) indicates that the large linear dunes in the Namib are part of an actively evolving pattern and there is no evidence to suggest that the area of the dune field has changed significantly (Lancaster, 1989). This suggests that the large linear dune pattern in the Namib Sand Sea is near its most organized state. Dune fields that have significantly higher defect densities than their minimum either represent dune fields that are evolving toward their minimum defect density state, or dune fields that have been modified by changing climatic or geomorphic conditions. In the latter case, the higher defect density results from crestlines that have been truncated or crestlines that have been broken by a younger generation of dunes.

All else being equal defect density and spacing evolve interdependently. Fig. 12 shows that as spacing increases, defect density decreases. The Algodones Dune Field, Gran Desierto and Agneitir Sand Sea depart from the overall trend with high values of defect density for their associated spacing. These dune fields were noted above as departing from the spacing to area relationship (Fig. 10) owing to their reduced dune-field areas, as recognized by relict crestlines and other geomorphic evidence. Plotting the minimum defect density values calculated from the relict areas of these dune fields indicates a stronger correlation between spacing and defect density. The plotted defect density value of the Namib Sand Sea, a dominantly linear dune field, stands apart from the overall data trend with a lower defect density value, and clusters with the minimum values

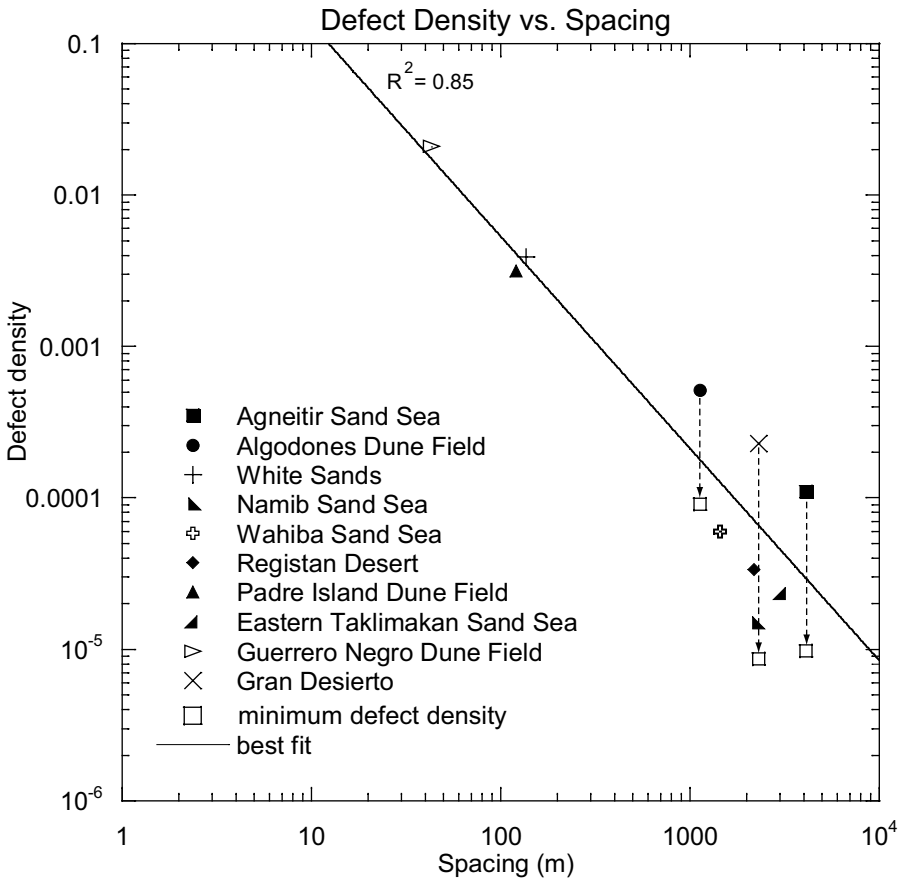

Figure 12. Plot showing measured crest spacing vs. defect density. The solid line indicates the best fit line for the data. The open squares show the relationship of the minimum defect density values based on the relict dune-field areas to spacing of the Algodones Dune Field, Gran Desierto and Agneitir Sand Sea. Dashed arrows correlate each measured defect density value to the respective minimum defect density value.

of Gran Desierto and Agneitir Sand Sea, which are also linear dune fields. This may point to the highly organized state of the Namib and, in general, the stability of linear dune fields.

In Figs. 10, 11 and 12 both transverse crescentic and longitudinal linear dunes were plotted along the same trend. That both dune types plot well along a single trend line suggests that the areal limit boundary conditions applies to both dune types. This is expected because bedform patterns emerge through dune-dune interactions, which occur through dune migration. The areal limit boundary condition limits the space in which

dune migration can occur, and consequently, constrains the number of interactions and the maximum spacing that can occur within an area. Transverse dunes may be more impacted by areal limits, at least in the dune-field length as shown in Fig. 5 and demonstrated by the model (Fig. 9), because the migration and interactions are predominantly unidirectional in the streamwise direction. Linear dunes emerge under the influence of a bidirectional wind regime and interactions probably occur in the streamwise direction as linear dunes elongate, as well as laterally as defects attach to crestlines and form Y-junctions. In contrast to these dune types, star dunes, which form under multidirectional winds, interact with their nearest neighbors only and can develop a large spacing in a small area (Ewing et al., 2007).

The role of boundary conditions in pattern development

Source-area geometry and areal limits as detailed above describe the impact of single boundary conditions upon pattern development. Because all dune fields involve a wind regime and sediment supply there must be at least interplay between these two boundary conditions within the same dune field. Probably in natural dune fields there is an interplay between several boundary conditions at any one time. Additionally, at different stages of pattern development one boundary condition may dominate over others, and with changing climatic, eustatic or tectonic parameters, boundary conditions may change to modify an existing pattern. Simple dune-field patterns (i.e., a single constructional event; Kocurek and Ewing, 2005) reflect the interaction among boundary conditions and the changing impact of boundary conditions through stages of pattern development. Complex patterns (i.e., multiple superimposed simple patterns; Kocurek and Ewing, 2005) reflect changes in boundary conditions through time.

Wind regime, sediment supply, source-area geometry, areal limits and antecedent conditions stand out as primary boundary conditions on dune-field pattern formation. Antecedent conditions are geomorphic conditions, such as a near-surface water table,

vegetation and topography, existing prior to a dune-field pattern constructional event. Minimally, a dune-field pattern will reflect the wind regime, sediment supply and source-area geometry. Although areal limits and antecedent conditions may significantly impact the pattern as primary controls, the presence of these boundary conditions is determined by the local geomorphic setting.

Boundary condition interplay

Consideration of wind regime, source-area geometry, and sediment supply can account for the simple dune-field pattern at Guerrero Negro Dune Field (Fig. 3A) in the absence of significant impact by areal limits and antecedent conditions. The northeast-southwest crestline orientation emerges transverse to the onshore northwesterly winds. The dune spacing increases over the distance of the dune field owing to the beach line source and the crescentic ridge morphology arises from a high and continuous sediment supply from the beach. The high defect density, apparent in Fig. 11, suggests the dune-field pattern is not yet impacted by areal limits and it is reasonable to suggest the impact of antecedent conditions would be neutral given the geomorphic setting of the dune field on a low-relief barrier island.

In another example, consideration of wind regime, source-area geometry and sediment supply by themselves are insufficient to account for the simple pattern at White Sands Dune Field. Similar to Guerrero Negro, the crestline orientation at White Sands is transverse to the overall wind regime, here dominated by southwesterly winds with a subordinate north-northwesterly component. Deflation of upwind playas and in situ sediments provides an episodic and sufficient sediment supply for the formation of crescentic ridges. The high defect density noted in Fig. 11 suggests that the impact of areal limits is minimal at its current stage of development. In this case, however, the antecedent condition of pre-existing topography affects the spatial variability of the crest spacing at

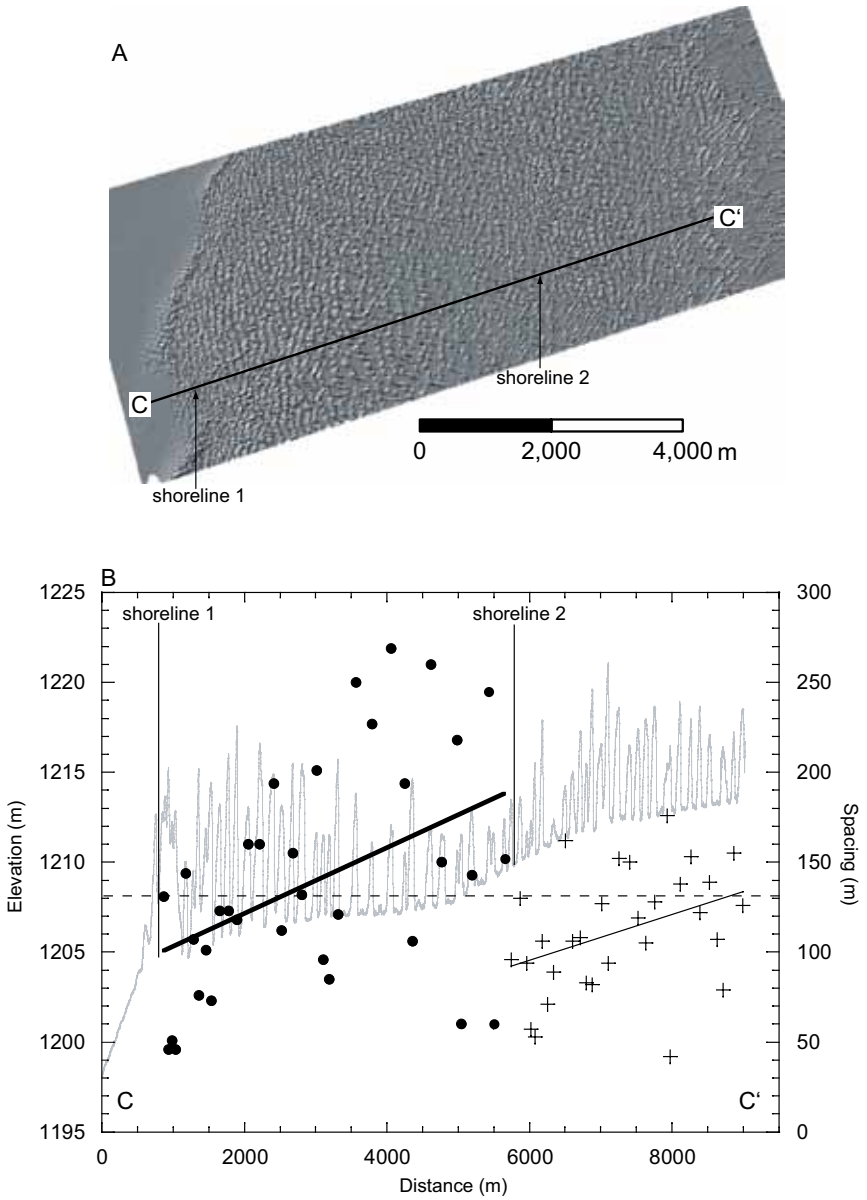

Figure 13. (A) Hillshade rendering of a DEM derived from airborne LiDAR over the core of White Sands Dune Field. Dunes are largely migrating from the southwest to the northeast along the orientation of the transect C to C'. Arrows denote the location of paleo-shorelines along the profile identified in the DEM. Note the change in spacing along the transect. (B) Plot showing a profile (gray line) through the dune field along the C to C' transect noted in Fig. 13A. Elevations on the left y-axis correspond to the profile. The solid, black dots indicate the spacing between dune crests along the profile between shoreline 1 and shoreline 2, and the thick, black line is the best fit line to these data. The black crosses indicate the spacing between dune crests along the profile between shoreline 2 and the termination of the profile, and the thin black line within these data is the best fit line. Spacing measurements correspond to the right y-axis. The x-axis is the distance along the profile and corresponds to both the profile and spacing data. Shorelines 1 and 2 are labeled on the profile by solid straight black lines and correspond to the shorelines noted in Fig. 13A. Note the increase in dune spacing, apparent by the best fit lines, initiates at each shoreline and can be seen in the profile.

White Sands.

The crest spacing at White Sands increases from the upwind margin toward the middle of the field, then abruptly decreases, followed by another increase in spacing (Fig. 13A, 13B). A high-resolution airborne LiDAR survey of the dune field indicates that the increasing trends in spacing at the upwind margin and from the middle of the field are coincident with topographic steps in the underlying surface over which the dunes are migrating (Ewing et al., 2008) (Fig. 13A-B). The topographic steps can be related to the basin-wide geomorphology as paleoshorelines of paleo-Lake Otero (Langford, 2003; Ewing et al., 2008). Apparently, deflation of lake strata to each successive shoreline acted as a line source for the dune sediments and created the characteristic increase in spacing over distance. Although the trend of increasing spacing over distance is apparent in Fig. 13B, a high degree of scatter occurs in the spacing data and the correlation is weaker than that of the Guerrero Negro Dune Field (Fig. 3C). This appears to be the result of other antecedent boundary conditions at White Sands, such as a near-surface groundwater table and partial vegetation of the dunes in some areas (Kocurek et al., 2007; Langford et al., 2009).

Boundary conditions at different stages of pattern development

Although wind regime is the dominant control on crestline orientation, the impact of the variation within the wind regime decreases with time as the pattern evolves to achieve a gross bedform-normal orientation (Fig. 14A). At a juvenile stage of pattern development (i.e., high defect density and low dune volumes) the reconstitution time of a crestline is short and the pattern responds rapidly, reorienting to seasonal changes in the wind regime (Rubin and Ikeda, 1990). As the pattern develops, the reconstitution time of the dune pattern exceeds that of the cycle time of the wind regime and the impact of seasonal fluctuations in the wind regime on the crestline orientation is lessened (i.e., the

crest assumes its gross bedform-normal orientation).

Similarly, the impact of sediment supply decreases through time (Fig. 14B). At the onset of a pattern constructional event much of the available sediment supply is depleted quickly (Kocurek and Lancaster, 1999). As dune growth occurs, the contribution of the sediment supply proportionally decreases with an increase in dune size. With point- and line-sourced dune fields, the impact of sediment supply decreases as dunes migrate away from their source.

Typically the source-area of a dune field remains fixed over the course of a single constructional event, thus for simple patterns, the impact of a point, line or plane source-area geometry on pattern development remains constant through time (Fig. 14C). In constrast, as evident from Fig. 8, the impact of areal limits increases with time as a dune-field pattern

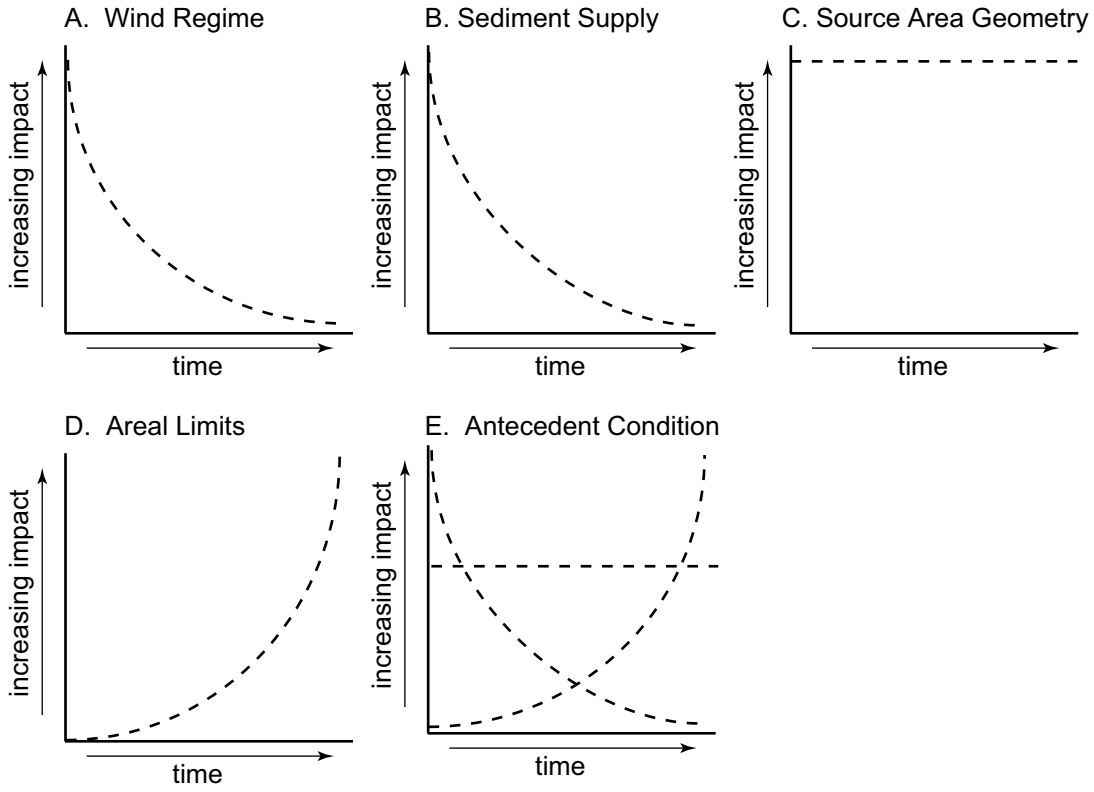

Figure 14. Schematic figures showing the changing impact of (A) wind regime, (B) sediment supply, (C) source-area geometry, (D) areal limits and (E) antecedent conditions over a pattern constructional event.

grows to occupy its geomorphic container (Fig. 14D).

Antecedent conditions is a broad category of boundary conditions. The impact of an antecedent condition may increase, decrease, fluctuate or remain the same over the course of pattern development depending on its type (Fig. 14E). For example, vegetation may act to disrupt an emerging pattern; however, if dune growth outpaces the vegetation growth, the impact of the vegetation on the pattern development will decline over time. The impact of a near-surface groundwater table, which decreases sediment availability, will remain the same as long as the water table is sufficiently high. Antecedent topography may influence a pattern over the course of pattern development, as with the White Sands example, or may have an increasing impact over time, as with the influence of relict linear-dune topography on the organization of an emergent star-dune pattern superimposed on the linear-dune pattern (Beveridge et al., 2006; Ewing et al., 2007).

Changing boundary conditions through time

The formation of complex dune-field patterns (i.e., multiple pattern constructional events) necessarily indicates temporally changing boundary conditions. In the simplest case, a new pattern is created superimposed on an older pattern with a change in wind regime. However, additional pattern complexity may arise with a change in source-area geometry or sediment supply, which becomes imprinted on the older pattern. The template of the older pattern may continue to impact the younger pattern as it develops or the signature of the older pattern may become subdued or erased, as with the relict dunes in the Algodones Dune Field (Derickson et al., 2008).

Conclusions

As a self-organized, pattern-forming system, aeolian dune-fields have been typically viewed in models in which the emergence and ordering of a pattern occurs through autogenic, dune-dune interactions (Werner, 1995; Werner and Kocurek, 1999).

Simulations, however, have not succeeded in capturing the richness of patterns observed in nature because much of this diversity arises from the influence of the boundary conditions within which the dune-field pattern formation occurs.

Two newly recognized boundary conditions presented here, source-area geometry and areal limits, demonstrate that within a given set of environmental conditions a characteristic dune-field pattern emerges that reflects boundary condition controls. Point- and line-sourced dune-field patterns show a signature of increasing spacing and crest length over distance, whereas plane-sourced patterns emerge equally across the dune field. The areal limit boundary condition arises from the spatial limits of the geomorphic container within which the pattern develops and acts to limit pattern evolution as the pattern grows to occupy its container.

The example of the interplay of boundary conditions at White Sands demonstrates clearly how pattern morphology may be used to interpret boundary conditions that might not otherwise be obvious. In this example, the changes in crest spacing across the dune field reflected subtle topographic changes that only became apparent with high-resolution topographic data. This indicates how dune-field patterns respond to and reflect changes in the external environment in a systematic manner and are not a simple product of the autogenic processes. Rather, it is the coupling of the internal processes and the external environment that give rise to diverse aeolian dune-field patterns imprinted on planetary surfaces. Recognizing these controls becomes important for decomposing patterns to reconstruct past dune building events and climatic change, and for modeling efforts aimed at simulating the evolution of natural dune-field patterns.

Chapter 2: Aeolian-dune interactions and dune-field pattern formation: White Sands New Mexico

ABSTRACT

Pattern formation is a fundamental aspect of self-organization in fields of bedforms. Time-series aerial photographs and airborne LiDAR show that fully developed, crescentic aeolian dunes at White Sands, New Mexico, interact and the dune pattern organizes in systematically similar ways as wind ripples and subaqueous dunes and ripples. Documented interactions include: (1) merging, (2) lateral linking, (3) defect repulsion, (4) bedform repulsion, (5) off-center collision, (6) defect creation, and (7) dune splitting. Merging and lateral linking are constructive interactions that give rise to a more organized pattern. Defect creation and bedform splitting are regenerative interactions that push the system to a more disorganized state. Defect/bedform repulsion and off-center collision cause significant pattern change, but appear to be neutral in overall pattern development. Measurements of pattern parameters (number of dunes, crest length, defect density, crest spacing, dune height), dune migration rates, and the type and frequency of dune interactions within a 3,500 m box transect from the upwind margin to the core of the dune field show that most pattern organization occurs within the upwind field. Upwind dominance by constructive interactions yields to neutral and regenerative interactions in the field center. This spatial change reflects upwind line-source and sediment-availability boundary conditions arising from antecedent paleo-lake topography. Pattern evolution is most strongly coupled to the pattern parameters of dune spacing and defect density, such that spatially or temporally the frequency of bedform interactions decreases as the dunes become farther apart and have fewer defects.

Introduction

Aeolian dune fields form some of the most striking patterns in nature. These patterns represent both the external environmental conditions under which the fields evolved and the internal dune dynamics of self-organization. Dune-field self-organization implies that pattern development occurs as the result of dune-dune interactions (Werner, 1995). Interpreting the climatic and geomorphic histories of these landscapes and the mechanisms by which the patterns develop requires separating the signatures of the internal system dynamics from the environmental controls.

Although air-sand interactions are a well-recognized grain-scale internal dynamic, dune-dune interactions are a relatively unexplored dune-scale internal dynamic of aeolian systems. Dune interactions are the collisions and exchange of sediment between dunes as they migrate. Although aeolian dune interactions have been well documented in field studies of barchan dunes (Elbelrhiti et al., 2005; 2008) and in the early stages of dune-field formation (Kocurek et al., 1992), in large measure, our impression of dune interactions comes largely from observations of wind ripples (Sharp, 1963; Anderson, 1990; Landry and Werner, 1994), subaqueous dunes and ripples (Allen, 1973; Coleman and Melville, 1994), and models of ripple and dune evolution (Forrest and Haff, 1992; Anderson and Bunas, 1993; Nishimori and Ouchi, 1993; Tufillaro, 1993; Landry and Werner, 1994; Werner, 1995; Werner and Kocurek, 1999; Katsuki et al., 2005) (Fig. 15).

The external environmental conditions under which dune interactions occur and the pattern evolves are boundary conditions of the system (Ewing and Kocurek, in press). Although some boundary conditions such as wind directionality are well recognized controls on the type of dune-field pattern (Rubin and Hunter, 1987; Werner and Kocurek, 1997), others such the areal limit of a dune field and the geometry of the sediment source-area, are only now being explored (Ewing and Kocurek, in press).

This paper demonstrates for the first time that fully developed, aeolian crescentic

dunes behave and interact in many of the same ways as wind ripples, and subaqueous ripples and dunes. Seven different types of interactions, which have been previously documented in wind ripples, or subaqueous ripples and dunes, are documented at White Sand Dune Field in New Mexico using aerial photographs and airborne LiDAR. The type and frequency of interactions, as measured along a transect within the dune field, demonstrates the relationship between the dune interactions, the boundary conditions and changes in field-scale pattern. The paper concludes that: (1) bedform interactions are similar across scales (i.e., ripples and dunes) and environments (i.e., air and water), (2) much of the pattern morphology arises from the signature of the dynamics of interacting dunes, and (3) boundary conditions affect the type and frequency of interactions, which gives rise to changes in the field-scale pattern.

Methods

Dune interactions at the White Sands Dune Field were identified and studied using digitally scanned aerial photographs from 1963 and 1985, Digital Orthophoto Quarter Quadrangles (DOQQs) from 1996, 2003, 2005 (1 m/pixel spatial resolution), and a Digital Elevation Model (DEM) (1 m/pixel spatial resolution) generated from a June 2007 airborne LiDAR survey. The 1963 and 1985 images, which were provided in digital format from White Sands National Monument, were geo-referenced to the 1996 and 2005 DOQQs acquired from the New Mexico Resource Geographic Information System Program (http://rgis.unm.edu/intro.cfm). Large pedestal dunes, which are permanent vegetated structures within the active dune field and are apparent in all images, were used as ground-control points and a first-order polynomial transformation was used to correct the 1963 and 1985 imagery. Owing to the low resolution of the 1963 and 1985 imagery the transformation resulted in relatively high RMS error values. Migration rates (~3 m/yr), however, measured from the 1963 and 1985 images match well with rates measured from the 1996 and 2005

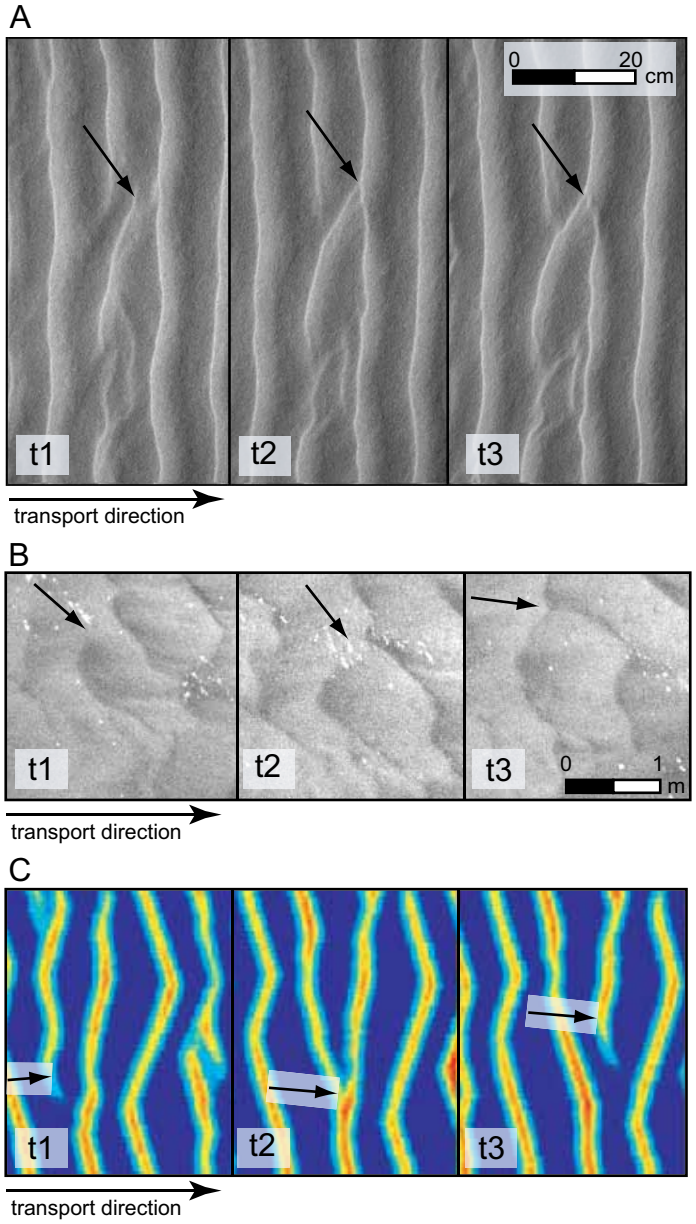

Figure 15. Interacting bedforms. (A) Translation of a wind ripple defect through a wind ripple field by defect repulsion interaction (See Fig. 20 and text for discussion). Transport direction is from left to right and the lighting is from the right. At (t1) the ripple termination migrates on to the stoss slope of the downwind ripple. At (t2) the defect attaches to the downwind ripple crestline forming a Y-junction, and at (t3) the downwind crestline is broken, a new ripple defect forms and begins migrating downwind. (B) Defect repulsion in subaqueous dunes in the North Loup River, Nebraska. The subaqueous dunes show the same behavior as the wind ripples. Images courtesy of David Mohrig. (C) Cellular automaton model showing defect repulsion described in the wind ripples in (A). Model images courtesy Erin Eastwood.

imagery and previously reported values from field studies (McKee, 1966; Fryberger, 2000; Kocurek et al., 2007), indicating that the geo-rectification was sufficient.

Dune interactions were identified through visual inspection of the imagery data in Geographic Informations System (GIS) software. Repeated surveys across the coverage area (~50 km^2) and between the time-series imagery revealed the systematic dune behavior. Time-series images of the different types of dune interactions are presented here as results. Within each image series, the frame of the image remains static (i.e., only the dunes are moving within the frame) and the scale of the images are the same. North is to the top of each image and the dune migration direction is generally to the ENE.

In order to quantitatively characterize the dune interactions, dune crestlines were manually digitized using GIS software following the methods of Ewing et al. (2006). Crestlines were chosen as the morphological elements by which to characterize the interactions because crestlines are an emergent, large-scale, slow-evolving property of the system from which measurements of the pattern-scale variables crest length, crest spacing and defect density can be made (Werner and Kocurek, 1999; Werner, 2003; Ewing et al., 2006).

In order to assess the interplay between the boundary conditions and dune interactions, every crestline along a 500 m x 3,500 m box transect, oriented from the upwind margin of the dune field to the center of the field, was digitized from the 1985, 1996, 2003, 2005, and 2007 data. Each crestline, at each time step along the transect, was inspected to determine if the crestline was interacting with another crestline. The type of interaction was recorded after the interaction was completed. In order to capture the spatial variation in the type and frequency of interactions, the transect was split into seven 500 m x 500 m boxes. The number of dunes, total dune crest length, defect density (# defect pairs/crest length), and crest spacing were calculated for each box. Defects are breaks or imperfections in the bedform field-scale pattern (Mabbutt and Wooding, 1983; Werner and Kocurek, 1997) and

tangibly represent the ends or terminations of ripples and dunes that migrate faster than the main bedform. The ends of crestlines at the box edges (i.e., edge defects) were not calculated into the defect density. Average spacing (λ) between crestlines was measured as

$\lambda = A/L$,

where A is the total area of the box (250,000 m^2) and L is the total measured crestline length within the box. Dune height was measured every 25 m along each crestline from the 2007 LiDAR data. Average dune migration rates were calculated every 25 m along each crestline from the difference between the 1996 and the 2007 data. The migration distance was measured in the resultant transport direction (60°) (Fryberger, 2000), from the position of the 1996 crestline to the intersection of the 2007 crestline.

AEOLIAN DUNE INTERACTIONS

White Sands Dune Field, New Mexico

The White Sands Dune Field occupies ~400 km^2 of the Tularosa Basin in New Mexico (Fig. 16). Initiation of the gypsum-sand dune field is thought to have occurred with the onset of regional aridity during the mid-Holocene and progressed through the step-wise deflation of previously stored pluvial and playa Pleistocene Lake Otero sediments (Langford, 2003; Kocurek et al., 2007). Erosional shorelines created by a falling water table acted as line sources for the input of gypsum sand into the dune field (Ewing and Kocurek, in press). Today, sediment input derives primarily from the deflation of gypsum precipitated in modern playas, which are situated to the southwest of the dune field.

Morphologically, the dunes in the core of White Sands are characterized as continuous, sinuous, crescentic ridges and barchanoid dunes, which average 8-12 m in height. Small, isolated barchan dunes occur on the deflationary plain, Alkali Flat, to the west of the main dune field. The eastern and southern margins of the dune field consist of vegetated parabolic dunes. Dune migration rates range from 1-7 m/yr and are typically

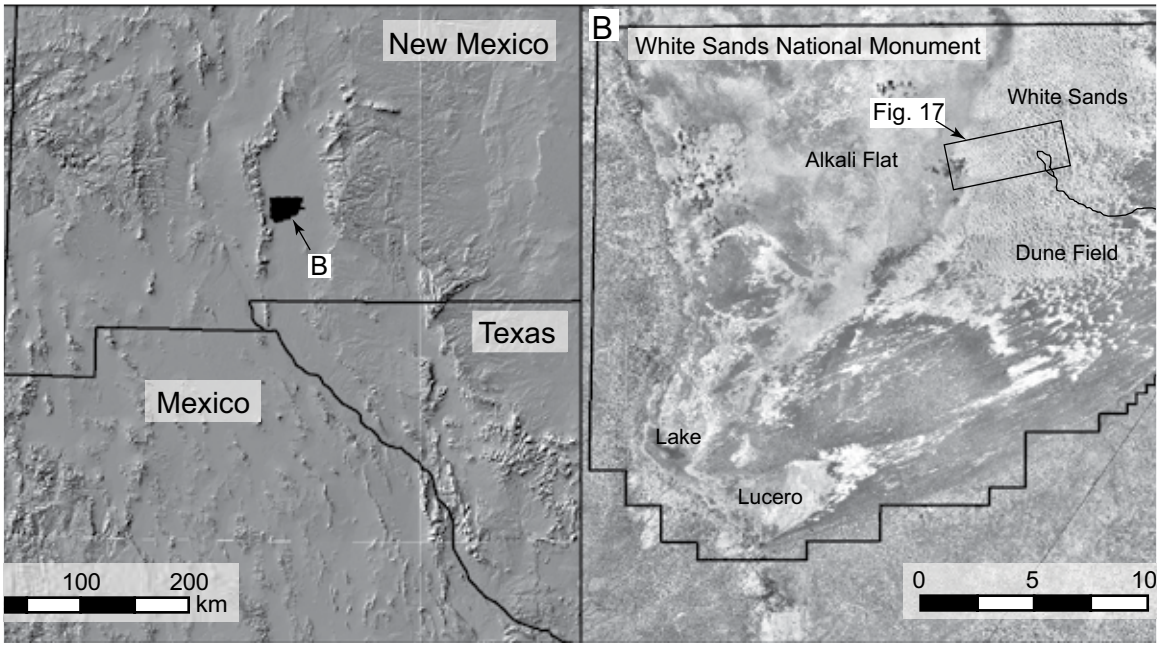

Figure 16. (A) Location map of White Sands National Monument. (B) Study area within the White Sands Dune Field.

faster at the upwind, western margin. At the pattern-scale, the dune crestlines are oriented NNW (345°), have an average length of 247 m and average spacing of 136 m (Ewing et al., 2006). The dune-field defect density is 0.0039.

The dune-field pattern at White Sands is significantly influenced by a strong seasonal wind regime (Kocurek et al., 2007). The wind regime at White Sands is dominated by winter-spring winds from the southwest and west (Fig. 17). A subordinate, but important, component of the wind regime occurs with fall-winter winds from the north and northwest. The dominant crestline orientation (345°) of the crescentic ridges is borderline transverse (75°) to the resultant wind vector of 60° (Fryberger, 2000; Ewing et al., 2006) in the classification of Hunter et al. (1983).

The pattern is also strongly influenced by the line source-area geometry. The line source-area geometry creates a spatial change in the pattern in which crest spacing increases in the dune migration direction away from the upwind source area (Ewing and Kocurek, in

press). Dunes originating at the upwind margin of the dune field are smaller, migrate faster, and, owing to their high defect density, are more susceptible to reorientation by the northerly component of the wind regime (c.f., Werner and Kocurek, 1997). The resulting pattern at the upwind margin is that of more irregularly oriented and closely spaced crestlines, which form a network-type pattern. The pattern becomes more organized toward the center of the dune field where crestlines are more widely spaced and have a fewer number of defects.

Classification of types of dune interactions

From ripples and dunes, in air and water, eleven types of bedform interactions have thus far been identified (see review by Kocurek et al., in press). These interactions can be viewed as forming a panoply of whole bedform, defect and remote interactions, which range from constructive to regenerative in terms of pattern development. Whole bedform interactions occur as the main bodies of migrating bedforms approach each other in the streamwise direction. Defect interactions encompass dune behavior in which the defect is the primary interacting element. Remote behavior occurs with the exchange of sediment from dune to dune without the collision between the main bodies or defect of the dunes.

Constructive interactions are those that yield fewer numbers of dunes than are interacting and change the field-scale pattern toward fewer, larger, more widely spaced dunes with longer crestlines. Regenerative interactions are those that yield a greater number of dunes than are interacting. In terms of the pattern variables, regenerative interactions result in a decrease in spacing and dune-crest length, and an increase in defect density. Neutral interactions are those that yield the same number of dunes as are interacting (i.e., the status quo of the number of dunes in the field is maintained). Unlike constructive and regenerative interactions, neutral interactions do not clearly change the pattern-scale variables (i.e., spacing, crest length or defect density), although some may have constructive or regenerative attributes (c.f., Landry and Werner, 1994; Werner and Kocurek, 1999).

Type examples of seven dune interactions within the crescentic dunes at White Sands were identified and classified as pattern constructive, neutral or regenerative. Of the seven interactions, merging, lateral linking, and off-center collision had been previously documented in aeolian dunes (Kocurek et al., 1992; Elbelrhiti et al., 2005). Bedform repulsion, defect repulsion, splitting and defect creation are all newly recognized as aeolian dune interactions in this study, although these have been documented in either wind ripples or subaqueous ripples and dunes (Allen, 1973; Landry and Werner, 1994; Endo et al., 2004). Although specific examples are used for each type of interaction identified, these interactions are implied throughout the dune field by characteristic morphologies imparted to the pattern by the interactions. From a single snapshot of the central portion of the White Sands Dune Field all the interactions and the stages of interactions described here can be

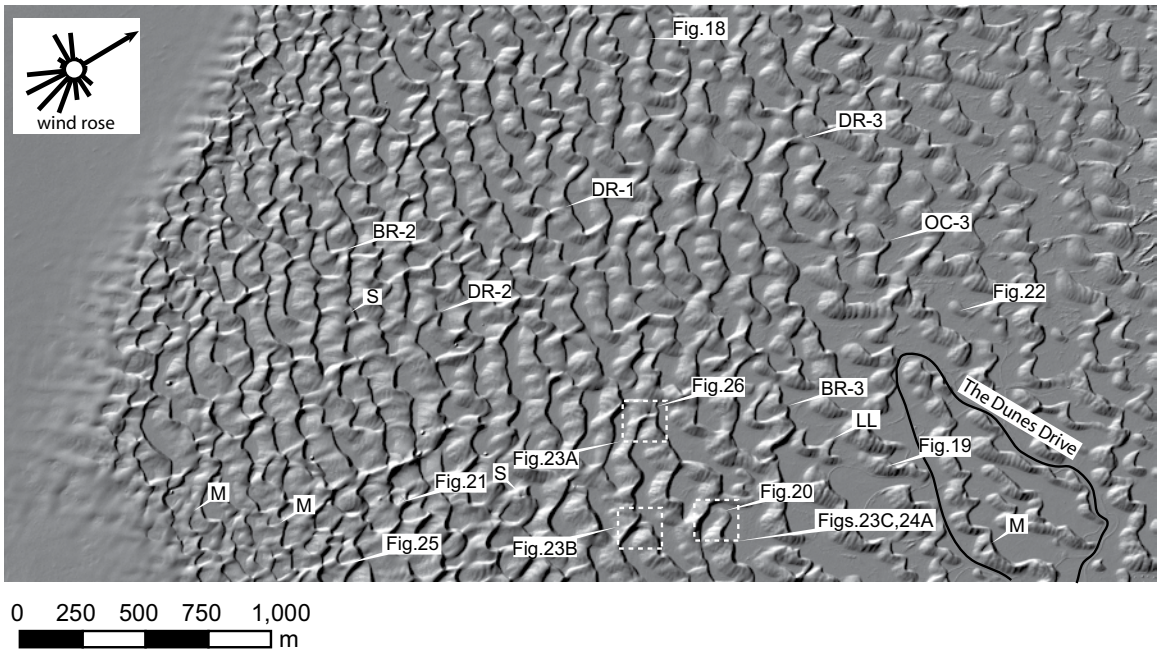

Figure 17. LiDAR image of the study area shown in Fig. 16B. The locations of the Figs. 18-26 are shown on the image. Letters and letters with hyphenated numbers refer to types of dune interactions. The hyphenated numbers following a letter indicating the stage of the interaction with 1 being the earliest and 3 being the latest. M= merging; S= splitting, LL= lateral linking; BR= bedform repulsion; DR= defect repulsion; OC= off-center collision. Wind data from Holloman Airforce Base (Fryberger, 2000).

indentified from the dune morphology (Fig. 17), as will be illustrated in detail below.

Constructive interactions

At White Sands lateral linking and merging are the dominant constructive interactions. Lateral linking can be viewed as a type of lateral defect-merger, which increases crest length by nearly the sum of the crestline lengths of the interacting dunes and decreases the number of interacting dunes by half. Merging ("absorption" in Endo and Taniguchi, 2004; "coalescence" in Katsuki et al., 2005; Herrmann, 2006), occurs as a smaller dune collides and combines with a larger dune.

Fig. 18A-D shows the evolution of lateral linking over 44 years at White Sands. In Fig. 18A the north-facing defect of dune 1 is beginning to link with the south-facing defect of dune 2. The lateral merging continues through 1985 and by 1996 (Fig. 18C) the crestlines are linked together. By 2007 the lateral linking is complete and little trace of the interaction remains (Fig. 18D).

Fig. 19A-C shows a sequence of merging interactions occurring over 33 years. In 1963 (Fig. 19A) dune 2 is colliding with dune 3, which is colliding with dune 4. By 1985 (Fig. 19B) dune 2 and dune 3 have merged to one dune, which is colliding with dune 4. Dune 1 has shed part of its crestline, which has become a separate barchan dune, dune 1', which is beginning to collide with dune 2+3. By 1996 (Fig. 19C), the collision and merging of dune 2+3 with dune 4 has destabilized dune 4, which splits and becomes, dune 2+3+4 and 4'. Dune 1' has significantly decreased in size by 1996 (Fig. 19C).

Lateral-linking has been previously recognized in the early stages of aeolian dune-field formation (Kocurek et al., 1992) and in wind-ripple development (Sharp, 1963; Landry and Werner, 1994). Merging has been recognized in aeolian dunes (Kocurek et al., 1992), wind ripples (Sharp, 1963; Landry and Werner, 1994) and subaqueous dunes (Allen, 1973; Coleman and Melville, 1994). A complete merging interaction, in which the dune

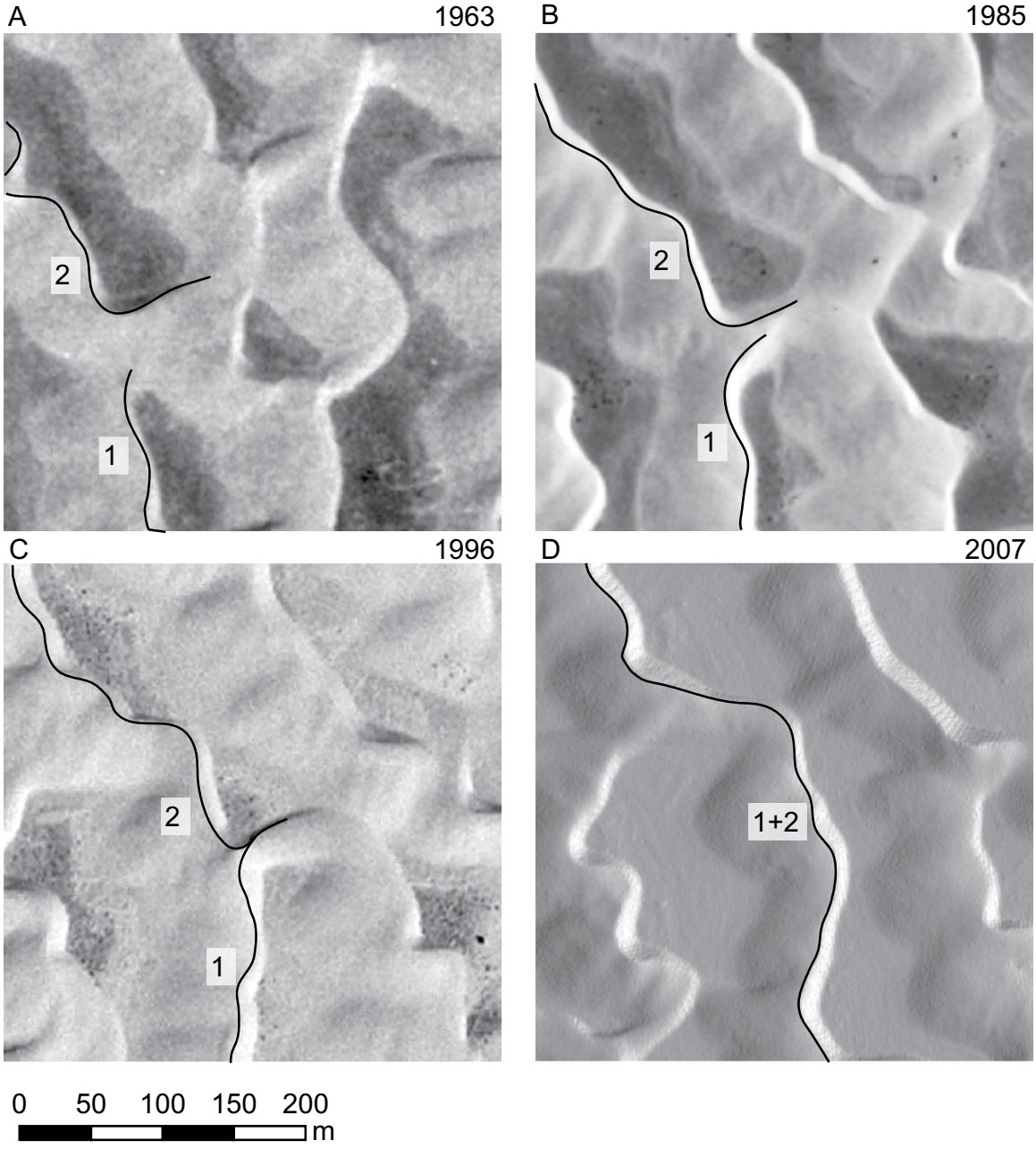

Figure 18. (A) 1963, (B) 1985 and (C) 1996 aerial photographs and (D) 2007 airborne LiDAR imagery showing a lateral linking interaction (see text for discussion). In Figs. 18-22 and 25-26 the interacting dunes are numbered. Dunes that combine over time are indicated by a plus sign (+). A prime sign (‘) following a dune number indicates a newly created portion of a crestline that split.

volume increases by the sum of the interacting dunes and the number of interacting dunes decreases by half, appears to occur only when the upwind dune is significantly smaller

than the downwind dune (Schwammle and Herrmann, 2003; Endo and Taniguchi, 2004; Katsuki et al., 2005; Herrmann, 2006; Elbelrhiti et al., 2008; Diniega et al., in press). Non-coaxial collisions and collisions between dunes of near equal size impart instabilities into the interaction such that it becomes neutral, as with off-center collisions (see below), or regenerative, as with calving (Hersen, 2005; Elbelrhiti et al., 2005, 2008) or defect creation (see Fig. 19C, 25A). The absolute and relative size between merging dunes, which

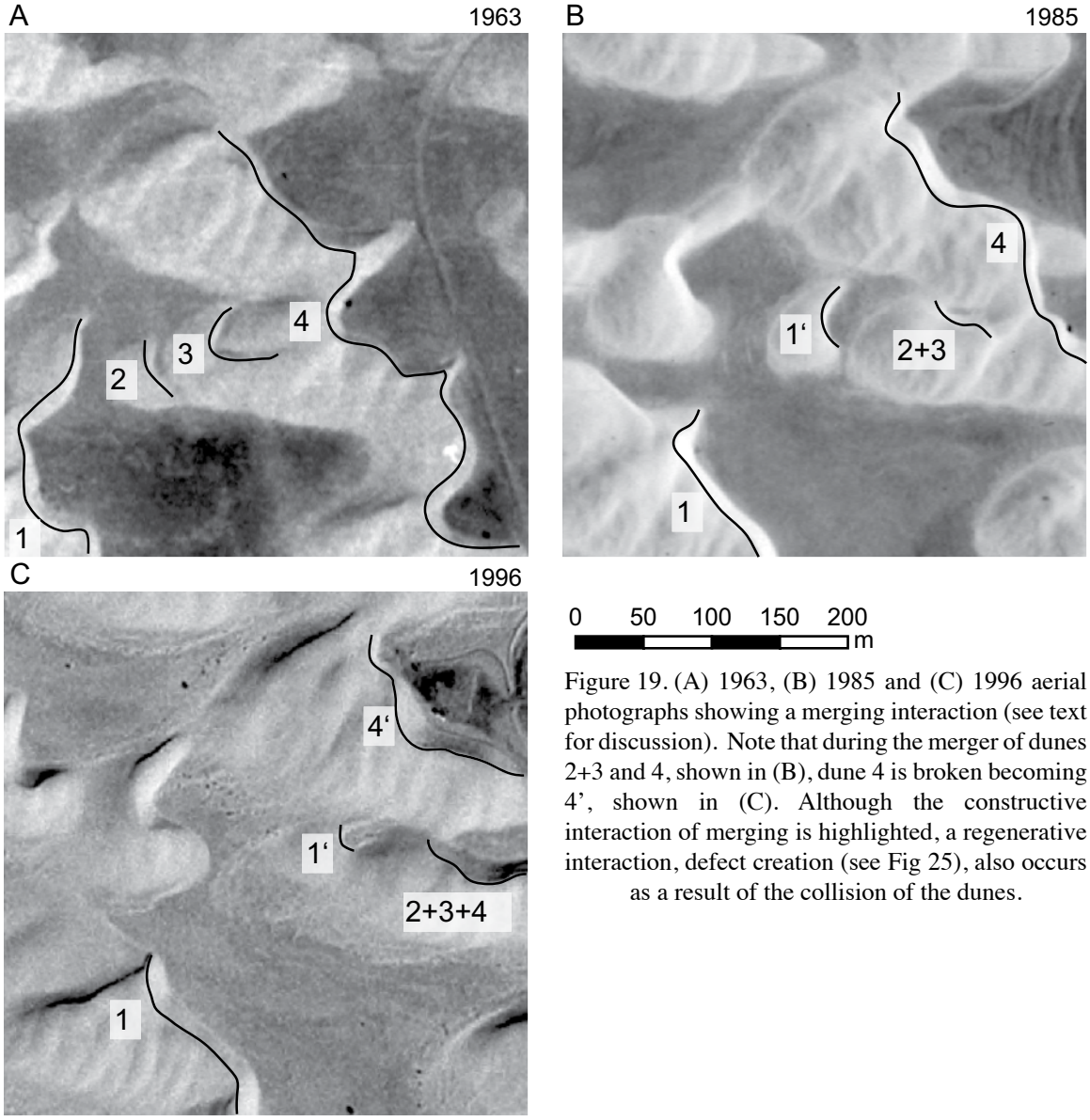

Figure 19. (A) 1963, (B) 1985 and (C) 1996 aerial photographs showing a merging interaction (see text for discussion). Note that during the merger of dunes 2+3 and 4, shown in (B), dune 4 is broken becoming 4', shown in (C). Although the constructive interaction of merging is highlighted, a regenerative interaction, defect creation (see Fig 25), also occurs as a result of the collision of the dunes.

determines whether a merger will occur, is poorly constrained.

In terms of pattern development, the lateral linking process creates a convexity along the crestline during the stage when the two defects coalesce (Fig. 18B-C). The morphologic characteristics of this dynamic are numerous throughout the White Sands Dune Field, implying that it is lateral linking that gives rise to much of the crescentic sinuous pattern (Fig. 17). Although merging is apparent in the dune field (Fig. 17), the majority of merging interactions likely occurs at the onset of the dune-field formation and diminishes as the dunes grow more organized (Kocurek et al., 1992). Additionally, dunes which may be merging, but are smaller than the spatial resolution of the data, cannot be accounted for.

Neutral interactions

Defect repulsion, bedform repulsion, and off-center collision are documented here as neutral interactions at White Sands. Defect repulsion occurs as a migrating defect attaches to a downwind crestline, forming a Y-junction. The upwind defect captures the downwind crestline and new defect is created at the point of intersection, which detaches from the Y-junction and migrates to the next downwind crestline. Defects propagate through the field via this interaction. Bedform repulsion is similar in behavior to defect repulsion, but involves an entire dune or two defects rather than a single dune termination. During this interaction, an upwind dune approaches a downwind dune, but does not merge. Rather, the downwind dune diminishes in size and migrates away from the upwind dune. Off-center collisions are non-coaxial collision between dunes, during which a smaller dune is ejected from the downwind dune.

Fig. 20A-D shows defect repulsion occurring between aeolian dunes over 44 years. In the 1963 image (Fig. 20A) the north-facing termination of dune 1 (marked by an arrow) is situated near the crestline on the stoss slope of dune 2, which forms a Y-junction. By

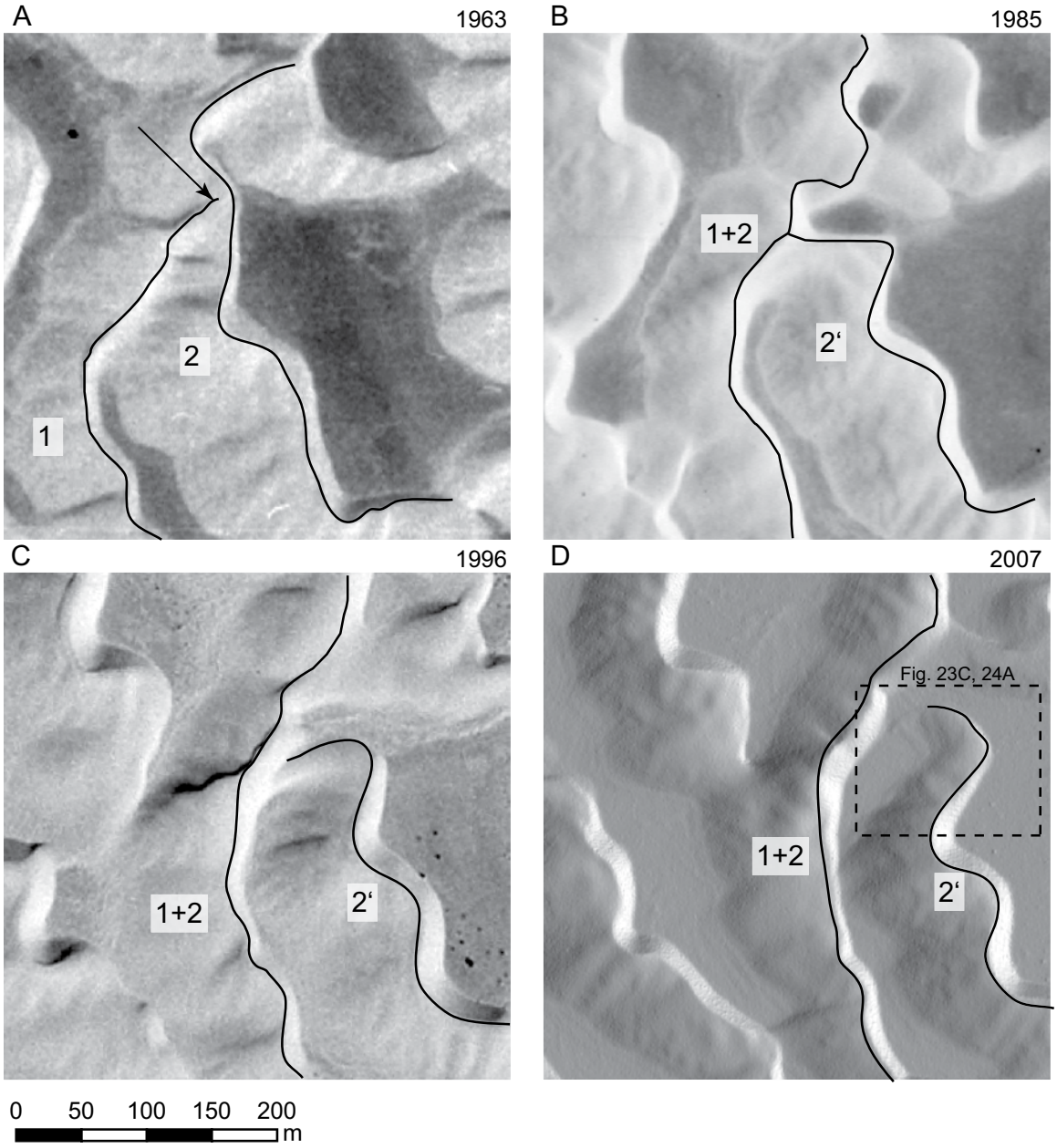

Figure 20. (A) 1963, (B) 1985 and (C) 1996 aerial photographs and (D) 2007 airborne LiDAR imagery showing defect repulsion (see text for discussion). The dashed box in 6D, refers to location of Fig. 23C and 24A.

1985 (Fig. 20B) the north-facing defect of dune 1 has captured the crestline of dune 2, becoming dune 1+2. The crestline of the new downwind dune, dune 2', has formed a large, downwind, convex curvature at the point of attachment. By 1996 (Fig. 20C), the convex-curved portion of dune 2' has detached from dune 1+2 at the initial point of attachment and

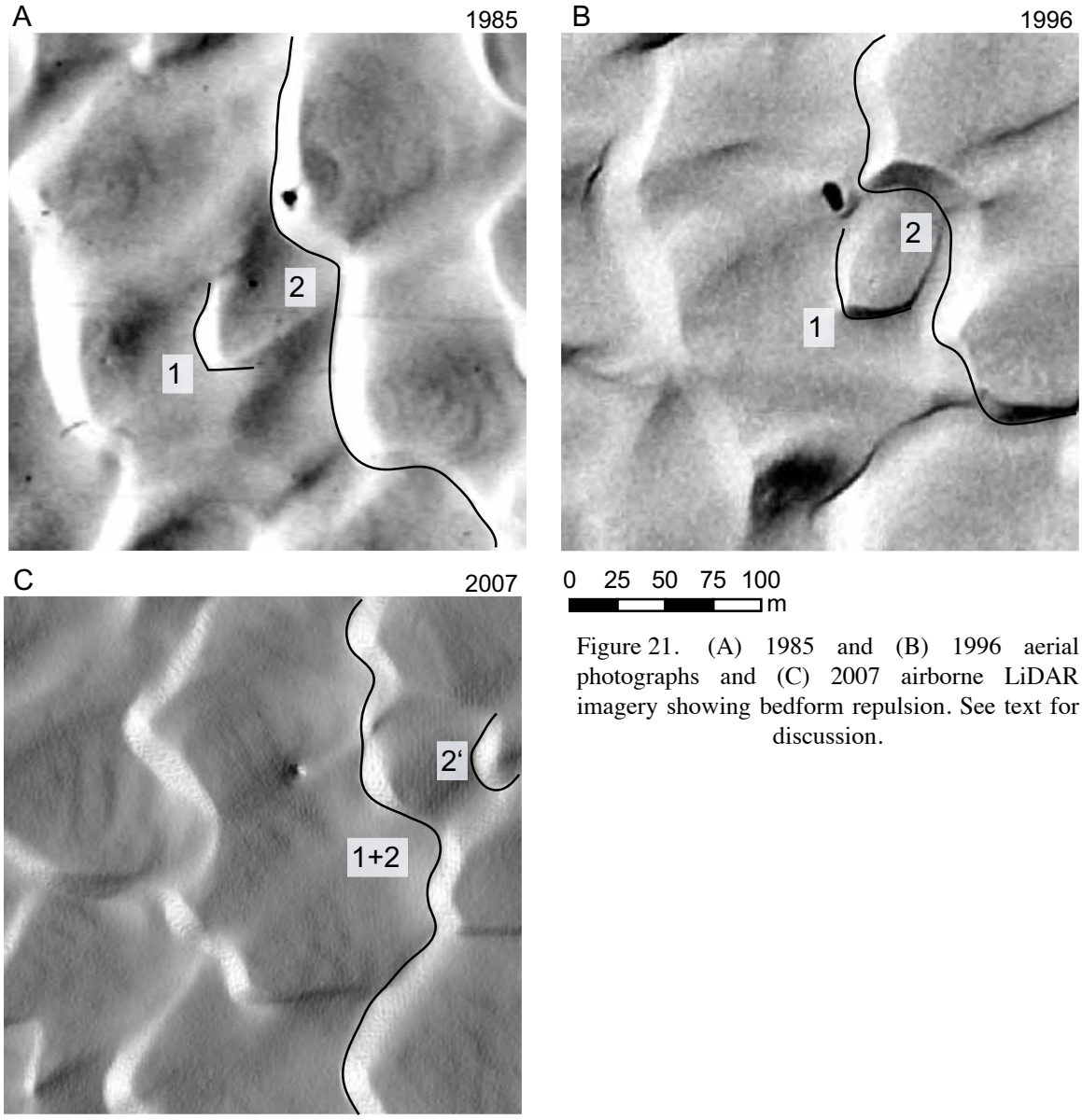

Figure 21. (A) 1985 and (B) 1996 aerial photographs and (C) 2007 airborne LiDAR imagery showing bedform repulsion. See text for discussion.

is now the north-facing defect of dune 2'. In 2007 (Fig. 20D) the north-facing defect of dune 2' is fully detached from dune 1+2 and freely migrating downwind.

Bedform repulsion between aeolian dunes is shown in Fig. 21A-D. In this time-series of photographs bedform repulsion occurs between dune 1 and dune 2 over a period of 22 years. In Fig. 21A (1985), a barchan dune, dune 1, is approaching a larger crescentic dune, dune 2. As dune 1 approaches dune 2, the crestline of dune 2 is beginning to deform.

In 1996 (Fig. 21B), a large downwind convexity has developed in dune 2 in response to the approach of dune 1. By 2007 (Fig. 21C), the crestlines of dune 1 and dune 2 have combined into dune 1+2 and the convexity of dune 2 has detached and has begun migrating downwind as a small barchan dune, dune 2'. Little trace of the interaction is visible in crestline 1+2.

Fig. 22A-C shows an off-center collision between two crescentic dunes occurring

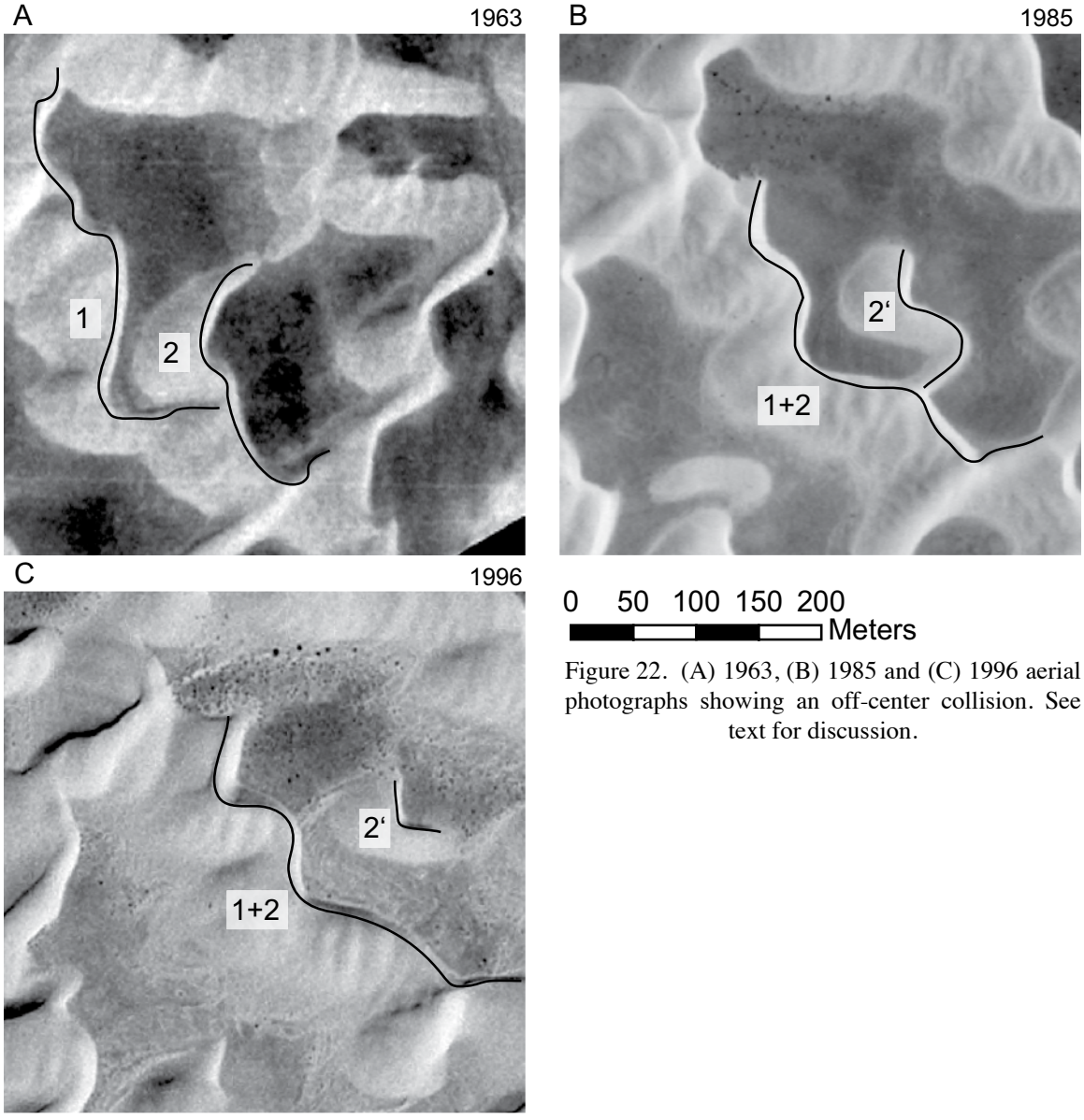

Figure 22. (A) 1963, (B) 1985 and (C) 1996 aerial photographs showing an off-center collision. See text for discussion.

over 33 years, which results in the ejection of a single barchan dune. This example appears to be along the transition from off-center collisions to defect repulsions, however, because a single barchan dune is ejected, this interaction most closely resembles examples of off-center collisions (c.f., Hersen, 2005). In 1963 (Fig. 22A), the south termination of dune 1 has migrated upon the stoss slope of dune 2. Dune 2 has begun to deform at the point of intersection and form into a barchanoid shape. By 1985 (Fig. 22B), dune 1 and dune 2 have completely joined forming dune 1+2 and the south-facing defect of dune 2 has mostly detached and become dune 2'. By 1996 dune 2' has separated from dune 1+2 and is freely migrating downwind as a barchan dune.

Defect repulsion is widely recognized in wind ripples (Fig. 15A) (Anderson and McDonald, 1990), cellular automaton models of wind ripples and dunes (Fig. 15C) (Landry and Werner, 1994; Werner, 1995) and apparently occurs in subaqueous dunes (Fig. 15B). Bedform repulsion has been observed in wind ripples (Landry and Werner, 1994) and was proposed, but not directly observed, for aeolian barchan dunes (e.g., soliton model (Schwammle and Herrmann, 2003) and "ejection" (Katsuki et al., 2005)). Similar behaviors have been reported in crescentic fluvial dunes (Venditti et al., 2005). Off-center collision has been described in barchan-shaped ripples created in a laboratory flume (Hersen, 2005; Katsuki et al., 2005) and between barchan dunes in the field (Elbelrhiti et al., 2008). Off-center collisions should decrease as the dunes grow in crest length and the probability of whole dune collisions decreases. Off-center collisions may be thought of as the barchan dune end-member of defect repulsion.

Defect repulsion, bedform repulsion, and off-center collision interactions go through morphologically distinct stages during which the dune topography is deformed and the dune crestlines are reorganized. Broadly, these stages reflect the early, middle and late phases of the interaction (Fig. 23A-C). The early stage is the response or deformation of the crestlines as two dunes approach each other. During the early stage, an upwind

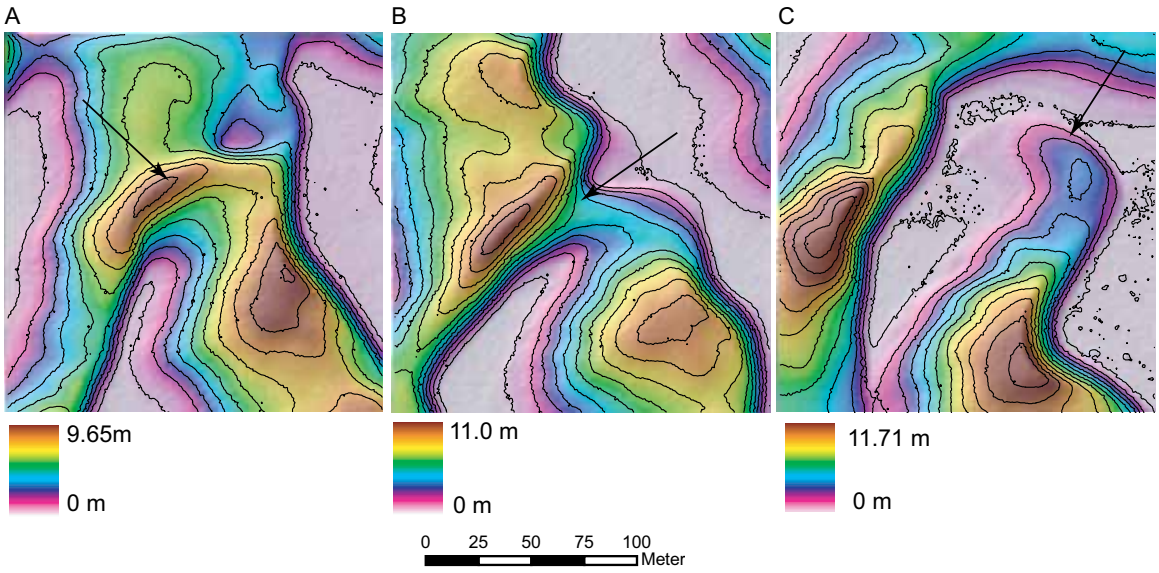

Figure 23. Contoured DEM showing three stages of defect repulsion. Defect repulsion is described in the text and shown in Fig. 1 and Fig. 20A-D. Each panel is from a 2007 LiDAR derived DEM and represents a stage of a defect repulsion interaction recognizable by the morphology of the pattern. Fig. 17 shows the location of A-C within the White Sands Dune Field. (A) An upwind dune defect (black arrow) is attached to the stoss slope of a downwind dune. (B) The downwind dune is in process of separating from the upwind dune and is separating at the point of attachment (black arrow) of the upwind defect. (C) The downwind dune is fully detached and the newly formed defect (black arrow) is migrating downwind (see also Fig. 23A).

dune defect migrates onto the stoss slope of the downwind dune. Near the attachment of the defect to the dune, the crestline of the downwind dune begins to deform into a streamwise-convex nose (Fig. 20A, 21A, 22A, 23A). Reorganization of the crestlines occurs during the middle stage. During the middle stage, the upwind defect "welds" itself on to the downwind crestline at the point of intersection (Fig. 20B, 20C, 21B, 22B, 23B). Crestlines reorganize such that the upwind crestline becomes the larger primary crest, the downwind dune becomes smaller near the point of intersection and the convex nose becomes exaggerated and sharper in the downwind direction. The portion of the downwind crest that remains attached to the upwind dune is the initiation of the new, trailing defect (discussed below) of the downwind crestline. A return toward a steady-state form occurs in the late stages. During the late stage, the main bodies of the interacting dunes fully separate and the new, downwind dune defect detaches from the upwind dune and begins to

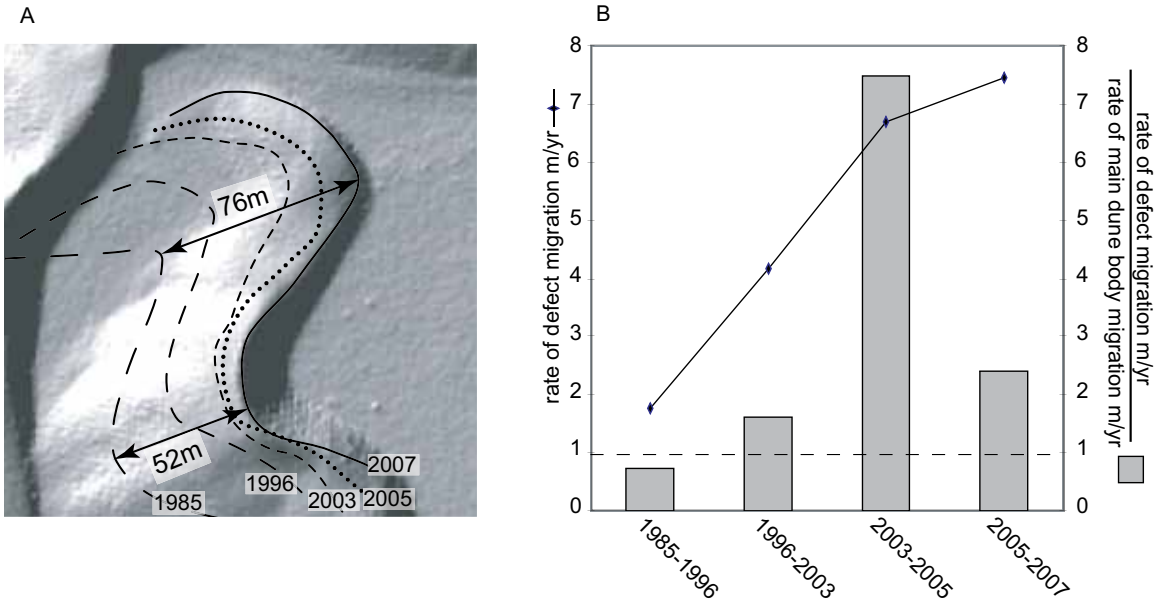

Figure 24. (A) DEM hillshade of a trailing defect. See text for discussion of trailing defects. Lighting is from the top left of the image. The defect emerged from the defect repulsion interaction shown in Fig. 20A-D. The lines represent the location of the dune crestline in 1985, 1996, 2003, 2005, and in 2007. The double-sided arrows show the total crestline migration at the defect (top arrow) and at the point of maximum concave curvature and height of the main dune (bottom arrow). (B) Plot showing the rate of defect migration and the migration rate of the main body of the dune. The left Y-axis shows the rate of defect migration and is shown as a line on the plot. The right Y-axis shows the ratio of defect migration to the main dune migration and is plotted as gray bars. The dashed line is associated with the right Y-axis and shows the point at which the main dune and the defect are migrating at the same rate.

swing around the main body of the dune (Fig. 20D, 21C, 22C, 23C). At a wider scale, the entirety of these interactions introduces sinuosity along the interacting crestlines. Each of these interactions at each stage of development is recognizable throughout the White Sands Dune Field (Fig. 17).

Trailing defects are one of the most distinctive pattern morphologies that emerge from neutral interactions and appear throughout the White Sands Dune Field (Fig. 17). Trailing defects are most visible in the central portion of the field, where dunes are more widely spaced, and most obscured in the upwind margin, where the dunes are more closely spaced. The term “trailing defect” is applied to this form of defect because the defect lags behind the main body of dune. This morphology is unlike typical defects, such as the horns of barchan dunes, which point downwind ahead of the main dune body (Werner and

Kocurek, 1997). Fig. 24A shows the migration of the trailing defect that emerged from the defect repulsion shown in Fig. 20A-D. Whereas the main body of the bedform migrated 2.4 m/yr over the 22 year period, the defect migrated 3.4 m/yr. The rate of defect migration increased beyond that of the main dune body after the defect became fully detached from the upwind dune in 1996 and the rate continued to increase as the defect swung around the dune main body (Fig. 24B). The ratio of the rate of defect migration to the migration of the main body of the dune increased from 1985 to 2005 and decreased as the defect migrates downwind of the main body of the dune in 2007.

Regenerative interactions

Defect creation and a type of crestline splitting are documented here as regenerative interactions at White Sand Dune Field. Defect creation is the simple break-up of one dune into two or more smaller dunes. Dune splitting refers to the emergence of a new dune on the stoss slope of a host dune that grows to nearly the size of the host dune. Fig. 25A-B shows

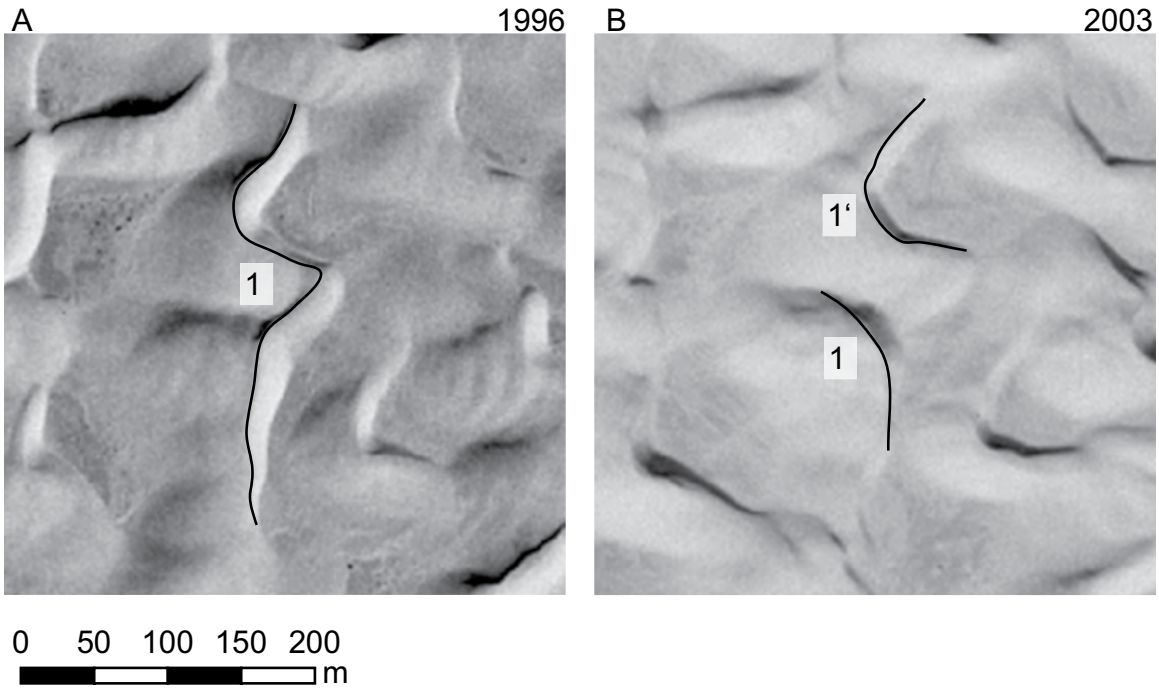

Figure 25. (A) 1996 and (B) 2003 aerial photographs showing defect creation. See text for discussion.

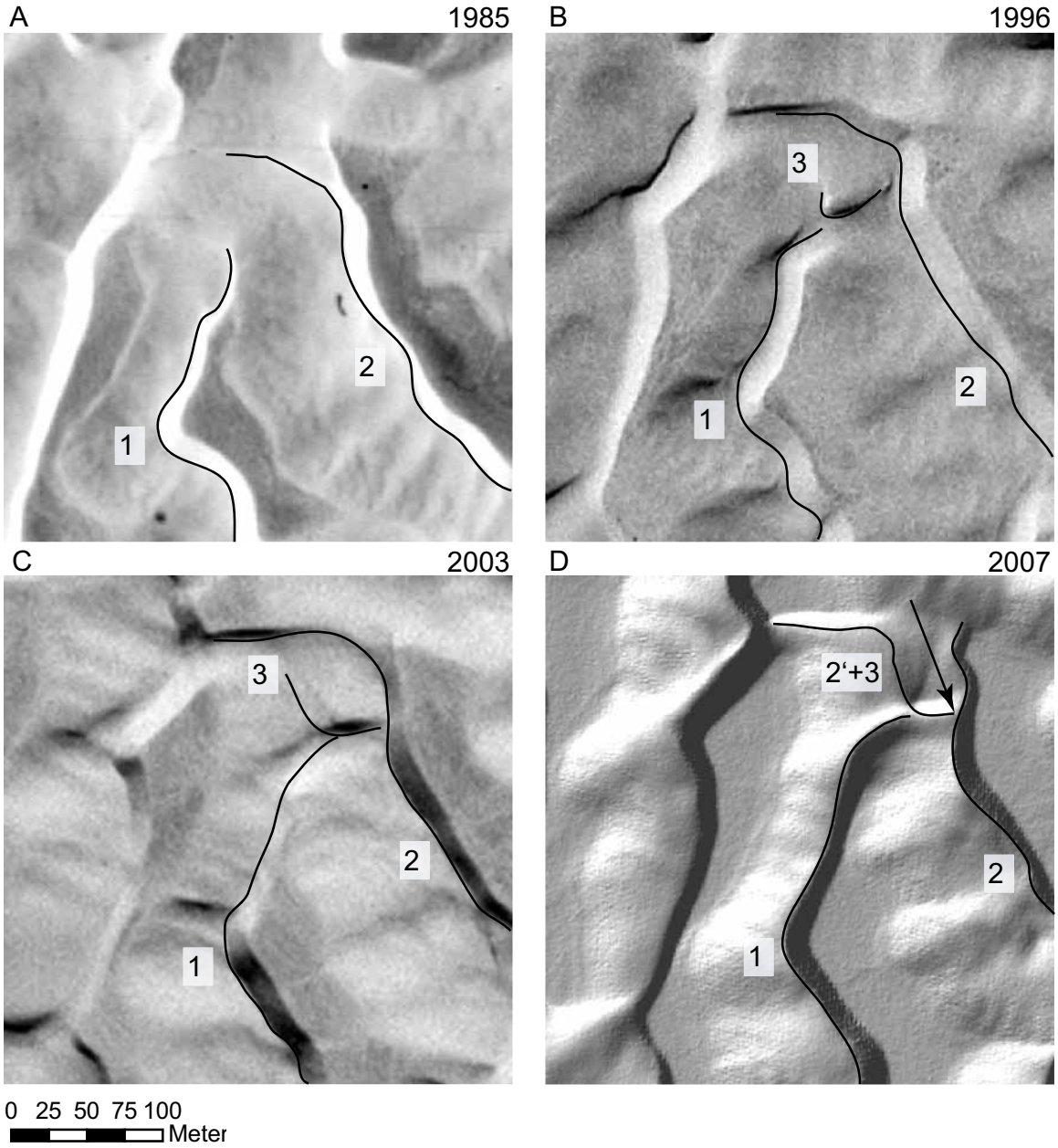

Figure 26. (A) 1985, (B) 1996 and (C) 2003 aerial photographs and (D) 2007 airborne LiDAR imagery showing dune splitting. Note the emergence of the dune 3 at the intersection of the north facing defect of dune 1 and the stoss slope of dune 2. See text for further discussion.

the simple break-up of a crescentic dune, dune 1, into two smaller dunes, dune 1 and dune 1'. Fig. 26A-D shows an interaction that is considered here as a type of splitting. Figure 26A (1985) shows the north-facing defect of dune 1 migrating onto the stoss slope of dune

2. By 1996 (Fig. 26B) a new dune, dune 3, has emerged at the end of the termination of dune 1. The crestline of dune 2 is beginning to deform downwind of the newly formed dune 3. By 2003, dune 3 has grown in crest length and substantially deformed the crestline of dune 2. By 2007 (Fig. 26D, also shown with elevation contours in Fig. 23A), the north-facing defect of dune 3 captured the northern portion of the crestline of dune 2 through defect repulsion, becoming dune 2'+3. The newly detached north-facing defect of dune 2 is freely migrating downwind.

Although heretofore considered by itself, defect creation may also arise along with another interaction if a crestline is destabilized during another interaction, such as merging (see Fig. 19D) or occur more systematically at the field scale, as with the transition from crescentic dunes to barchan dunes (Endo et al., 2004). The northern area of the White Sands Dune Field is dominated by the latter (see Fig. 7 in Kocurek et al., in press). Splitting is common in shallow subaqueous dunes (Allen, 1973; 1976) and is thought to occur when the stoss slope elongates beyond a critical length (Dohmen-Janssen et al., 2008). The splitting described in this study departs from the descriptions in subaqueous dunes, yet arguably, should be considered a type of splitting owing to the emergence of a new dune, which grows to a sufficient size to break the crestline of the host dune.

Spatial variations in the pattern and dune interactions at the White Sands Dune Field

Spatial variations in the pattern at White Sands Dune Field

Spatial variations in the dune-field pattern at White Sands were measured by manually digitizing crestlines from aerial photographs from 1985, 1996, 2003, 2005 and a LiDAR DEM from 2007 along a 500 x 3,500 m box transect from the upwind margin to the core of the dune field (Fig. 27A, 27B). This transect was chosen because it captures a spatial change in the dune-field pattern from the emergence of smaller, closely-spaced

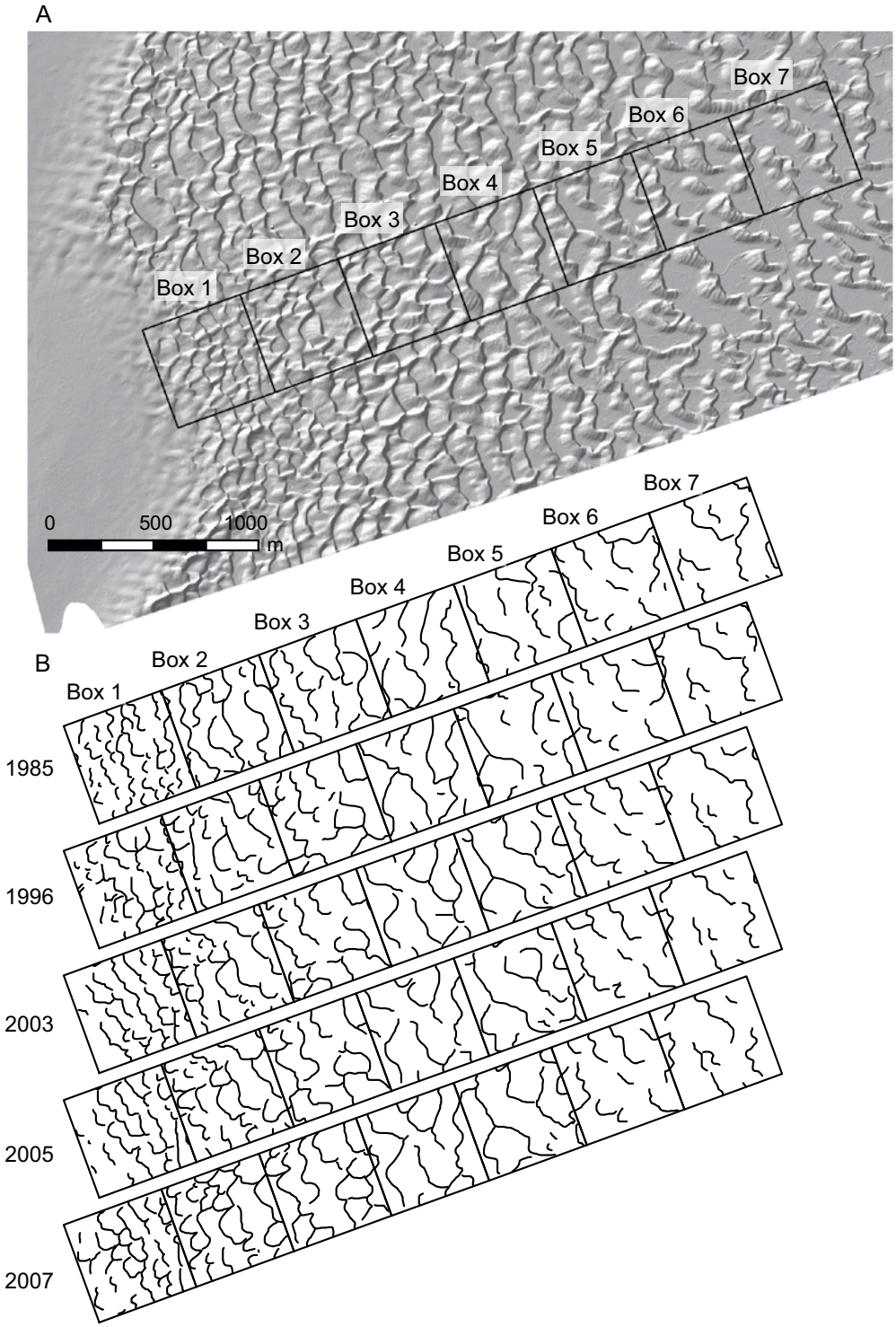

Figure 27. (A) DEM hillshade of the upwind and central portion of White Sands Dune Field showing the location of the 3,500 m box transect. Note that the boxes are labeled sequentially from the upwind margin, Box 1, to the interior of the dune field, Box 7 in the direction of dune migration. (B) Digitized dune crestlines along the box transect from 1985, 1996, 2003, 2005 and 2007.

Table 1. Statistical summary of dune-field pattern parameters

Data from 1985-2007	Box 1	Box 2	Box 3	Box 4	Box 5	Box 6	Box 7
Dune count	154	114	80	54	65	58	48
mean	30.6	22.6	15.8	10.6	12.8	11.4	9.4
std. dev.	5.7	9.8	6.6	4.4	5.3	4.7	3.7
coeff. var.	0.19	0.43	0.42	0.41	0.41	0.41	0.41
Number of interactions	24	16	10	4	6	3	3
mean	4.8	3.2	2	0.8	1.2	0.6	0.6
std. dev.	3.6	3.3	1.9	1.3	1.8	0.96	0.96
coeff. var.	0.74	1.02	0.94	1.62	1.49	1.6	1.6
Crest length (m)							
sum	17,132	16,443	14,142	11,526	11,411	8,570	7,870
mean	111.97	145.51	179.01	217.47	178.30	150.35	167.44
std. dev.	79.90	116.87	138.71	160.52	157.98	102.64	124.50
coeff. var.	0.71	0.80	0.77	0.74	0.89	0.68	0.74
Spacing (m)							
mean	73.46	76.65	88.74	108.69	110.16	146.75	159.24
std. dev.	6.85	7.57	6.14	5.74	9.25	12.36	8.97
coeff. var.	0.093	0.099	0.069	0.052	0.084	0.084	0.056
Defect Density							
mean	0.0073	0.0050	0.0038	0.0029	0.0035	0.0046	0.0044
std. dev.	0.00095	0.0017	0.00028	0.00059	0.00034	0.00035	0.00021
coeff. var.	0.13	0.33	0.072	0.21	0.098	0.076	0.048
Migration rate (m/yr) from 1996-2007							
11 year mean	5.6	3.8	2.9	3.1	3.4	3.1	3.88
std. dev	1.8	1.5	1.2	1.1	1.2	1.0	1.0
coeff.var.	0.32 (n=90)	0.38 (n=84)	0.38 (n=83)	0.36 (n=79)	0.35 (n=63)	0.33 (n=52)	0.27 (n=50)
Mean height (m) from 2007							
mean	5.3	6.5	7.1	6.3	5.4	5.1	3.7
std. dev.	2.3	2.5	2.7	2.6	2.4	2.2	1.7
coeff. var.	0.43 (n=159)	0.38 (n=164)	0.38 (n=136)	0.40 (n=103)	0.44 (n=105)	0.43 (n=72)	0.46 (n=64)

dunes at the upwind margin of the field to larger, more widely-spaced dunes downwind. The number of dune crestlines, crest length, defect density, crest spacing, height, and migration rate were measured within seven 250,000 m^2 boxes along the transect. The total numbers of crestlines and interactions within each box were measured over the 22 year period. The crest spacing, crest length and defect density within each box is the average of the average measured at each of the 5 time intervals over the 22 year time period. Dune heights were measured from the 2007 DEM. Migration rates are averaged as per year values over the eleven year period from 1996 and 2007. The methods section describes those used for

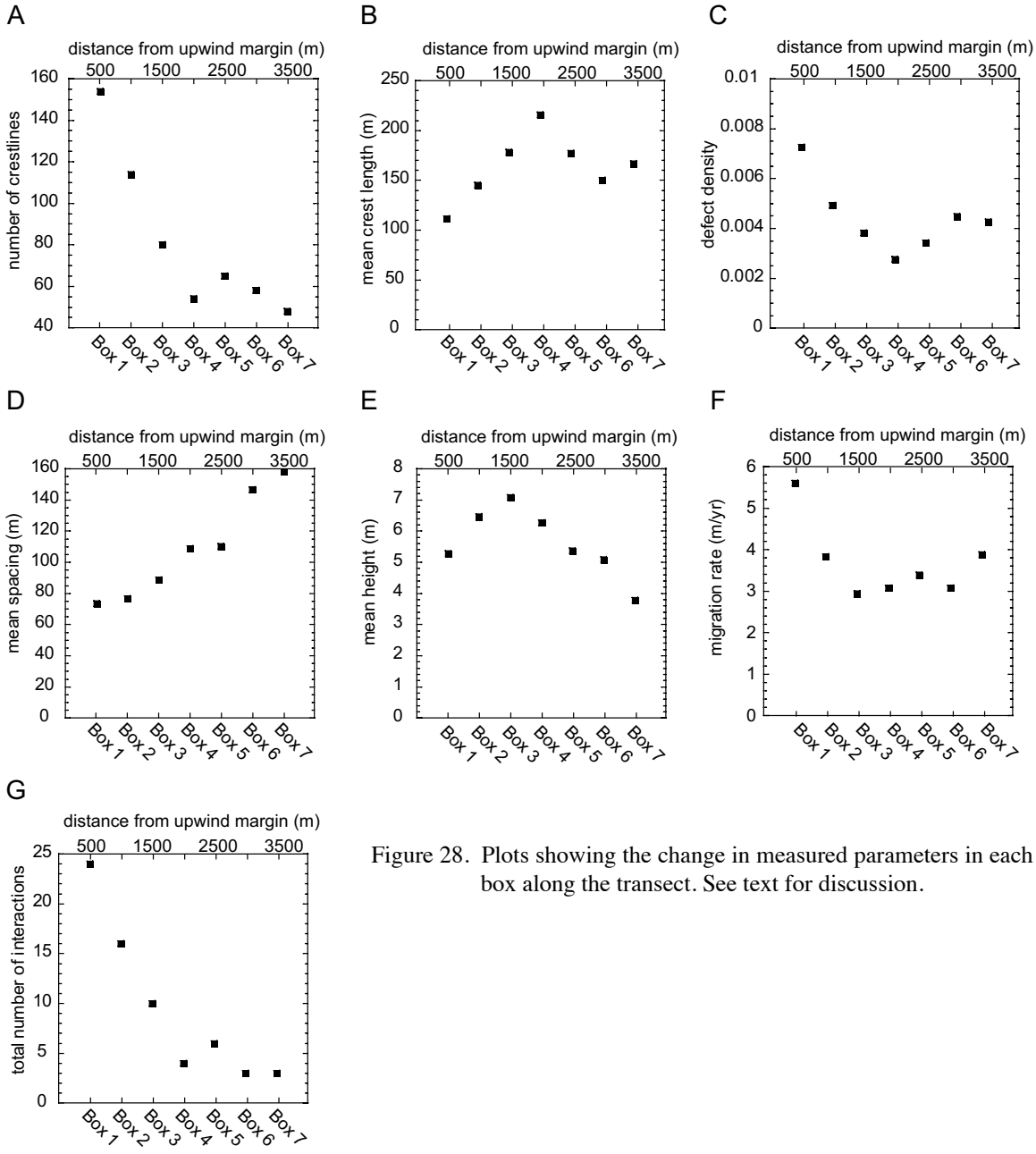

Figure 28. Plots showing the change in measured parameters in each box along the transect. See text for discussion.

measuring and calculating each measured parameter. A statistical summary of the data is presented in Table 1 and a graphical summary of the data is presented in Fig. 28 A-G.

Along the transect, the number of dune crestlines decreases significantly in the first 2000 m downwind of the upwind margin and changes little in the last 1500 m (Fig. 28A). Mean crest length increases over the first 2000 m, decreases over the next 1000 m and

increases in the remaining distance of the transect (Fig. 28B). Defect density decreases over the first 2000 m, increases for 1000 m, and then decreases to the end of the transect (Fig. 28C). Mean spacing increases over the entire distance of the transect (Fig. 28D). Mean height increases over the first 1500 m and then declines sharply to the end of the transect (Fig. 28E). Dune migration rates drop sharply over the first 1500 m, then fluctuate around 3.2 m/yr over the next 1500 m and climb to nearly 4 m/yr in the last 500 m (Fig. 28F). The number of dune interactions decreases in the first 2000 meters, then remains relatively constant over the remainder of the transect (Fig. 28G).

Overall, the measured parameters change the most and co-vary within the first 1500 m of the transect. Over the first 1500 m, dune height and migration rate co-vary, with migration rate decreasing as height increases. The pattern parameters of spacing, crest length and defect density co-vary over the first 1500 m, with spacing and crest length increasing and defect density decreasing. This trend matches well with previous studies, which show that these parameters evolve interdependently toward greater organization over time (Werner and Kocurek, 1999; Ewing et al., 2006), however, this trend occurs as a function of the distance from the upwind line source area (Ewing and Kocurek, in press).

Over the last 2000 m of the transect, the relationships among the pattern parameters do not indicate a clear trend toward greater or lesser organization, but do show a difference from the first 1500 m. Over the latter interval, although spacing continues to increase, crest length decreases and defect density increases. Dune height begins to decrease and the number of dunes, migration rate and number of dune interactions reaches a near steady state. These changes in the pattern parameters correspond to a change in the morphologic characteristics of the dunes and the interdune areas. The dune morphology changes from continuous crescentic ridges to barchan-shaped near 2500 m along the transect. Barchan dunes are the dominant dune type by the end of the transect. The interdune areas transition from small, trough-like depressions in the first 1500 m to more widely-spaced interdune

flats over the last 2000 m.

The absence of a correlation among the pattern parameters and a change in morphologic characteristics of the dunes over the last 2000 m along the transect relate to a field-wide change in the dune and interdune regime (i.e., the dune patterns in these areas are evolving under different boundary conditions). The central area of White Sands has wet interdune areas and partially cemented dune stoss slopes (Schenk and Fryberger, 1988; Kocurek et al., 2007). The wet interdune areas trap sand moving across the interdune surface and the partially cemented stoss-slopes limit erosion of the stoss-slope, both of which limit the amount of sediment available for transport in this area of the dune field. Overall, the spatial change in the dune pattern over the first 1500 m of the transect relates to the line-source area geometry, whereas the changes over the last 2000 m of the transect relate to a change in the availability of sand.

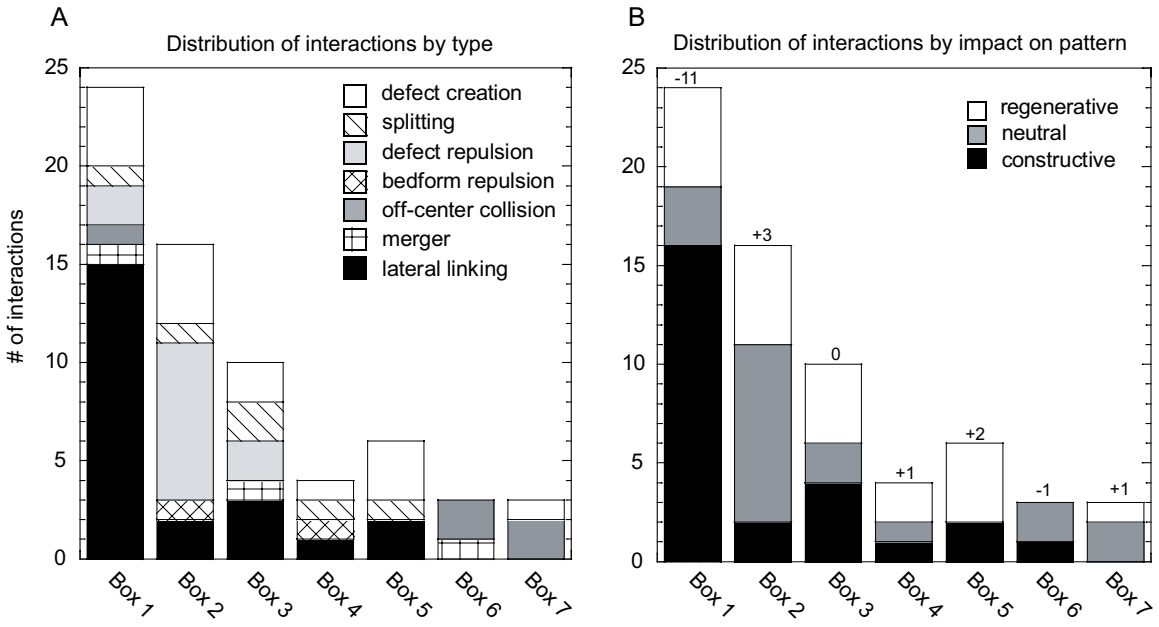

Figure 29. Bar plots showing the total number of interactions in each box classified by interaction type (A) and impact on pattern (B). The numbers above the columns in (B) are the net sum of crestlines where constructive interactions reduce the total number of crestlines and are negative numbers, neutral interactions do not change the number of crestlines, and regenerative interactions increase the number of crestlines and are positive. The net sum of all crestlines along the entire transect is -5.

Spatial variations in the type and frequency of dune interactions

Do the type and frequency of dune interactions vary with spatial changes in the dune-field pattern? The type and frequency of dune interactions within White Sands Dune Field were measured along the 3,500 m transect (Fig. 29A). The most upwind area, Box 1, has the most and the greatest diversity of interactions along the transect. Lateral linking dominates the interactions within Box 1 and defect creation has the next greatest abundance. Box 2 is dominated by defect repulsion and to a lesser degree by defect creation. Box 3 has a near equal distribution of interaction types, although lateral linking is most abundant. Defect creation, splitting, bedform repulsion and lateral linking appear equally in Box 4. Box 5 has a slight overall increase in the number of interactions and is dominated by defect creation. Boxes 6 and 7 have equal numbers of interactions and off-center collisions are the most prevalent type.

Figure 29B shows the types of interactions classified by the impact on the pattern as constructive, neutral or regenerative. Box 1 is strongly net constructive with a loss of 11 crestlines over the 22 year period. Although neutral interactions are most common in Box 2, it is net regenerative with the creation of 3 crestlines. Box 3 remains neutral and Box 4 is regenerative with the creation of one crestline. Box 5 is net regenerative with the creation of two crest lines, Box 6 is net constructive with the loss of one crestline and Box 7 is net regenerative with the creation of 1 crestline. Overall, within the measured transect from the upwind margin, the dune field is net constructive with the loss of five crestlines, nearly all of which were lost during the first 500 m.

In terms of pattern development, the strongly constructive upwind margin of the field corresponds to an increase in dune height (Fig. 28E), and an increase in pattern organization with a decrease in the number of dunes (Fig. 28A) and defect density (Fig. 28C), and an increase in crest length (Fig. 28B) and spacing (Fig. 28D). Although the first 500 m (Box 1) is the only constructive area along the transect in the first 2500 m, the constructive trend

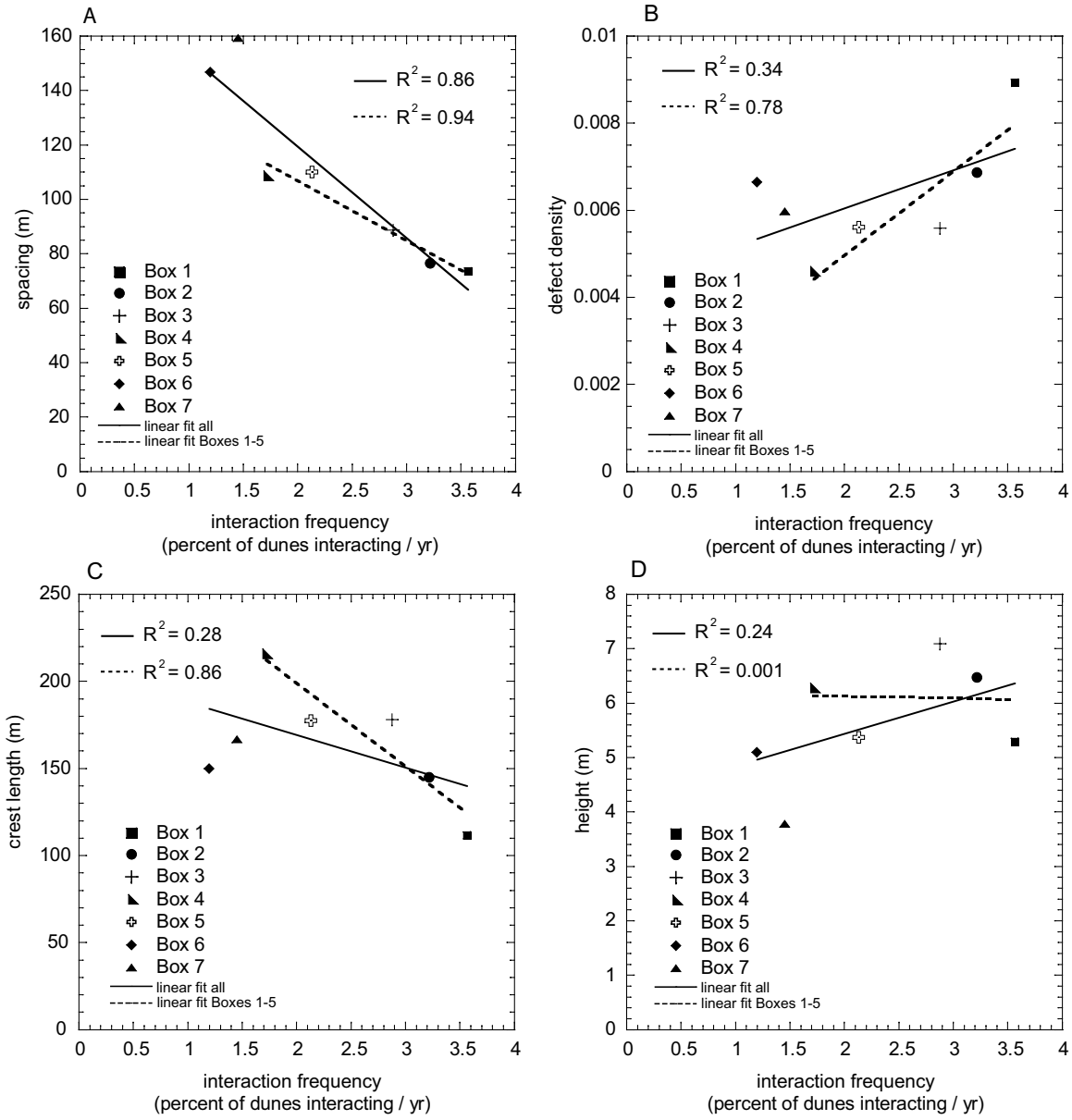

Figure 30. Plots showing dune pattern parameters spacing (A), defect density (B), crest length (C) and height (D) versus the interaction frequency (percent of dunes interacting per year) within each box along the transect. The solid line is a linear regression line through all data points. The dashed line excludes the data from Boxes 6 and 7. Note that the fit does not improve for height when data are excluded. See text for discussion.

in the pattern continues through the first 1500 m. Beyond 1500 m, the interactions are dominantly neutral and regenerative, which corresponds to a decrease in the correlation among the pattern parameters. The dominance of basically neutral interactions over the field interior is supported by Rachal and Dugas (2009), in which no overall constructive

trend was found in measurements of dune-pattern parameters from aerial photos of White Sands that span 60 yr.

Interplay of dune interactions and pattern variables

The dune-pattern variables of spacing, crest length and defect density are plotted against the frequency of dune interactions in order to gauge the interplay between dune interactions and pattern development (Fig. 30A-D). The frequency of interactions is the percentage of dunes interacting per year and calculated as the average number of interactions per year in each box divided by the average number of dunes in each box. Linear regression lines are fit to all the data in each plot to highlight the presence or absence of a trend between the interaction frequency and the pattern. A linear regression line is also fit to Boxes 1-5 only because Boxes 6 and 7 appear as outliers in Fig. 30A-D and, geomorphically, Boxes 6 and 7 fall within a different dune and interdune regime, with barchan dunes as the dominant dune type. Figure 30A shows a robust relationship between spacing and the percentage of dunes interacting, where spacing increases as the number of dune interactions decreases. Although a relationship between defect density and crest length is not apparent with a linear fit through all the data points, a more clear relationship emerges with the exclusion of the data from Boxes 6 and 7 (Fig. 30B-C). No relationship is apparent between dune height and the number of dunes interacting, even with the exclusion of Boxes 6 and 7 (Fig. 30D).

The trends between the pattern variables and the percent of dunes interacting per year indicate a strong coupling between dune interactions and pattern development. Excluding the barchan-type dunes in Boxes 6 and 7, the pattern becomes more organized (e.g., greater spacing and crest length and lower defect density) as the number of interactions decrease. In turn, the increased pattern organization that emerges from interactions causes a feedback, which decreases the probability that an interaction will occur. This is most

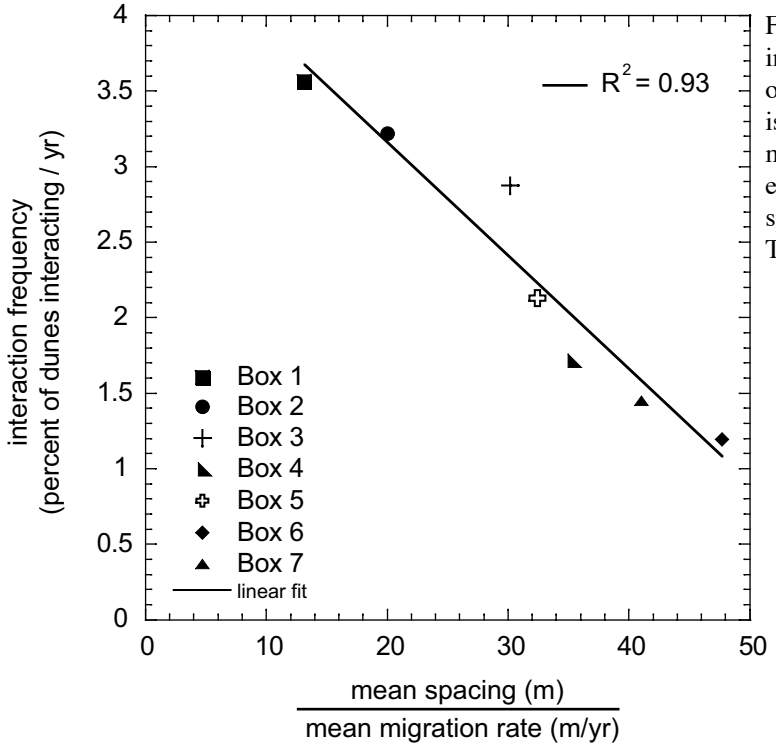

Figure 31. Plot showing interaction frequency vs. the ratio of spacing to migration rate, which is the time needed for a dune migrating at the average rate within each box to migrate the average spacing distance within each box. The solid line is a linear regression line through all the data points.

apparent with the spacing-to-interaction-frequency relationship. As spacing increases, the growing distance between dunes becomes the controlling limit on the frequency of dune interactions (i.e., all else being equal dunes that are farther apart interact less frequently; Fig. 30A). Similarly, as defect density decreases there are fewer numbers of defects though which interactions can take place and the interaction frequency decreases (Fig. 30B). Boxes 6 and 7 in Fig. 30B are an exception, where spacing and defect density increase as the interaction frequency decreases. The increase in defect density results from the break-up (i.e., a regenerative regime of the pattern by defect creation) of continuous crescentic dunes into barchan dunes. This transition begins in Box 5 and is apparent qualitatively (Fig. 27A) and quantitatively by the increase in the number of dunes (Fig. 28A) and defects (28C) within the area. The spacing likely increases because of the decreased sediment availability (see 4.1 above), which would reduce the number of barchan dunes. In turn, the total crestline length decreases and spacing increases within the area (see Table 1).

The continued increase in spacing in Boxes 6 and 7 suggests that dune spacing may be a stronger feedback on interaction frequency than defect density, at least within a crescentic-to-barchan transitional dune-pattern regime.

Figure 31 shows a strong relationship between the frequency of interactions and the ratio of spacing and migration rate, such that the frequency of interactions decreases as spacing increases or migration rate decreases. The ratio of spacing to migration rate is the time needed for a dune migrating at the average rate within each box to migrate the average spacing distance within each box. The inclusion of spacing and migration rate for comparison to the interaction frequency provides a dimensionless relationship by which interactions of bedforms of different scales can be assessed.

Conclusions

Time-series images of the White Sands Dune Field show that large-scale, fully developed, aeolian crescentic dunes do not simply translate in isolation with dune migration, but rather interact with each other in much the same way as wind ripples and subaqueous bedforms. With this observation, it is apparent that not only are bedform patterns similar across system type and scale, but also that bedform patterns emerge though the same types of interactions. These observations are consistent with the hypothesis that bedform patterns are self-organized, emergent structures arising within the complex system of sediment transport, in which the bedforms themselves are the interacting elements that give rise to the pattern.

The documented dune interactions at White Sands include: (1) merging, (2) lateral linking, (3) defect repulsion, (4) bedform repulsion, (5) off-center collision, (6) defect creation and (7) splitting. Merging and lateral linking are constructive interactions that give rise to a more organized pattern. Defect creation and bedform splitting are regenerative interactions that push the system to a more disorganized state. Defect/bedform repulsion

and off-center collision cause significant pattern change, but appear to be neutral in overall pattern development. Most of these bedform interactions result in characteristic dune morphologies that can be identified in the field, including trailing defects that arise from defect/bedform repulsion and off-center collision.

Time-series documentation of the type and frequency of dune interactions at White Sands shows a spatial arrangement that reflects the boundary conditions of the field. Most of the constructive development in the field occurs near the upwind field border, which serves as a sediment line-source boundary condition. Constructive interactions yield in the field interior to a dominance of neutral and regenerative interactions, the latter of which reflects a boundary condition of lower sediment availability.

The ability of dunes to interact and the pattern to evolve is a function of the pattern parameters of dune spacing and defect density – the frequency of bedform interactions decreases as dunes get farther apart and the number of defects decreases. Greater spacing and lower defect density both occur with greater pattern self-organization, which may occur over time or spatially within the field.

Chapter 3: Dune-field pattern formation and recent transporting winds in the Olympia Undae Dune Field, north polar region of Mars

ABSTRACT

The Olympia Undae Dune Field in the north polar region of Mars is complex. Observations from High Resolution Imaging Science Experiment (HiRISE) imagery show that the reticulate dune-field pattern in the field center of the Olympia Undae Dune Field is comprised of two sets of nearly orthogonal dune crestlines, apparent slipfaces, wind ripples, coarse-grained wind ripples and deflated interdune areas. Geomorphic evidence and dune-field pattern analysis of dune crest length, spacing, defect density and orientation measured from HiRISE imagery indicates that the pattern represents two constructional generations of dunes. The oldest and most well organized generation forms the primary component of the pattern and is transverse to circum-polar easterly winds. The younger pattern emerged with both circum-polar easterly winds and katabatic winds and is reworking the older pattern. The younger pattern appears to represent an influx of sediment to the dune field associated with the development of the Olympia Cavi re-entrant and katabatic winds channeling through the re-entrant. A third, yet older dune generation is represented by aeolian dune cross-strata exposed in the deflationary sequence surface upon which the current dunes exist. Mapped secondary flow fields indicate that the most recent transporting winds are from the NE and most likely related to the katabatic winds. A model of the pattern reformation based on the reconstructed primary winds and resulting secondary flow fields shows that the development of the secondary pattern is controlled by the boundary condition of the older dune topography.

Introduction

Aeolian dune fields create some of the most striking patterns on Mars. Although the fluid/grain properties of the aeolian sediment transport system on Mars are different from those on Earth (Greely and Iverson, 1985), the robust, self-organizing nature of this complex system dictates that the emergence of dune-field patterns on Mars will be much the same as on Earth (Werner, 1999; 2003; Kocurek and Ewing, 2005; Ewing and Kocurek, in review; Kocurek et al., in press). Martian patterns, like those on Earth, reflect the internal dune dynamics of self-organization and the geomorphic and climatic boundary conditions within which the dune-field patterns evolve (Ewing and Kocurek, in press).

One means of interpreting the geomorphic and climatic history of a dune field is through analysis of the dune-field pattern (Kocurek and Ewing, 2005; Ewing et al., 2006; Ewing and Kocurek, in press). On Earth, dune-field pattern analysis via measurements from remote images of dune fields, statistical analysis of the measurements, and geomorphic observation has yielded robust interpretations of the evolution of regional-scale dune fields (Beveridge et al., 2006; Ewing et al., 2006; Derickson et al., 2008). This type of analysis is well-suited to study the evolution of dune fields on Mars because the measurements and analysis are at the scale of the pattern (i.e., not the fluid/grain scale) and the measurements are taken remotely (i.e., no *in situ* data is required).

The purpose of this study is to analyze in detail the dune-field patterns of the Olympia Undae Dune Field in the north polar region of Mars in order to elucidate the most recent wind conditions and the dune-field evolution. All dune crestlines and a representative sample of wind-ripple crestlines within High Resolution Imaging Science Experiment (HiRise) image PSP_001432_2610 were measured and statistically analyzed to assess the spatial relationships of the dune-field pattern in the center of Olympia Undae (160.3 W, 81.1 N; Fig. 32). Wind ripples were mapped to determine the flow fields of the most recent sediment transport event within the dune field. A model of the evolution of the

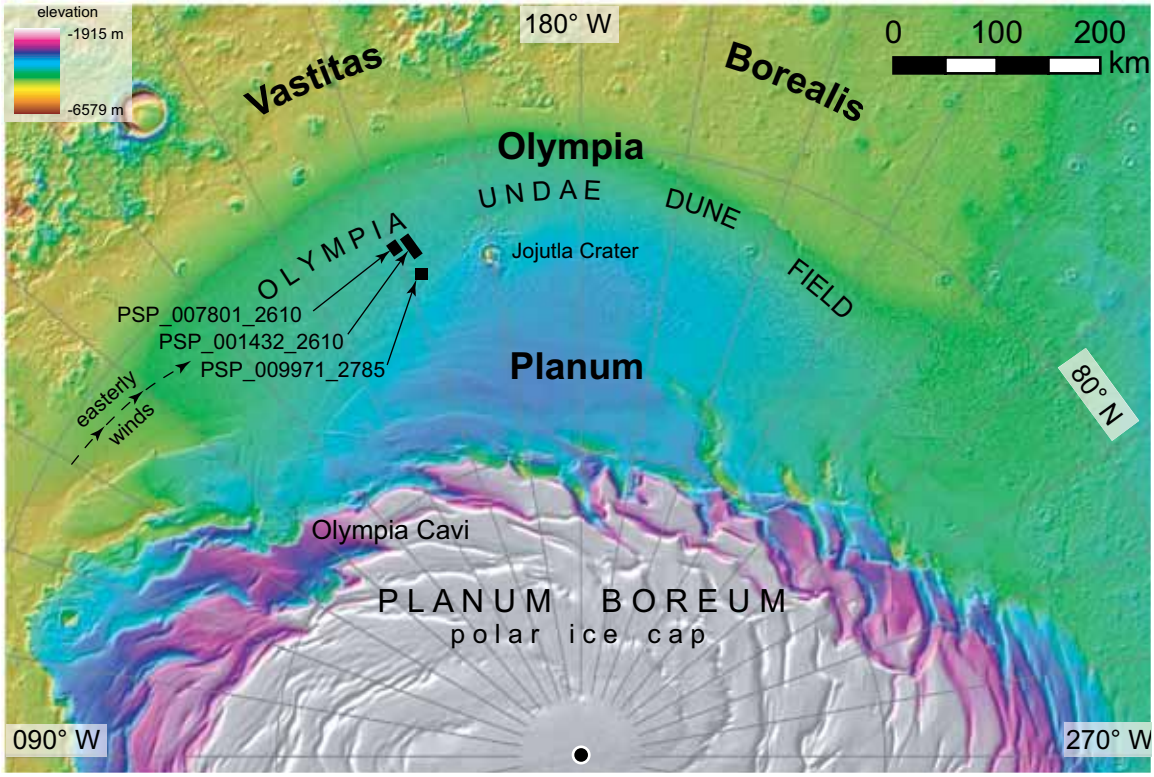

Figure 32. MOLA digital elevation model (DEM) of the north polar region of Mars centered on the Olympia Undae Dune Field. Note the elevation color ramp in the upper left corner. HiRISE image PSP_001432_2610 is the primary study area shown in detail in Fig. 33. PSP_007801_2610, shown in Fig. 36, shows the seasonal defrosting of the dune field. PSP_00971_2785 is shown in Fig. 43 and is used as a comparison for the flow fields reconstructed within the study area. Note the general orientation of circum-polar easterly winds.

pattern, which relates the spatial relationships of the pattern and the mapped flow fields, is developed and discussed in the context of the polar wind regime and regional, spatial changes of Olympia Undae Dune Field pattern. This paper concludes that: (1) the dune-field pattern is complex (i.e, comprised of two generations of dunes) - the youngest pattern emerged with both easterly and katabatic winds and is reworking the older pattern formed primarily by easterly winds, (2) the most recent transporting winds are from the northeast and are related to katabatic winds descending the residual polar ice cap, (3) katabatic winds from Olympia Cavi dominate the current state of dune-field pattern development in the center of the field, (4) the current pattern development occurs within an overall stabilized system through the accumulation of sediment by ice, and (5) an older dune constructional

event is apparent by aeolian dune cross-strata exposed within the interdune areas.

Motivation for dune-field pattern analysis

Two nearly orthogonal crestline orientations define the reticulate crestline pattern within the study area in the Olympia Undae Dune Field (Fig. 33). Crestline orientation relates to the sediment-transporting wind regime, such that dunes orient to maximize the sediment transport perpendicular to the crestline – gross bedform-normal transport (Rubin and Hunter, 1987). Gross bedform-normal transport implies that for a given wind regime a simple crestline pattern emerges, which represents a single generation of dune construction (Kocurek and Ewing, 2005; Ewing et al., 2006). A complex pattern (i.e., multi-generational) arises with the superposition of multiple simple patterns and can be distinguished by multiple statistical populations of dune crestlines separated in scale or orientation. The reticulate pattern in the study area can represent either a simple pattern created under a single wind regime, or a complex pattern comprised of two generations of dune construction. In the former interpretation, the composite pattern would be classified as a star-dune pattern created by a bimodal wind regime with a divergence angle between the dominant and subordinate winds of ~90° (see Fig. 2 in Rubin and Hunter, 1987; Fig. 4 in Werner and Kocurek, 1997; Fig. 4 in Kocurek and Ewing, 2005). In this case, the star pattern would indicate a strongly bimodal polar wind regime at the time of pattern construction, with winds blowing from a relatively narrow range of directions. In the interpretation that the pattern is complex, each crestline trend formed under a different wind regime. In this case, the pattern represents a change in the transporting winds over time, which may relate to changes in the polar climate regime. Quantitative analysis of the crestline pattern along with geomorphic observation, provide a means to constrain the range of winds and constructional events that gave rise to the pattern in the Olympia Undae Dune Field.

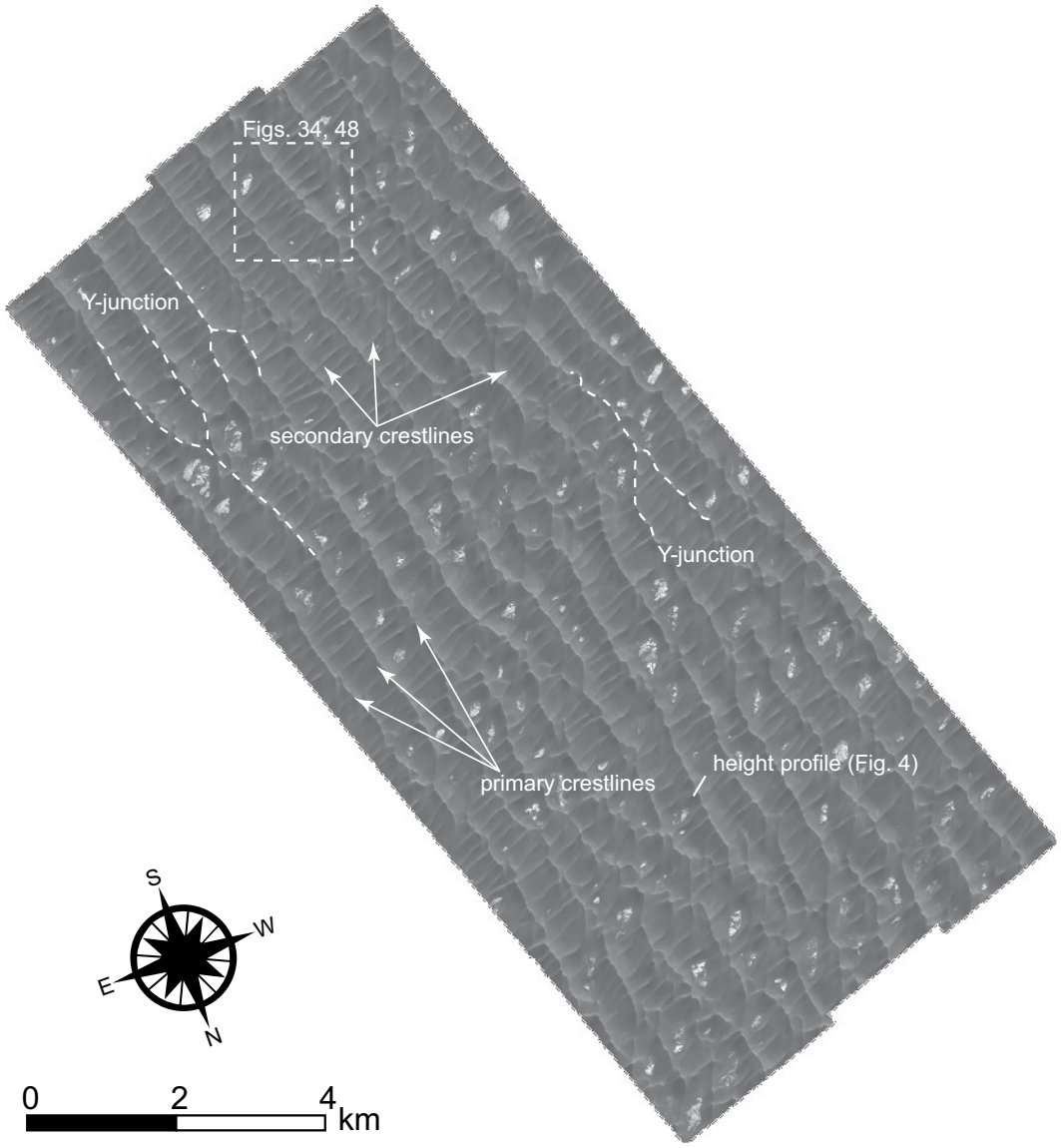

Figure 33. Study area - HiRISE image PSP_001432_2610. Lighting is from 196° W longitude. The primary and secondary crestlines are indicated on the image. Y- junctions are highlighted by dashed white lines along the primary dune crestlines. The location of Figs. 3 and 17, and a height profile shown in Fig. 34 are indicated on the image.

The Olympia Undae Dune Field

The Olympia Undae Dune Field is the largest sand sea in the north polar region of Mars, spanning from ~120°–230° W and ~79°–83° N (Tsoar et al., 1979; Lancaster and Greeley, 1990; Tanaka et al., 2005) with a total area of 385,000 km^2 (Hayward et al., 2008). The majority of the dune field mantles Olympia Planum, which is a large platform that rises nearly 800 m above the surrounding plains of Vastitas Borealis near the base of Planum Boreum (Fig. 32).

The Olympia Undae dunes have been primarily described and classified as crescentic ridges and barchan dunes. Crescentic ridges comprise the core of the field and barchan dunes flank the southern and western margins (Tsoar et al., 1979; Lancaster and Greely, 1990; Tanaka and Hayward, 2008). The dunes in the field center are thought to be mostly transverse to circum-polar easterly winds, whereas the dunes along the southern margin of the field appear to reflect a westerly wind belt (Tsoar et al., 1979; Howard, 2000; Tanaka and Hayward, 2008).

Estimations of the wind directions in Olympia Undae, based primarily on crestline orientation and slipface direction, indicate winds are largely from the east to the west with subordinate northeasterly winds in the western part of the field (Tsoar et al., 1979; Tanaka and Hayward, 2008). However, wind directions based on crestline and slipface orientation alone are not reliable indicators of wind direction except in the case of a dominantly unidirectional wind regime. Because crestlines are oriented to be as perpendicular as possible to all constructive winds (i.e., gross bedform-normal transport of Rubin and Hunter, 1987), in non-unimodal wind regimes, the crestline orientation shows the direction of net bedform migration, but not directly the constructive wind directions that cause the crestline orientation. For example, a crescentic dune crestline may be transverse (i.e., the

incidence angle between the crestline and the resultant transport vector is between 75-90°; Hunter et al., 1983) under a bimodal wind regime in which the divergence angle between dominant and subordinate winds are between 0 and ~70° (see Fig. 2 in Rubin and Hunter, 1987 and Fig. 4 Kocurek and Ewing, 2005). Thus, a dune crestline may be transverse to the resultant transport direction, but not to the constructive winds. The interpretation of an east-to-west wind direction in Olympia Undae based on the crescentic dune morphology may be oversimplified. The apparent dispersion direction of gypsum detected within the dune field from the east to west (Langevin et al., 2005) substantiates the net transport wind direction indicated by the orientation of the dune crestlines, but does not provide any further details of the wind regime. Katabatic winds from the north and northeast, descending off Planum Boreum, have been interpreted from frost streaks and constitute an additional component of the wind regime in Olympia Undae (Tsoar et al., 1979; Howard, 2000; Tanaka and Hayward, 2008).

The dunes of Olympia Undae are thought to be mostly inactive, stabilized features (Breed et al., 1979; Schatz et al., 2006; Feldman et al., 2008; Tanka et al., 2008). Based upon a model that used Mars Odyssey Neutron Spectrometer data, Feldman et al. (2008) suggested that the bulk of the dune volume is stabilized by ice (i.e., niveo-aeolian) deposited through water vapor diffusion into the sediment pore space or through the entrainment of ice precipitation, and that a thin (~10 cm) more mobile layer of sediment mantles the stabilized portion of the dunes. Their model is supported by a surface morphology that includes surface fractures, steep-walled pits, the apparent absence of grainflow avalanches, and an overall topographically subdued crestline appearance. Dune inactivity in Olympia Undae is further supported by time-series observations from Viking and Mars Orbiter Camera imagery made by Schatz et al. (2006), who found no evidence of dune movement over 4-15 Martian years in both the equatorial latitudes and in the north polar region in Chasma Boreal. Although no dune movement is observed, some sediment mobility is implied by

sand streaks, which emanate from the horns of barchan dunes (Tanaka et al., 2008) and in three instances, the erosion and disappearance of small dome dunes (Bourke et al., 2008; 2009).

Dark dune sediments thought to be composed of basaltic andesite or weathered basalt comprise nearly all of Olympia Undae (Bandfield et al., 2000; Wyatt et al., 2004; Fishbaugh et al., 2007). Gypsum comprises a secondary component of the dune mineralogy and ranges in concentration up to 24% near the eastern margin of the dune field and decreases westward (Langevin et al., 2005; Fishbaugh et al., 2007; Horgan et al., 2009a). The dune crests show the highest concentrations of gypsum, with lesser amounts occurring on the dune slopes and in the interdune areas (Roach et al., 2007; Horgan et al., 2009a; Lahtela et al., 2009).

Sedimentary deposits that flank and underlie much of the polar ice cap are thought to be the source for the dune sediments (Byrne and Murray, 2002; Fishbaugh and Head, 2005; Tanka et al., 2008). Recent detailed mapping of these deposits indicates that much of the dune sediment has eroded from the middle Amazonian, Planum Boreum cavi unit (Tanka et al., 2008). Primarily exposed along slipfaces near the base of the North Polar Layered Deposits in Olympia Cavi, the cavi unit makes up the majority of Olympia Planum, upon which Olympia Undae sits. In outcrop, the cavi unit appears as dune cross-bedded strata, interbedded with polygonally fractured ice layers and is interpreted as an ancient aeolian sand sea, which co-evolved with deposition of ice (Byrne and Murray, 2002; Fishbaugh and Head, 2005; Herkenhoff et al., 2007; Tanaka et al., 2008).

Geomorphology of study area

The area within the Olympia Undae Dune Field chosen for the dune-field pattern analysis covers 93 km^2 and is centered at 160.3 W, 81.1 N (Fig. 32). This area lies near the center of the Olympia Undae Dune Field, 80 km east of Jojutla Crater and 200 km south

from the base of Planum Boreum.

Six distinct morphologic features give rise to the dune-field pattern within in the study area. (1) NNW-trending crestlines form the largest, primary set of dunes that extend the length of the study area (Fig. 33). (2) A smaller, secondary set of NE-trending crestlines are oriented nearly perpendicular to the primary crestlines (Figs. 33-34). At the dune-scale, (3) apparent slipfaces are present along the primary dune crests (Figs. 34-35), (4) wind ripples are ubiquitous over nearly all sediment-covered surfaces of the dune field (Fig. 34B), and (5) more widely spaced coarse-grained wind ripples occur within the interdune areas and on the eastern slopes of the primary dunes (Fig. 34B). (6) The substrate underlying the dunes is exposed in interdune areas that are not covered by sediment (Figs. 33-34, 7B).

Primary dunes

The largest-scale dunes within the study area are straight-crested and regularly spaced. The dune slopes and crests are subdued in appearance, only becoming sharp at the brinks of the apparent slipfaces that occur along the crestlines. The basic element of the crests extend over the length of the image, giving rise to a continuous appearance with Y-junctions, typical of well-organized linear dunes and wind ripples (Fig. 33). In detail, however, disconnections occur were the crests are offset, typically where they are intersected by secondary crests or slipfaces (Fig. 34A). Feldman et al. (2008) estimated dune heights within a nearby area in Olympia Undae at 75 m. Height estimates in this study range from 10-20 m based upon the reconstructed flow-fields (see below) and 65 m based on a photoclinometry profile (Fig. 35A). Dune profiles show the primary dunes have a slight asymmetry, with the steepest slopes occurring on the western side of the crestlines (Fig. 35A). From this profile, the W-facing slopes are interpreted as the primary lee slope of the dunes, and the E-facing slopes are the primary stoss slope, which imply a general transport direction from the east to the west.

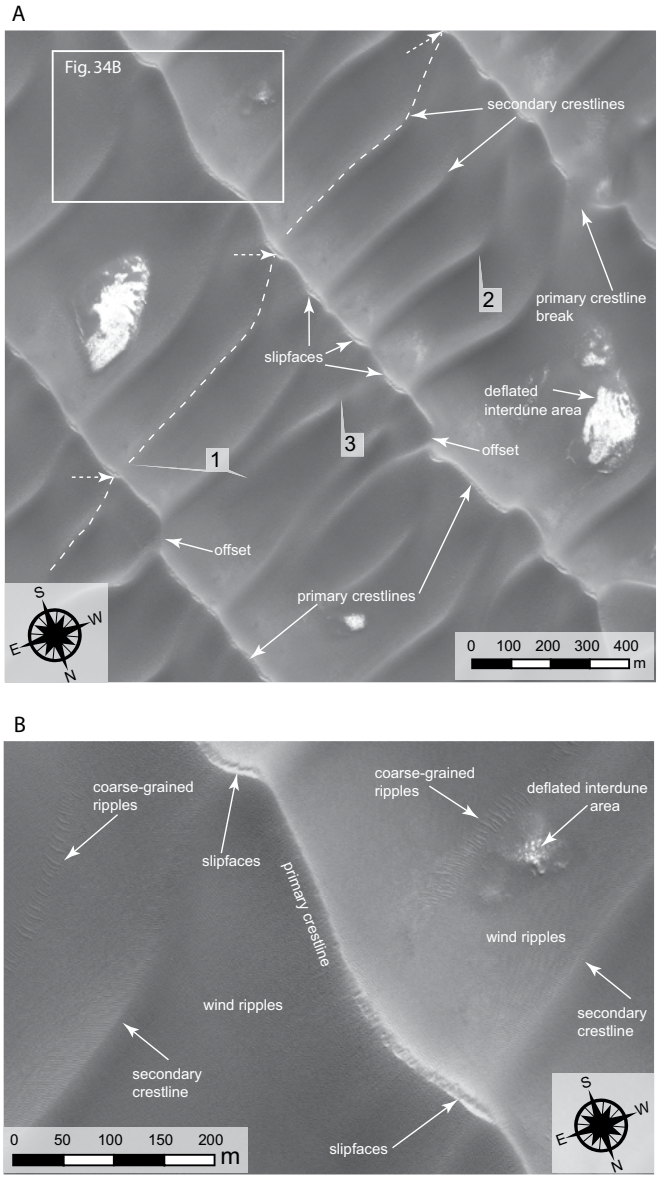

Figure 34. Detail images showing the geomorphic elements of the study area. (A) Inset located in Fig. 33. Lighting is from 196° W. Primary crestlines, secondary crestlines, apparent slipfaces and interdune areas are labeled on the image. Label number 1 indicates an unattached eastern termination of a secondary dune. Label number 2 indicates a bend in the secondary crest line. Label number 3 shows a secondary dune that is unattached at both the eastern and western terminations. The dashed white lines follow the alignment of three secondary crestlines across three primary dunes, showing typical deflections S up the stoss slope of the primary dunes and slight S off set subsequent secondary crests. Note that slipfaces occur at the intersection of the secondary crestline and the primary crestline. Examples of breaks or offsets in the primary crestline are labeled. (B) Inset from Fig. 34A showing all the geomorphic features that make up this dune-field pattern. At this scale, the sharp brink along the slipfaces, widely-spaced coarse-grained ripples (see text for discussion) and wind ripples that mantle the dunes surfaces are visible.

Profile measurements were extracted by a simplified photoclinometric procedure that assumes uniform albedo along a profile line and Lambertian photometric properties of the surface (i.e., brightness is only dependent on the solar incident angle) (see Bourke et al., 2006; Zimbleman, in press). Although the albedo of the dune surface appears uniform across the profiles, this method does not account for differences in surface mineralogy that may alter the surface brightness. Gypsum, which is most concentrated at the dune crests in Olympia Undae (Roach et al., 2007; Horgan et al, 2009a), may introduce non-Lambertian properties to the dune surface that cause higher than expected slope values. Because of the method assumptions, the heights derived from slopes, are considered maximum values and are intended as exploratory data.

Secondary dunes

The secondary dunes are rounded, topographically-subdued features that extend nearly perpendicular to and are bound by the primary crestlines. Height profiles could not be extracted from these dunes using the photoclinometric method because the dune orientation is nearly parallel to the solar azimuth angle. Without a height profile, presence of a distinct stoss and lee slope cannot be determined from dune asymmetry, however, based upon ripple orientations the SE-facing slopes appear to be the lee slopes. Although these crestlines are not connected to each other, they typically align across the primary crestlines, giving rise to the reticulate pattern (Fig. 34A). The secondary dunes most commonly extend up the eastern slopes of the primary dunes, typically deflected southward as they approach the primary crestline and terminate where they intersect the crestline of the primary dunes (Fig. 34A). In contrast, the eastern terminations of the dunes are usually unattached to the primary crestlines and terminate at the base of the western, lee slopes of the primary dunes or within the interdune areas (Fig. 34). Less common are secondary crestlines that remain entirely unattached at both their eastern and western terminations (Fig. 34).

Slipfaces

The subdued appearance of the primary crestlines is broken quasi-periodically in the along-crest direction by scarps, which commonly form at the intersection of the secondary and primary crestlines (Fig. 34). These features are typically arcuate in shape, with a wider, steeper center that tapers in the along-crest directions. Similar features were described as elongate depressions by Feldman et al. (2008). Based upon the sharp brink, the striated appearance of the scarp surface and on evidence presented below that these features are transverse to one dominant wind direction, these scarps are interpreted to be depositional slipfaces.

The slipfaces themselves shallow downslope and terminate at a rampart (Fig. 35A-B), and beyond which, the dune slope is covered with degraded wind ripples (Figs. 34B). Grainflow, which would be expected on a depositional slipface, may be represented by the downslope-striated structures, but distinct grainflow lobes are not apparent possibly because they are (1) below the resolution of the image, (2) not recently active, or (3) indurated, eroded, and oversteepened.

Wind ripples

Ripples are omnipresent within the dune field except on the slipfaces and within the deflated interdune areas (Fig. 34B). The majority of the ripples appear well-organized with typical Y-junctions and continuous crestlines. The ripples change orientation in a systematic way related to their position on the primary and secondary dunes, which corresponds to the dune-induced secondary air-flow over the dune field (see below). Where the secondary air-flow patterns should intersect, the ripples are more discontinuous and ripple interference patterns appear.

Although nearly the entire dune field is covered with ripples, the ripples on the SE-facing slopes of the secondary dunes are the most active-appearing within the field (Figs.

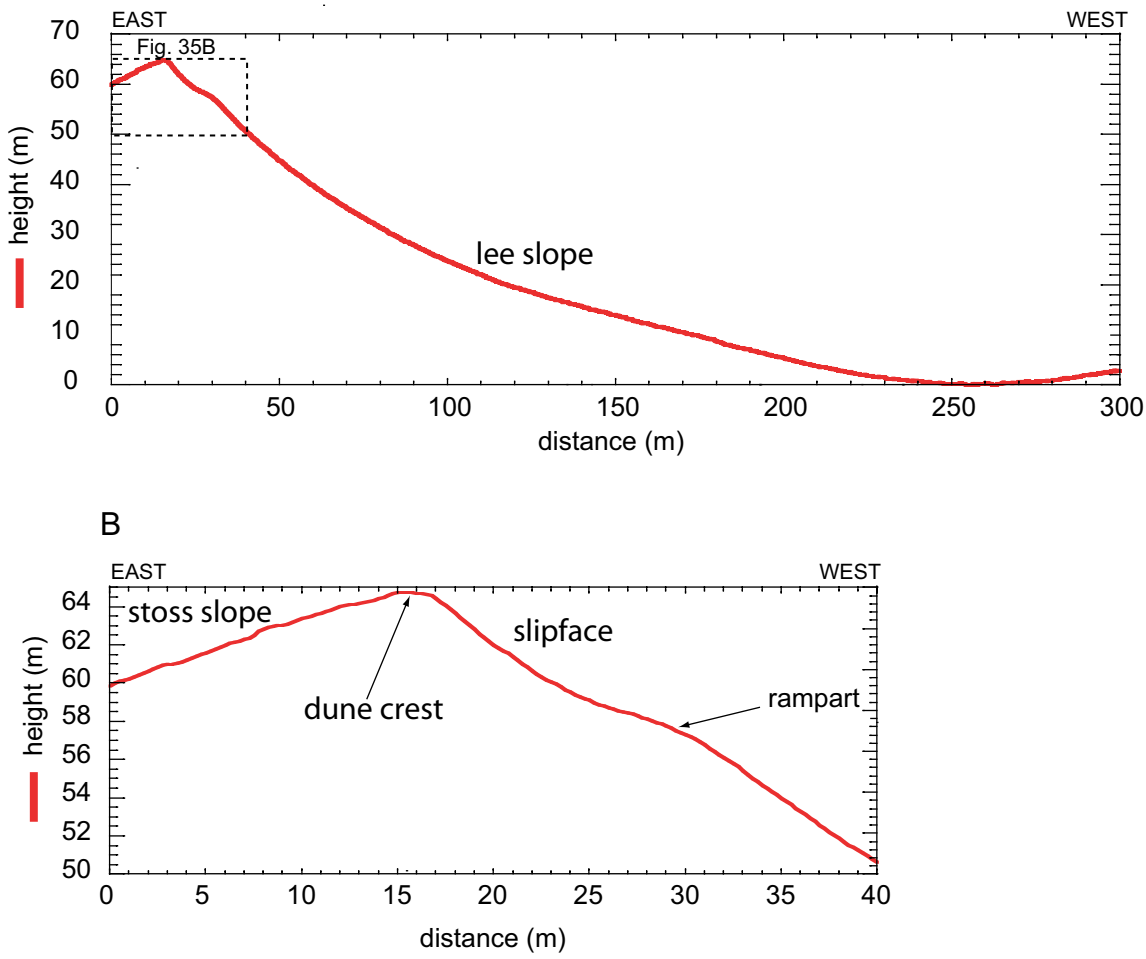

Figure 35. (A) Height profile across a primary dune crestline using a simplified photoclinometric method (location shown in Figs. 2, 7B) (see Bourke et al., 2006; Zimbleman, in press). The left Y-axis shows the dune height (thick, solid red line), which should be considered a maximum using this method (see text for discussion). The asymmetry of the dune suggests that the shallow-sloped E side is the stoss slope and that the steep, western slope is the lee. (B) shows that the slopes are steepest near the dune crest at the apparent slipfaces.

34B, 36A). These ripples are far more distinct and have more continuous crestlines than other ripples in the immediate area (Fig. 36A). In addition, ripples on the SE-facing slopes truncate surface fractures, which appear on the NW-facing slopes of the secondary dunes (Fig. 36A). In contrast, the wind ripples on the NW-facing slopes of the secondary dunes are subdued, discontinuous and truncated by the surface fractures (Fig. 36A). Feldman et al. (2008) interpreted similar surface fractures as indicators of the cohesion of the surface

sediments and tensional stresses related to the presence of subsurface ice.

The apparent greater mobility of the ripples on the SE-facing slopes of the secondary dunes may be related to the stability of the near-surface ground ice on Mars. Aharonson and Schorghofer (2006) show that the stability of near-surface ice the on Mars depends upon local slope. In the northern hemisphere, ice is more stable on N-facing slopes, which receive less sunlight than do the S-facing slopes. The SE-facing slopes of the secondary dunes appear to defrost earlier during the Martian spring (Fig. 36B-C), which is consistent with receiving greater amounts of sunlight, and in turn, less stable near-surface ice. If ice is the dominant dune-sediment cement, the near-surface sediment on the SE-facing slopes of the secondary crestlines would be available for aeolian transport for a greater percentage of the time than the surrounding sediment and may defrost to a greater depth, thus accounting for the apparent greater activity of ripples on these slopes. In contrast, the NW-facing slopes may remain mostly frozen and preferentially form the surface fractures. Feldman et al, 2008 also suggested that aspect-related high insolation receipts may explain the location of the H_20 minima in Olympia Undae as well as the formation of sublimation pits along dune crests.

Coarse-grained ripples

Ripples, which are more widely spaced than the ubiquitous wind ripples, occur within the interdune areas between the primary crestlines and on the E-facing slopes of primary dunes between secondary dunes (Figs. 34, 38C). These ripple crestlines display less variability in orientation and commonly deviate from the orientation of nearby smaller, wind ripples. On Earth, a scale separation in the size of wind ripples within the same area typically occurs because of a strongly bimodal grain-size population. The larger, more widely spaced ripples comprise the coarser fraction of sand and the surrounding smaller ripples comprise of the finer, more abundant sand fraction (Bagnold, 1941; Fryberger et al.,

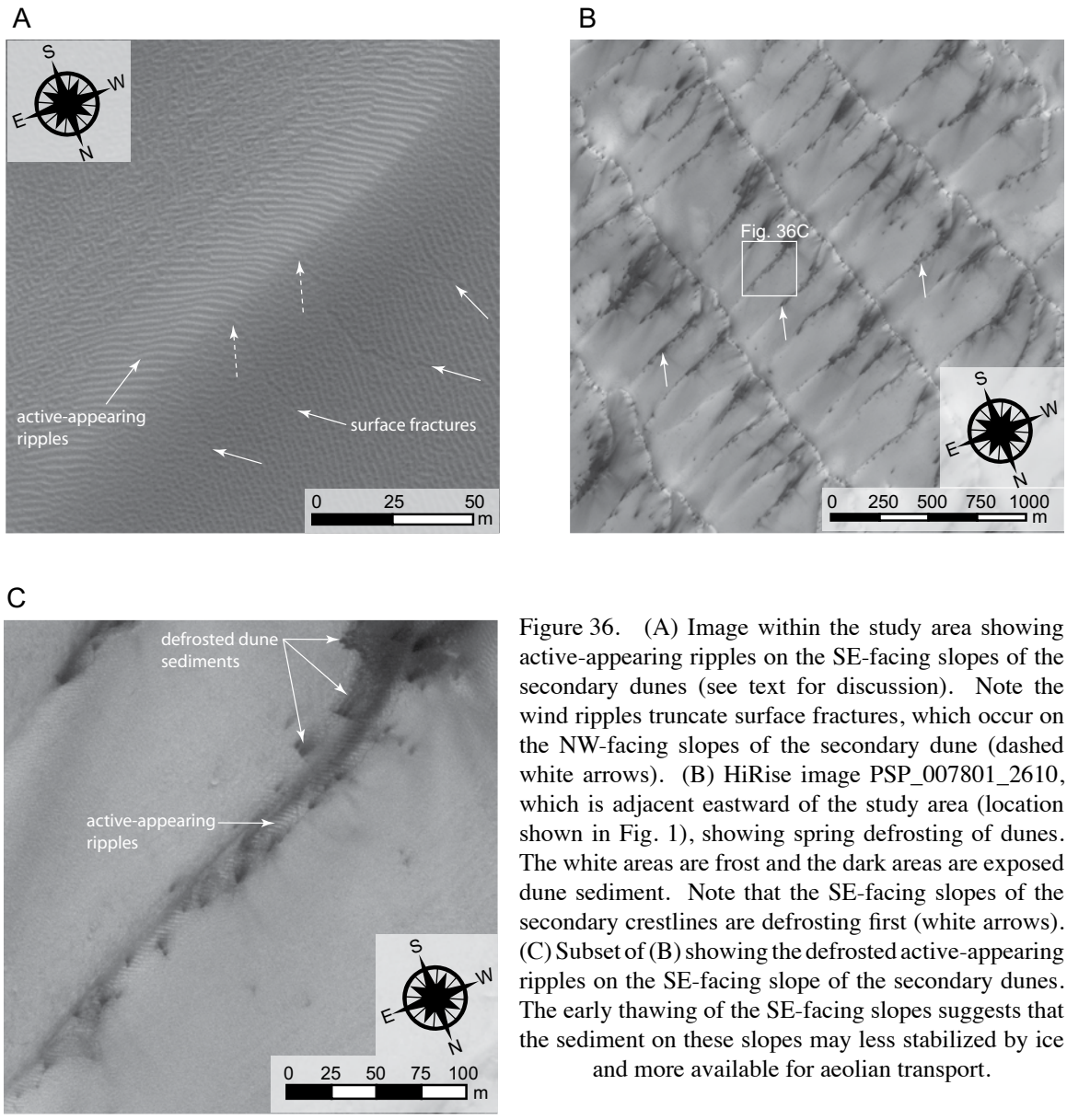

Figure 36. (A) Image within the study area showing active-appearing ripples on the SE-facing slopes of the secondary dunes (see text for discussion). Note the wind ripples truncate surface fractures, which occur on the NW-facing slopes of the secondary dune (dashed white arrows). (B) HiRise image PSP_007801_2610, which is adjacent eastward of the study area (location shown in Fig. 1), showing spring defrosting of dunes. The white areas are frost and the dark areas are exposed dune sediment. Note that the SE-facing slopes of the secondary crestlines are defrosting first (white arrows). (C) Subset of (B) showing the defrosted active-appearing ripples on the SE-facing slope of the secondary dunes. The early thawing of the SE-facing slopes suggests that the sediment on these slopes may less stabilized by ice and more available for aeolian transport.

1992; Jerolmack et al., 2006). The presence of two scales of ripple wavelengths, suggests a spatial sorting of the grains within this area of Olympia Undae. The concentration of coarser grains most likely represents a deflated lag where the finer grains have been removed.

Interdune areas

The interdune areas host a variety of geomorphic features related to the evolution of the dune field. Polygonal fractures are visible in many of the interdune areas and likely

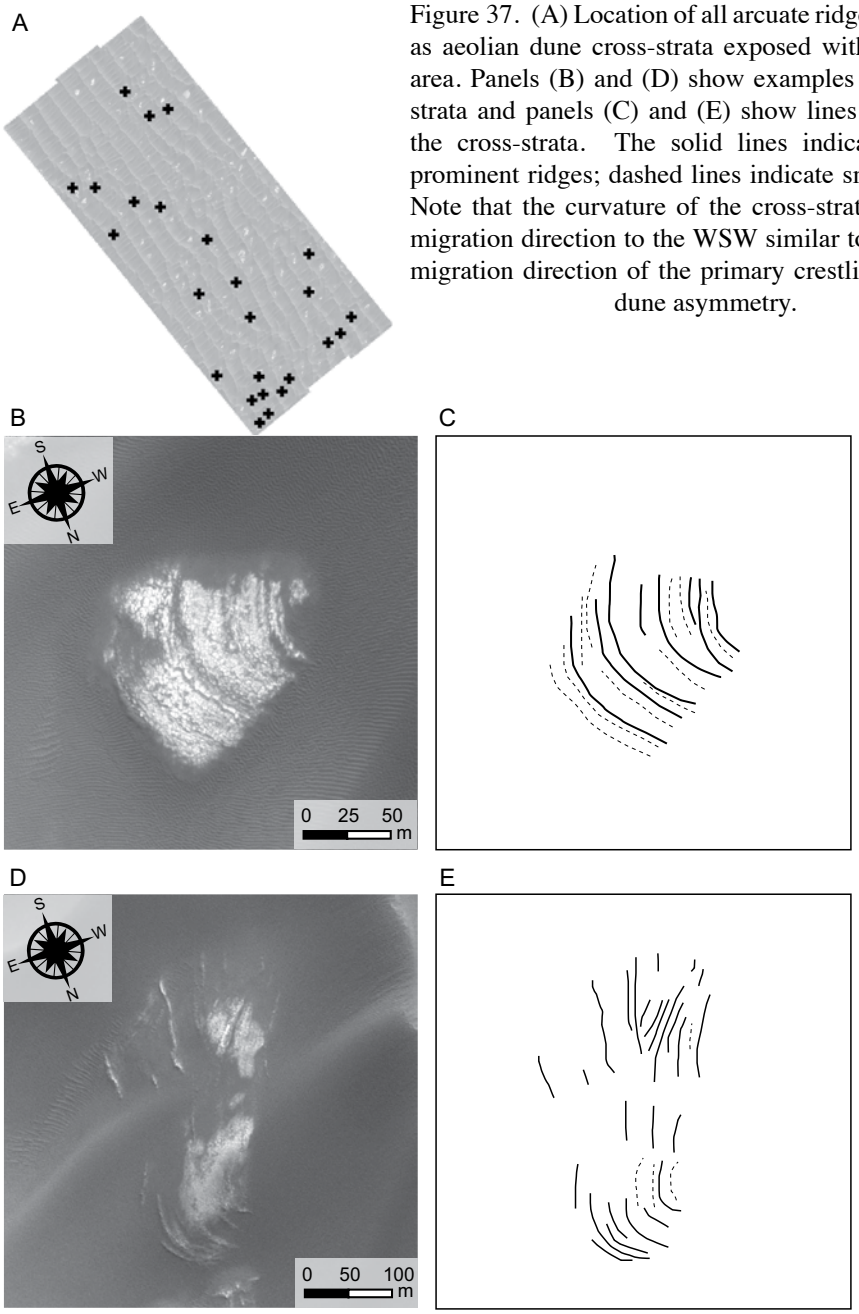

Figure 37. (A) Location of all arcuate ridges interpreted as aeolian dune cross-strata exposed within the study area. Panels (B) and (D) show examples of the cross-strata and panels (C) and (E) show lines traced along the cross-strata. The solid lines indicate the most prominent ridges; dashed lines indicate smaller ridges. Note that the curvature of the cross-strata indicates a migration direction to the WSW similar to the inferred migration direction of the primary crestlines based on dune asymmetry.

indicate the presence of ice (Feldman et al., 2008). Most notably, however, are the arcuate ridges (Fig. 37), which appear to consist of the same material as the underlying substrate and, in another location, have been interpreted as barchan dune cross-strata (Feldman et al., 2008). In the study area, these arcuate ridges can be clearly distinguished as large sets of aeolian dune cross-strata created by some type of crescentic dune (Fig. 37B-D).

Although the concave-westward curvature of the cross-strata indicates the dune migration was similar to the general, inferred migration direction of the primary dunes, as based upon their asymmetry (Fig. 35), the shape of the cross-strata does not match well with the crestline shape of the current dunes, indicating that the cross-strata are unrelated to the current generation of dunes. This suggests that the substrate exposed in the interdune areas is a deflationary sequence surface representing a previous dune constructional event and the current dune field represents a renewal of aeolian construction upon this surface. This interpretation is consistent with mapping of older stratigraphic units below the Olympia Undae dunes, including the Planum Boreum cavi unit (Tanaka et al., 2008).

METHODS

Every dune crestline and slipface brink and a representative sample of ripple crestlines were manually digitized from HiRISE image PSP_001432_2610 using geographical information system (GIS) software (Fig. 38). Dune and ripple crest spacing, crestline length, and defect density were measured using GIS. Defect density is $\varrho = N/L$, where ϱ is the defect density, N is the number of defect pairs (pairs of dune terminations) and L is the total crestline length within the field (Werner and Kocurek, 1999). Primary and secondary crestlines and slipfaces were digitized at a scale of 1:2000. Coarse-grained and fine-grained wind ripples were measured at 1:500. Crestlines that extend outside of the study area were not digitized. Where a break in the primary crestline occurs and is greater than ~50 m, the crestlines were terminated (see Fig. 34A). Breaks in the primary crestline were defined as portions of the crestline where the crest (i.e., a change from a positive to a negative slope) could not be clearly defined at the scale of digitization. Crestline breaks typically appear as troughs that off-set the trend of the primary crest, and coincide with the intersection of a secondary crestline and a slipface. Slipface brinks were measured as part of the primary crestlines, as well as analyzed individually.

Spacing was measured along transects perpendicular to the primary, secondary, coarse-grained and wind ripple crestlines. Spacing between slipfaces was measured as the distance from midpoint to midpoint of each slipface along the main crestline on which they occur. Defect density is a field-scale measurement and was determined for each set of crestlines. Dune, slipface and ripple crestline orientations were measured as straight lines between crestline terminations and plotted as rose diagrams. Because non-longitudinal line orientations near the pole may change significantly over relatively short distances, the azimuth orientation relative to north for lines greater than 500 m was calculated along 500 m line segments and averaged over the total number of line segments along the line. The maximum line orientation errors of a 500 m line between 79º and 83º degrees N latitude, which is the range of latitudes for the Olympia Undae Dune Field, are between ~0.05º and ~0.1º.

SPATIAL RELATIONSHIPS IN THE DUNE-FIELD PATTERN

Dune-field pattern measurements

The digitized primary and secondary dune crestlines are shown in Fig. 38A. Figure 38B shows the digitized crestlines overlain on a portion of the HiRISE image. Fig. 38C shows a sample of the digitized coarse-grained and ripple crestlines overlain on the HiRISE image. Measurements from these features are summarized in Table 1.

The distributions of dune and ripple crestline, and slipface brink lengths and spacing data were analyzed statistically using cumulative log-probability plots following the methods of Ewing et al. (2006) (Fig. 39A-B). This type of analysis provides a simple statistical basis by which the pattern morphologic features can be compared. Because of their distinct morphologic character (i.e., ripples, dunes and slipfaces), each feature was plotted as a separate population. In these plots, a single log-normally distributed population is represented by a straight-line segment of data (Sinclair, 1976). The median

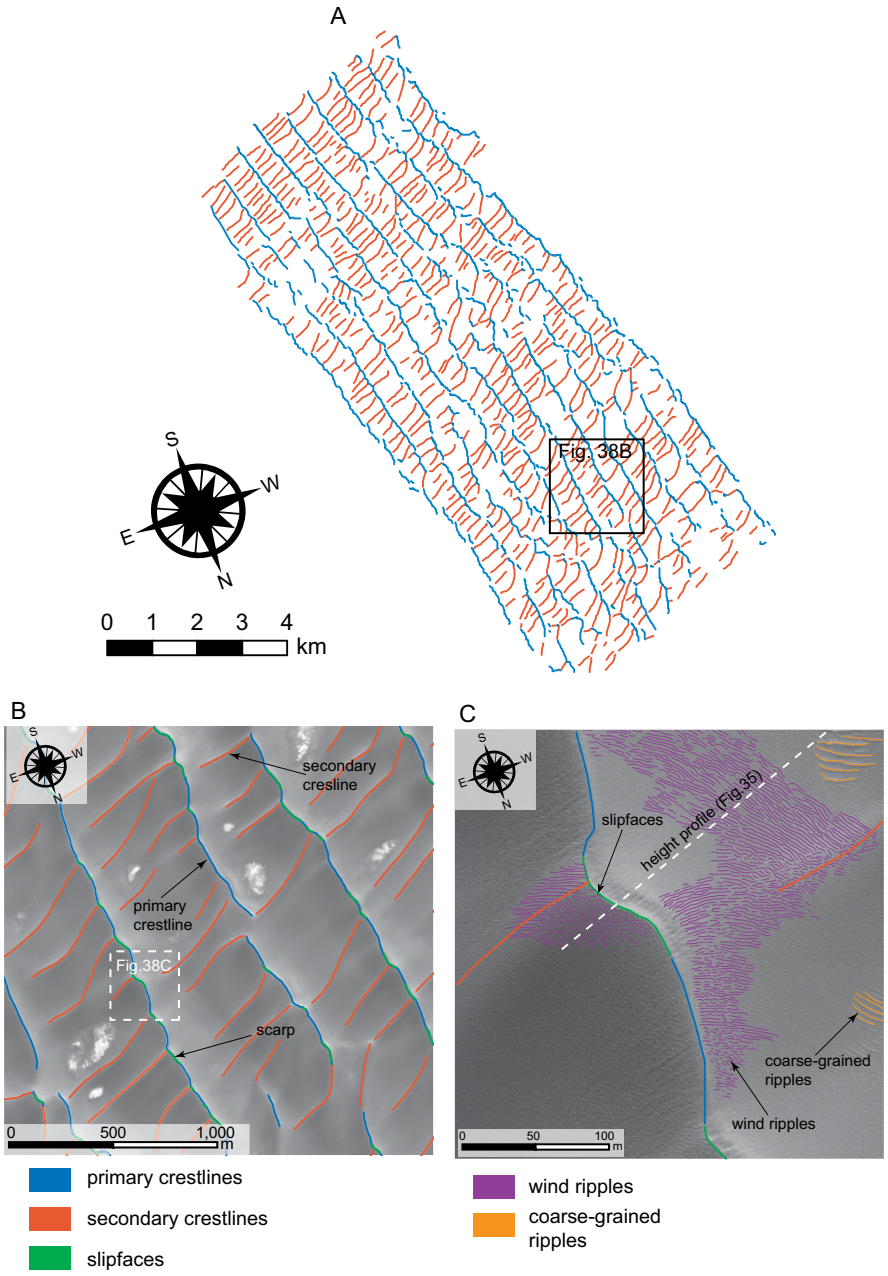

Figure 38. (A) Digitized primary dune and secondary dune crestlines and slipface brinks. (B) Digitized crestlines overlain on the study area HiRise image. Location image shown in (A). (C) Digitized coarse-grained and wind ripple crestlines overlain on inset of (B). Note the change in orientation of the ripples with respect to the topography of the primary and secondary crests.

value of the data is at the 50th percentile and the variability of the data is related by the slope of data trend, such that the lesser the slope the less variability. Numerically, the degree of variability in each population is related by the coefficient of variation, which is the ratio of

Table 2. Statistical summary of measure dune-field pattern parameters

	Primary crestlines	Secondary crestlines	Slipfaces	coarse-grained ripples	ripples
Crest length (m)					
count (n)	372	587	670	313	966
mean	360	386	62	28	10
median	217	389	52	27	6
std. dev.	425	153	40	12	11
coeff. var.	1.18	0.40	0.65	0.45	1.11
Spacing (m)					
count (n)	103	407	536	240	205
mean	637	215	199	5.6	2.1
median	640	187	187	4.9	2.2
std. dev.	133	89	93	2.6	0.5
coeff. var.	0.21	0.42	0.47	0.46	0.22
Defect density	0.0027	0.0026	0.016	0.035	0.099

the standard deviation over the mean ($C_v = \sigma / \mu$) (Table 1).

Figure 39A shows the cumulative log-frequency plots for the spacing data. The primary crestlines have the highest median and mean spacing values of all the data ($\mu_{primary}$ = 637 m) and the data plot as nearly a flat line, indicating a low degree of variability in the population. The secondary crestlines and the slipfaces have the same median spacing value at 187 m and overall nearly identical distributions of spacing values ($\mu_{secondary}$ = 215m, $\mu_{slipface}$ = 199 m). The coarse-grained ripple data show higher spacing values (μ_{coarse} = 5.6 m) and a higher degree of variability than the wind ripples (μ_{fine} = 2.1 m). All spacing data curves plot as a straight-line segments indicating these derive from a single log-normally distributed population, and each represents a separate population.

Figure 39B shows the cumulative log-frequency plots for crest length. Although the primary crestlines are the dominant morphologic feature in the study area and have a highly-organized and continuous appearance at the scale of the HiRISE image (Figs 34A, 38A), the crest lengths of the primary crestlines are highly variable, ranging over at least two

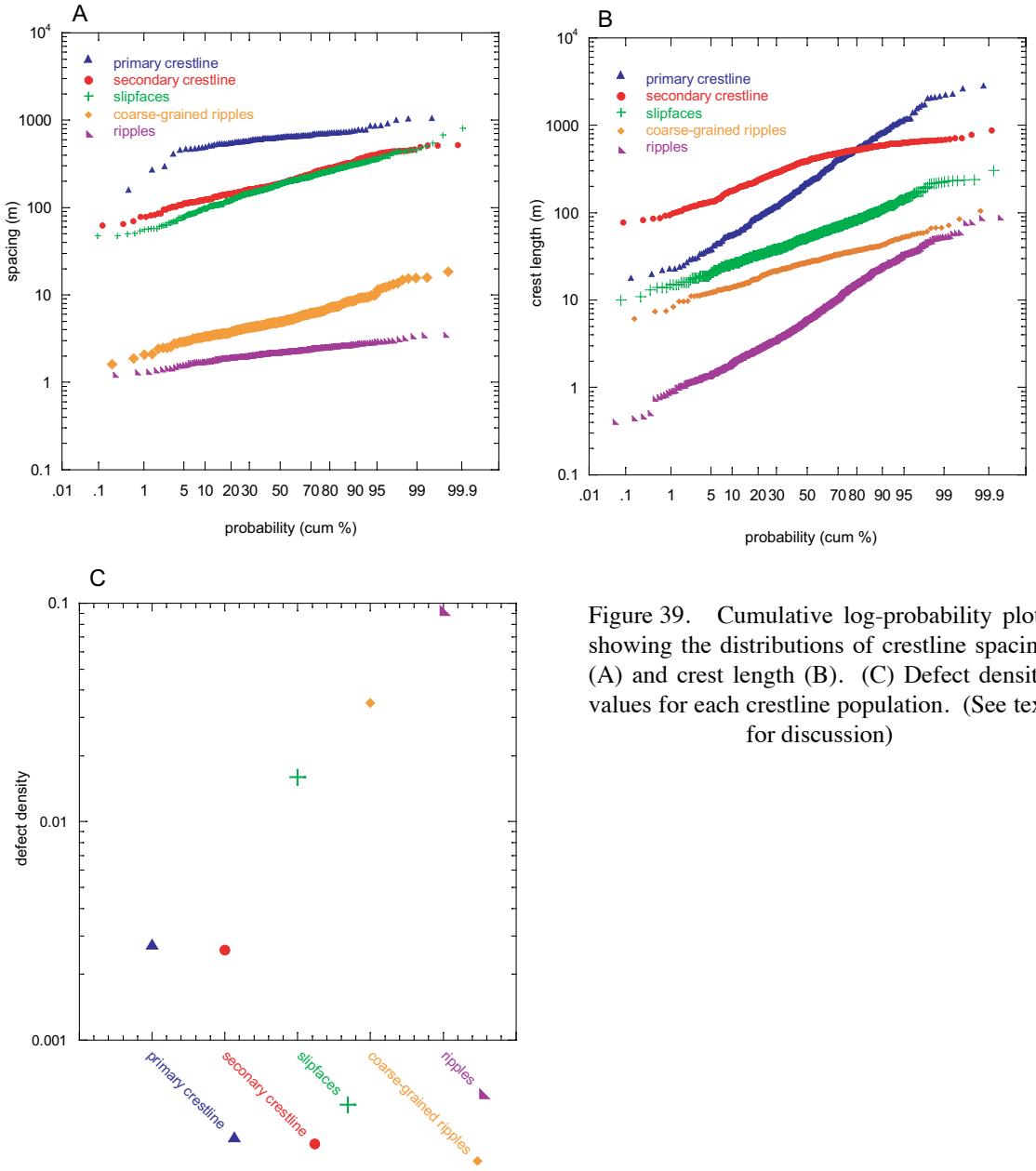

Figure 39. Cumulative log-probability plots showing the distributions of crestline spacing (A) and crest length (B). (C) Defect density values for each crestline population. (See text for discussion)

orders of magnitude ($\mu_{primary}$ = 360 m). At the lower range of values, the primary crestlines are disrupted by the secondary crestlines and slipfaces, which is apparent as breaks along the crestlines. At the higher range of values, greater crest lengths are not represented because they extend beyond the image. The secondary crestlines are less variable in length, and have median and mean values ($\mu_{secondary}$ = 386m), which are greater than that of the primary crestlines. The secondary crestline data are strongly top-truncated, which is indicated by

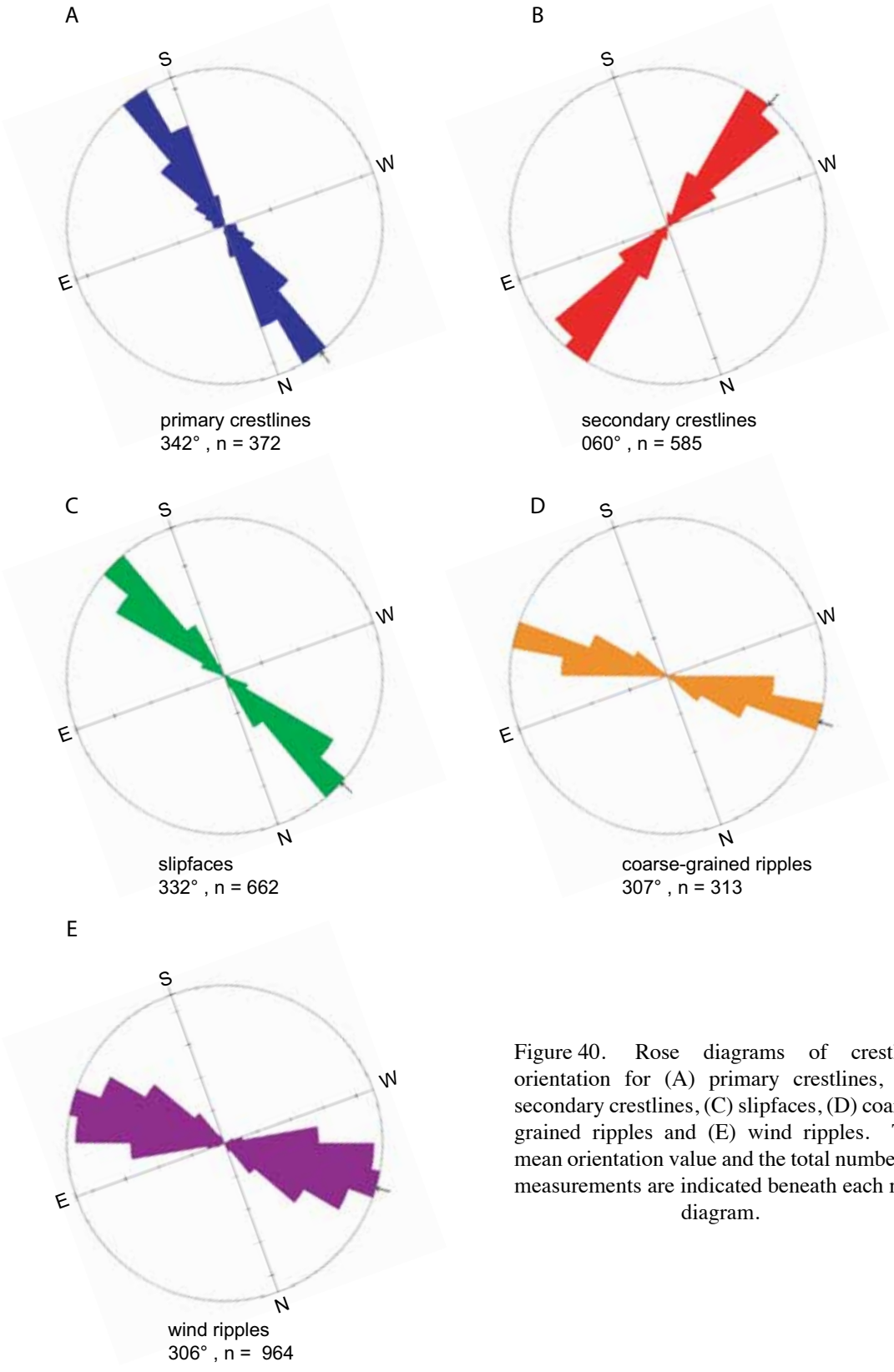

Figure 40. Rose diagrams of crestline orientation for (A) primary crestlines, (B) secondary crestlines, (C) slipfaces, (D) coarse-grained ripples and (E) wind ripples. The mean orientation value and the total number of measurements are indicated beneath each rose diagram.

the flattening of the data curve at the higher values. The top truncation of the data values may arise because the distribution of the secondary crest-length population is approaching a uniform distribution, which on this plot type creates a strongly top-truncated data curve. The slipface brink lengths ($\mu_{slipface}$ = 62 m) and coarse-grained ripples (μ_{coarse} = 28 m) show a moderate degree of variability, whereas the ripple crestline lengths (μ_{fine} = 10 m) is highly variable, ranging over two orders of magnitude.

Figure 39C shows the defect density for each crestline population. The primary crestlines ($\varrho_{primary}$ = 0.0027) and the secondary crestlines ($\varrho_{secondary}$ = 0.0026) show nearly the same values. The coarse-grained ripples (ϱ_{coarse} = 0.035) have a lower defect density than the wind ripples (ϱ_{fine} = 0.099), and the values of the slipfaces ($\varrho_{slipface}$ = 0.16) fall below the coarse-grained ripples and above the primary crestlines.

Figure 40A-E shows the range of dune and ripple crestline and slipface orientations as rose diagrams. The orientation values are reported relative to north. The orientations of the primary (342°) and secondary (060°) crestlines are nearly perpendicular. The slipface orientations (332°) trend closely with the primary crestlines. Although locally different, the mean trends of the coarse-grained ripples (307°) and fine-grained ripples (306°) are the same, indicating formation in the same wind regime and supportive of the interpretation that they represent a lagged concentration of coarse grains.

Spatial and geomorphic relationships of the pattern

The measured spatial relationships in the pattern variables along with geomorphic evidence indicate that: (1) the primary dunes are older and less active than the secondary dunes, (2) the secondary dunes and slipfaces co-evolved, (3) the secondary dunes and slipfaces are breaking up the primary dune pattern, and (4) the spacing between the primary dunes is an areal-limit boundary condition to the evolution of the secondary dunes.

The primary dunes have the greatest mean spacing and a very narrow range of

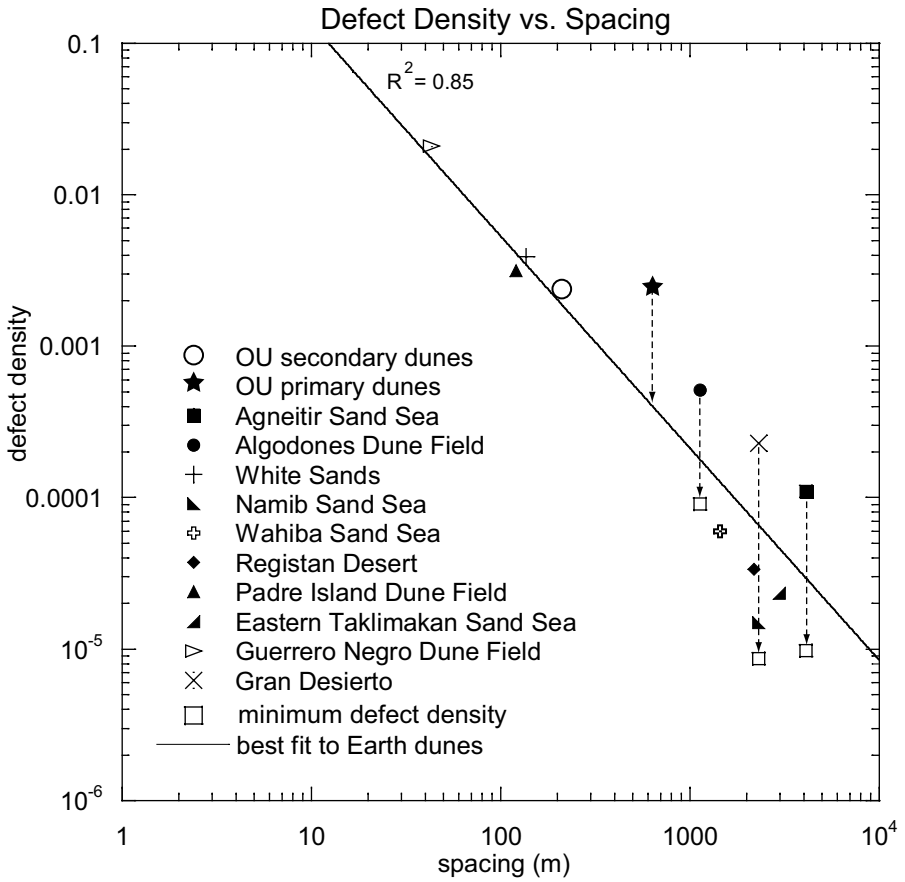

Figure 41. Plot showing the defect density versus the spacing for 10 dune fields on Earth and the primary and secondary dunes measured in the Olympia Undae Dune Field (OU). The open boxes represent the minimum defect density calculated from relict dune-field areas (see Ewing and Kocurek, in press) and these are connected with present field defect density by dashed arrows. The dashed arrows correlate the dune field with the minimum defect density for the dune fields on Earth. For OU the defect density is similarly too high for the crest spacing indicating that the primary dune pattern is being broken up. Note the defect density and spacing for the secondary dunes falls along the trend with the other dune-field patterns.

spacing values, which suggests these dunes are highly evolved and represent the oldest pattern in the study area (Ewing et al., 2006). In contrast, the range of primary dune crest lengths spans at least two orders of magnitude, which is reflected in the relatively high defect density. This contrasting state of pattern organization (i.e., spacing versus crest length and defect density) is well illustrated in Fig. 41, in which defect density is greater than expected for dunes with this spacing. By analog with Earth examples (Ewing and Kocurek, in press), the greater defect density occurs as the primary dunes are reworked and

segmented, as evident in Fig.s 34A and 38A.

The nearly identical distributions of the secondary dune and slipface spacing measurements suggest that the formation of these features is related (Fig. 39A), an interpretation supported by geomorphic observations. (1) Slipfaces typically occur where the western terminations of the secondary dunes intersect the primary dune crestlines (Fig. 34A-B). (2) The eastern terminations of the secondary dunes typically occur below a slipface (Fig. 34A-B). (3) The secondary crestlines and slipfaces typically align across the primary crestlines (Fig. 34A-B). The measurements and observations reasonably argue that the intersection of the secondary dunes with the primary crestlines causes the slipfaces to develop and the development of a slipface initiates the development of a secondary crestline in the lee of the primary dunes. In both cases, the development of the slipfaces and the secondary crestlines is breaking up the primary crestlines.

The values within the top-truncated portion of the secondary dune crest length population are nearly the same as the mean spacing of the primary dunes (Fig. 39A-B). This relationship suggests that the primary dune spacing creates an areal limit on the crest length development of the secondary dunes (Ewing and Kocurek, in press). The top truncation and the uniform distribution arise because the secondary dunes can only grow to the limit of the spacing between the primary dune crestlines, which creates a population in which the secondary dune crest lengths are the same as primary dune spacing. This relationship provides additional evidence that the secondary dunes are younger features than the primary crestlines, and is consistent with the secondary dunes breaking up the primary dune crests.

Overall, the dune-field pattern is best described as a complex pattern. The primary dunes emerged first, and during a later episode of pattern construction, the secondary dune pattern developed. The highly-organized state of the primary pattern suggests that it developed during a period in which more sediment was available for aeolian transport (i.e.,

the dunes were less stabilized), whereas the secondary pattern appears to have developed in a low sediment-availability environment following the stabilization of the primary pattern.

Determination of wind regimes

Given the geomorphic evidence of a complex pattern, within what wind regimes did the pattern arise? What is the most recent wind and does it relate to the pattern formation?

Determination of most recent flow fields

Given a crestline orientation determined by the overall wind regime (i.e., the gross bedform-normal orientation) the winds at any one time may strike the crestline at any angle, defining the incidence angle. A sinuous crestline on a single dune provides a spectrum of incidence angles for a given primary wind. Incidence angles have been defined as transverse (70-90^{o}), longitudinal (0-10^{o}) or oblique (10-70^{o}) (Sweet & Kocurek, 1990). These incidence angles each define a characteristic secondary flow configuration on the lee face, which is also a function of dune morphology and, to a lesser extent, atmospheric stability (Sweet & Kocurek, 1990; Walker & Nickling, 2003). With a longitudinal configuration, flow is attached and transport is along-slope. As the incidence angle becomes greater (i.e., oblique) the lee flow is deflected to blow along-slope, followed by flow separation in the form of a 3-D vortex with components of along-slope and reversed flow (e.g., Allen, 1982). A 2-D roller with a crest-normal return flow occurs as the incidence angle approaches 90^{o}.

In turn, the characteristic flow configurations give rise to specific surface processes and resultant lee-face surface features (Hunter, 1977): (1) grainfall in which grains blown passed the brink settle to the surface in paths modified by turbulence (Nickling et al., 2002), (2) grainflow or avalanching of the depositional grainfall, and (3) wind ripples. Grainfall and grainflow are gravity-driven processes and their exclusive presence is indicative of a transverse flow configuration where there is a general absence of tractional transport. Ripples are indicative of a flow configuration where tractional transport dominates,

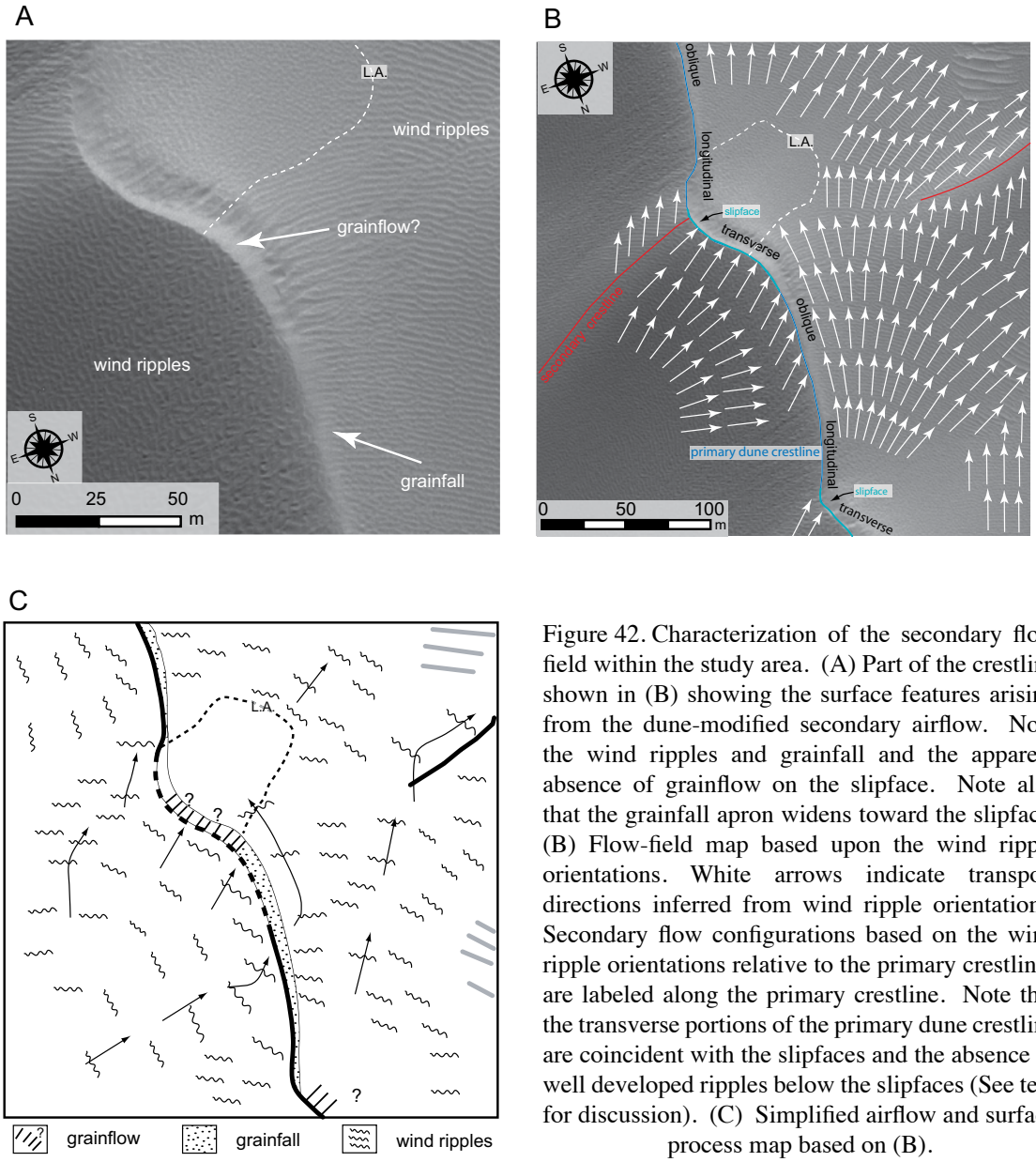

Figure 42. Characterization of the secondary flow field within the study area. (A) Part of the crestline shown in (B) showing the surface features arising from the dune-modified secondary airflow. Note the wind ripples and grainfall and the apparent absence of grainflow on the slipface. Note also that the grainfall apron widens toward the slipface. (B) Flow-field map based upon the wind ripple orientations. White arrows indicate transport directions inferred from wind ripple orientations. Secondary flow configurations based on the wind ripple orientations relative to the primary crestlines are labeled along the primary crestline. Note that the transverse portions of the primary dune crestline are coincident with the slipfaces and the absence of well developed ripples below the slipfaces (See text for discussion). (C) Simplified airflow and surface process map based on (B).

becoming increasingly prominent with decreasing incidence angle. Lee ripples have crests oriented parallel to the dip of the lee face as a function of along-slope transport and gravity (Howard, 1977). With oblique flow conditions both grainfall/grainflow and wind ripples can occur, depending upon the spatial dominance of gravity-driven versus tractional transport. Typically gravity-dominated processes on the upper lee face yield downslope to ripples migrating along-slope where tractional transport dominates. In total, lee-face

surface features are robust indicators of local flow condition as a function of the incidence angle.

Using the robust relationship between the dune-modified secondary flow and the resulting surface features, the flow fields within a representative area of the study area were mapped (Fig. 42A-C). Wind ripples are the clearest indicator of secondary flow and are used as the primary means to interpret the transport direction, although some evidence of grainfall is apparent. Figure 42A shows the different surface features apparent along a portion of the crestline shown in Fig. 42B. In Fig. 42A, wind ripples on the stoss slope become progressively more discontinuous and degraded as they approach the primary dune crestline, except where they occur along the SE-facing slope of the secondary dune where the ripples are continuous and more active in appearance (see above). Ripples in the immediate lee of the primary dune slipfaces appear mottled and discontinuous, whereas ripples in the lee the crestline to the N and S of the slipface are clearly defined and continuous. Evidence of grainfall appears as a bright dusting along the western side of the primary crest that obscures the eastern terminations of the wind ripples that appear downslope. The grainfall apron widens along-slope southward until it merges with the slipface. The presence of ripples above the slipface and a grainfall apron that widens toward the slipface suggest grainflow should be present on the slipface, however, the slipface face in Fig. 42A appears smooth with no clear evidence any surface features.

The secondary flow configuration interpreted from the ripple crestlines and the occurrence of grainfall (Fig. 38C; Fig 42A) is shown in Fig. 42B, with the generalized flow field illustrated in Fig. 42C. The flow configuration consists of a primary flow from the NE with modified secondary flow over the dune topography. In Fig. 42B, flow emerging from a hollow lower on the stoss slope is deflected to the SW in the direction of the primary flow as it approaches the primary crest. At the crest, flow is transverse to the slipface orientation, and longitudinal and oblique along areas without a slipface. In the lee of the

longitudinal and oblique areas, the SW flow is deflected S. Approximately 80 m W of this area flow recovers to the primary SW flow direction. At the transition from longitudinal to oblique flow, the grainfall apron appears. Although no clear flow direction could be determined in the lee of the slipface, ~80 m SW of the slipface, flow recovers to the SW, indicating the line of attachment for this separated flow. SW flow crossing the secondary dune crestline is deflected W and contours along the S-facing slope until reaching the next downwind primary crestline. Overall, the structure of the secondary airflow through the field is governed by the primary and secondary dunes and indicates that the last transporting wind must have blown from the NE to SW.

The distance from the crestline to the point where the airflow recovers to the primary flow direction depends largely upon dune height and incident angle (Sweet and Kocurek, 1990). In aeolian systems for both transverse and oblique flows, this distance is 4-8 dune heights downwind of the crest, which corresponds to estimates in fluvial systems (McLean and Smith, 1986) and estimates on Mars (Bourke et al., 2004). Using this measure, the estimated dune height of the primary dune at this location would be between 10 m and 20 m high.

Field-scale flow

In order to constrain the prevailing wind direction during the last transport event, flow fields were mapped over multiple dunes in the study area and in HiRISE image PSP_009971_2785, which is 10 km north of the study area (Figs. 32, 43C). Line segments were mapped perpendicular to the ripple orientations along multiple transects from the NE to the SW throughout each area (Fig. 43A-D). Fig. 43A shows 8 flow-path transects across the center portion of the study area. Areas outside the center of the image have a degraded spatial resolution and determining the ripple orientation was not possible. The consistent orientation of the paths shows that the general direction of transport is from the NE to the

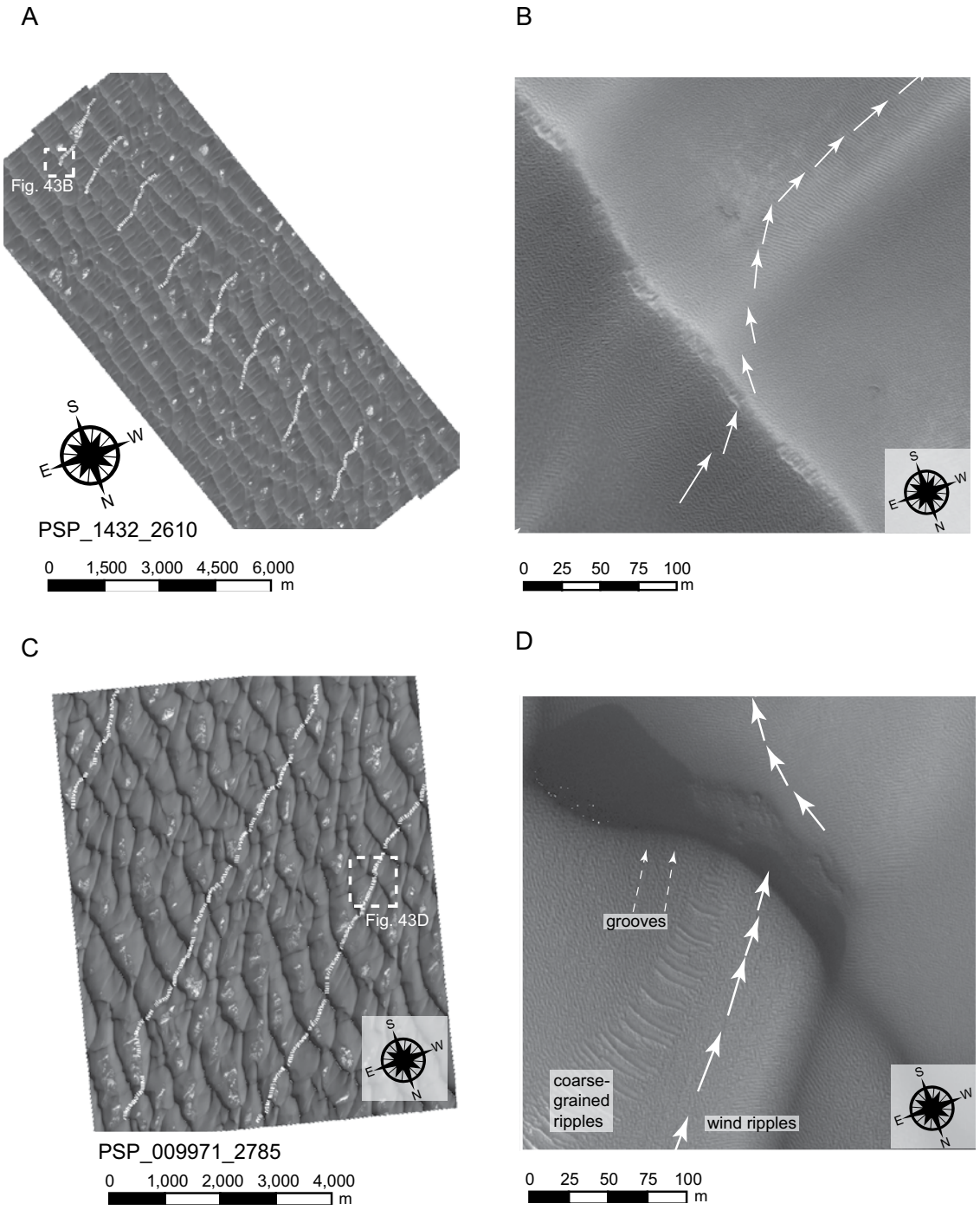

Figure 43. Field-scale flow pathways mapped by ripple orientation along transects from the NE to the SW. (A) Eight flow pathway transects mapped across the center of the study area. (B) Inset showing the flow pathway across a primary and secondary dune crestline within the study area. Location indicated on (A). (C) Three flow pathway transects mapped on HiRise image PSP_009971_2785, which lies 10 km N of the study area. Lighting is from 044° W (D) Inset of (C) showing the transport across a crestline. Note the transport direction is perpendicular to the wind ripples, coarse-grained ripples and parallel to erosional grooves in the dune slope (dashed white arrows).

SW, which is in agreement with the detailed mapping discussed above. Fig. 43B shows that the transport pathways through the dune field are controlled by the topography of the primary and secondary crestlines.

Although the dune-field pattern in HiRISE image PSP_009971_2785 is different from the study area, the flow paths indicate that transport is toward the SW, as in the study area. The inset image, Fig. 43D, shows the alignment of ripples, coarse-grained ripples and grooved features on the stoss slopes in the transport direction. The grooved features are more apparent in this area than in the study area to the south and have been interpreted as erosion of an indurated surface by aeolian abrasion and plucking (Horgan et al., 2009b).

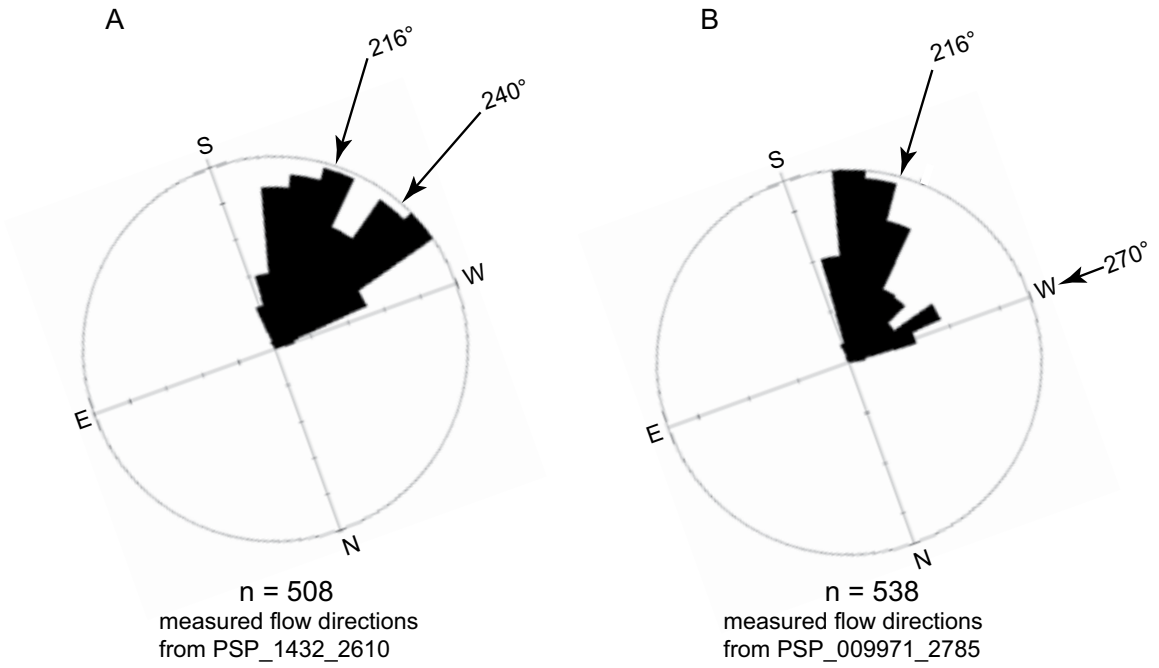

Figure 44. Rose diagrams of the transport directions mapped in (A) the study area and (B) HiRiSE image PSP_009971_2785. In (A) the mode at 216° is perpendicular to the measured ripple and coarse grained ripple orientation (see Fig. 40) and the mode at 240° is parallel to the orientation of the secondary dunes. In (B) a dominate mode occurs near 216° and a subordinate mode near 270°. The consistency of the transport direction toward 216° suggests the last significant transporting wind was from the NE at ~036°.

Flow-path vectors from the study area and HiRISE PSP_009971_2785 were plotted on separate rose diagrams to determine the transport direction of the winds that created the ripples (Fig. 44). Fig. 44A shows a bimodal distribution of transport vectors for the study area. One mode is near 216°, which is perpendicular to the average ripple orientation of 306° (Fig. 39E). Another mode occurs near 240°, which parallels the orientation of the secondary crestlines and reflects the transport along the lee-slope these crests. The two modes reflect the typical transport pathway shown in Fig. 43B. Fig. 44B shows the transport vectors for HiRISE image PSP_009971_2785. A dominate mode occurs near 216° and a much smaller mode occurs near 270°.

Although the transport directions reflect a range of dune-modified airflow, the consistency of transport toward the SW, near 216°, in both areas suggests the last significant transporting wind blew from the NE, ~ 036°.

Pattern construction

Pattern constructional winds

Theory, models (Tyler and Barnes, 2005) and empirical data (Tsoar et al., 1979; Howard, 2000; Langevin et al., 2005; Tanaka and Hayward, 2008) indicate circum-polar easterly winds are a persistent and dominant part of the wind regime around the residual polar ice cap. Although crestline orientation does not necessarily indicate the primary wind direction, the well-organized N-S oriented crestlines of the primary dune pattern (342°) and the above evidence reasonably argue that the primary dune pattern formed transverse to a circum-polar easterly wind. The influence of the NE wind is not apparent in the older pattern and is not needed to most simply explain the primary dune pattern. Within the study area an easterly wind transverse to the orientation of the primary dunes would be an ENE wind (072°).

In contrast to the simplicity of the primary dune pattern, the secondary crestlines

(060°) are highly oblique to the NE (036°) wind and longitudinal to the ENE (072°) wind. Neither of the winds alone well explain the orientation of the secondary crestline. However, the secondary crestlines can be well explained as longitudinal elements to the resultant transport direction between both winds, depending on the relative magnitude of each wind (i.e., the R value in gross-bedform normal transport; Rubin and Hunter, 1987). The secondary crestlines are longitudinal to the resultant between the ENE (072°) and NE (036°) winds, in which the ENE (072°) has a relative magnitude ~2x greater than the NE (036°) wind.

The NE wind appears to be related to katabatic winds descending Planum Boreum, which become deflected by Coriolis forcing. Katabatic winds refer to down-slope winds. Over large ice-sheets such as Greenland and Antarctica, katabatic winds arise from radiational cooling of the ice, which creates strong horizontal pressure gradients between the upland, ice-covered areas and the basinward ice-free area that, along with gravity, drive the cool, dense winds down-slope (Parish, 1988). Similarly, in the north polar region of Mars, katabatic winds are thought to arise from the contrast between the elevated, high-albedo Planum Boreum ice cap and relatively lower-albedo surrounding terrain (Tsoar et al., 1979; Siili et al., 1997; Howard, 2000). This contrast is thought to be particularly strong during the Martian summer in Olympia Undae when the expanses of low-albedo sands are frost free and warmer than the residual ice cap (Tsoar et al., 1979; Silli, 1997, Tyler and Barnes, 2005).

Howard (2000) mapped frost streaks on the Planum Boreum as indicators of katabatic winds and found that katabatic winds follow topography, draining into the major chasmae and re-entrants of Planum Boreum (see Fig. 1, Howard, 2000). The convergence of katabatic winds within the major drainages is thought to create strong winds, which erode the scarps and layered deposits, and over the long-term, may be a primary mechanism by which the re-entrants evolve. Sediment produced from the erosion of the layered deposits

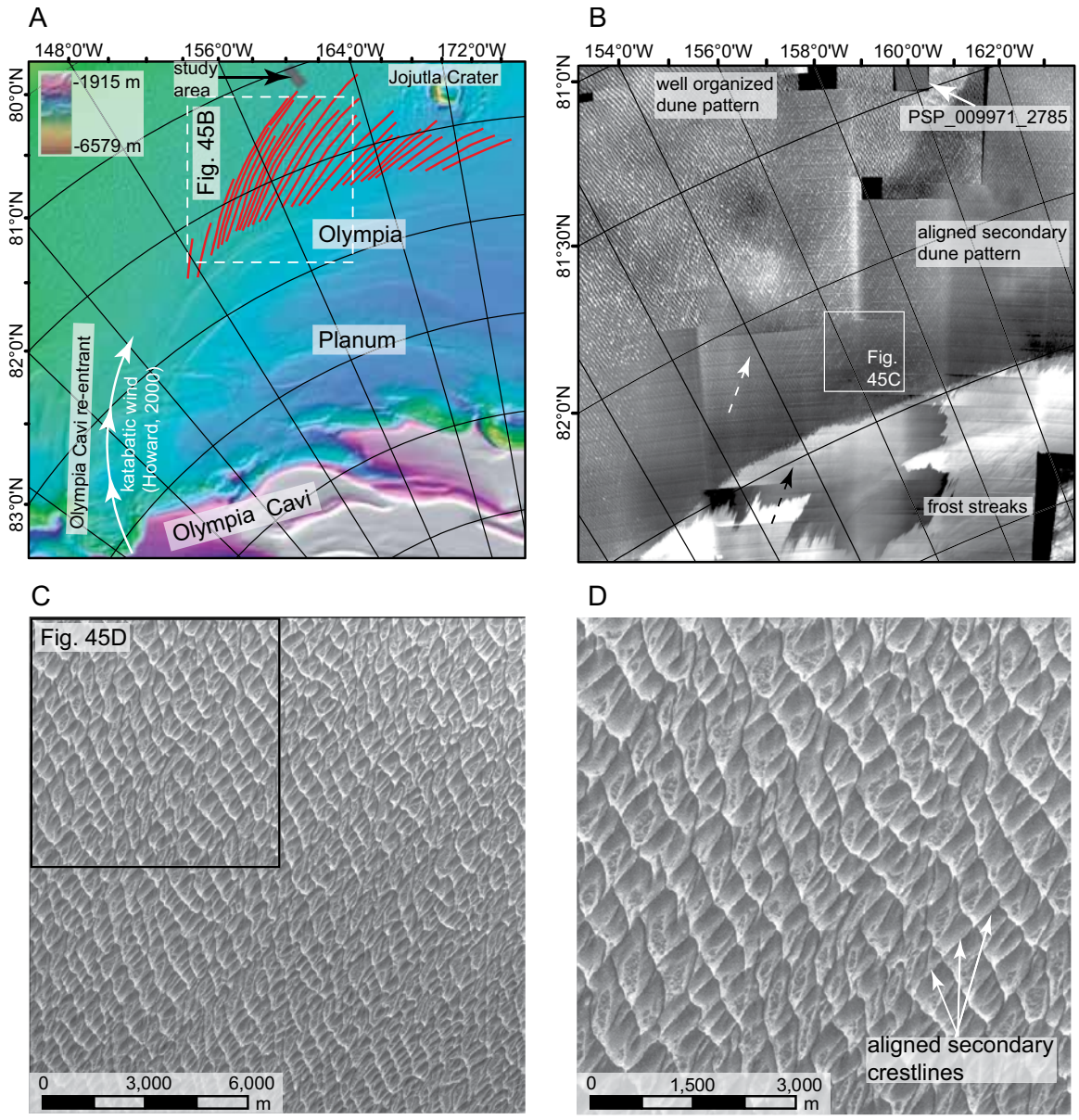

Figure 45. Regional-scale view of the center of the Olympia Undae Dune Field showing an E-W change in the dune-field pattern attributed to katabatic winds emerging from the Olympia Cavi re-entrant. (A) MOLA DEM with the trends of the secondary crestlines (red) mapped from the Themis mosaic shown in (B). The white arrows denote the trend of the katabatic winds mapped from frost streaks by Howard (2000). (B) Themis mosaic showing the E-W change in the dune-field pattern from well-organized crescentic dunes in the E of the re-entrant to a aligned secondary dune pattern to the west. Note the alignment of the frost streaks on the planum (noted by the black dashed arrow) with the secondary crestlines (dashed white arrow) in the dune field. (C) Context Camera (CTX) image of subset located in (B) showing the well aligned secondary crestlines and an overall star-dune type pattern. Note the prominence of the secondary crestlines is equal to that of the primary crestlines, whereas in the study area the secondary crestlines are more subdued. (D) Context Camera (CTX) image subset shown in (C) showing in detail the star-dune nature of the pattern.

is thought to provide sediment to dune fields, which are typically outboard of the re-entrants (Howard, 2000; Tanaka et al., 2008). A large re-entrant that extends from the Olympia Cavi escarpment connects Olympia Undae with Planum Boreum and is thought to be a primary drainage of katabatic winds (Fig. 45).

Katabatic winds are apparent at the field-scale by a distinct E to W spatial change in the dune-field pattern (Fig. 45). Westward of the re-entrant that connects the Olympia Cavi escarpment with Olympia Undae the secondary crestlines are strongly aligned, arcing out from the base of the Olympia Planum into the field center (Fig. 45A-B) Eastward the primary dunes are dominant and appear as well-organized crescentic dunes (Fig. 45A-B). The secondary crestlines are as prominent as the primary crestlines closer to Planum Boreum (Fig. 45C-D) but become subdued features southward into the field center, as with the secondary crestlines in the study area.

Mapping the orientation of the secondary crestlines from the re-entrant westward and from the northern margin of the field to the study area (Fig. 45A) shows that the orientations of the secondary crestlines range from ~40° at the mouth of the re-entrant to ~80° just north of Jojutla Crater (Fig. 46). Whereas the secondary crestline orientations are more dependent on the distance westward from the re-entrant rather than the distance from the base of Olympia Planum (Fig. 46), the prominence of the secondary crestline depends on distance from Planum Boreum. At the field-scale, the alignment and orientation of the secondary dunes appears to reflect the influence of katabatic winds draining from the Olympia Cavi re-entrant that are deflected westward around the base of the elevated, northern part Olympia Planum by Coriolis forcing. The waning prominence of the crestlines southward indicates that the katabatic winds decrease in intensity outward from the Olympia Planum.

Overall, the katabatic winds appear to be the most recent winds and related to the development of the second generation of dunes within the Olympia Undae Dune Field.

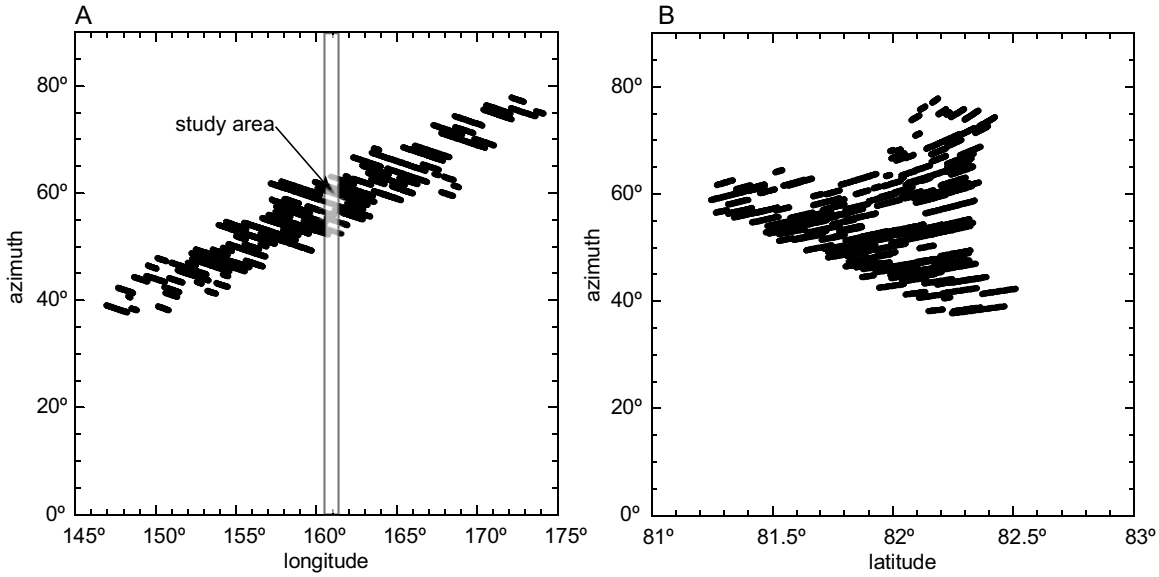

Figure 46. Azimuth vs. (A) longitude and (B) latitude plots showing the change in the orientation of the aligned secondary crests westward of the mouth of the Olympia Cavi re-entrant. The change in orientation is well-correlated to the distance west of the re-entrant (A), whereas it is poorly correlated with the distance south (B) from Planum Boreum. The location of the study area is indicated in (A).

The appearance of these winds as an influence on the dune-field pattern may have initiated with the erosion and retreat of the Olympia Cavi re-entrant. The development of this re-entrant would have channeled katabatic winds descending Planum Boreum, as well as injected into Olympia Undae a new supply of sediment derived from the erosion of the sedimentary units underlying Planum Boreum.

Crestline dynamics during constructional winds

Mapping incident angles and the resulting secondary flow patterns (c.f., Sweet and Kocurek, 1990) between the primary dune crestline and the NE wind and the ENE wind, provide a basis for a model of the development of the secondary crestline pattern and the current state of dune-field evolution. Figure 47A shows three slipfaces along a primary crestline with the secondary flow configuration shown for the NE wind. The center slipface is shown in more detail in Fig. 42A-B. The most developed areas of the

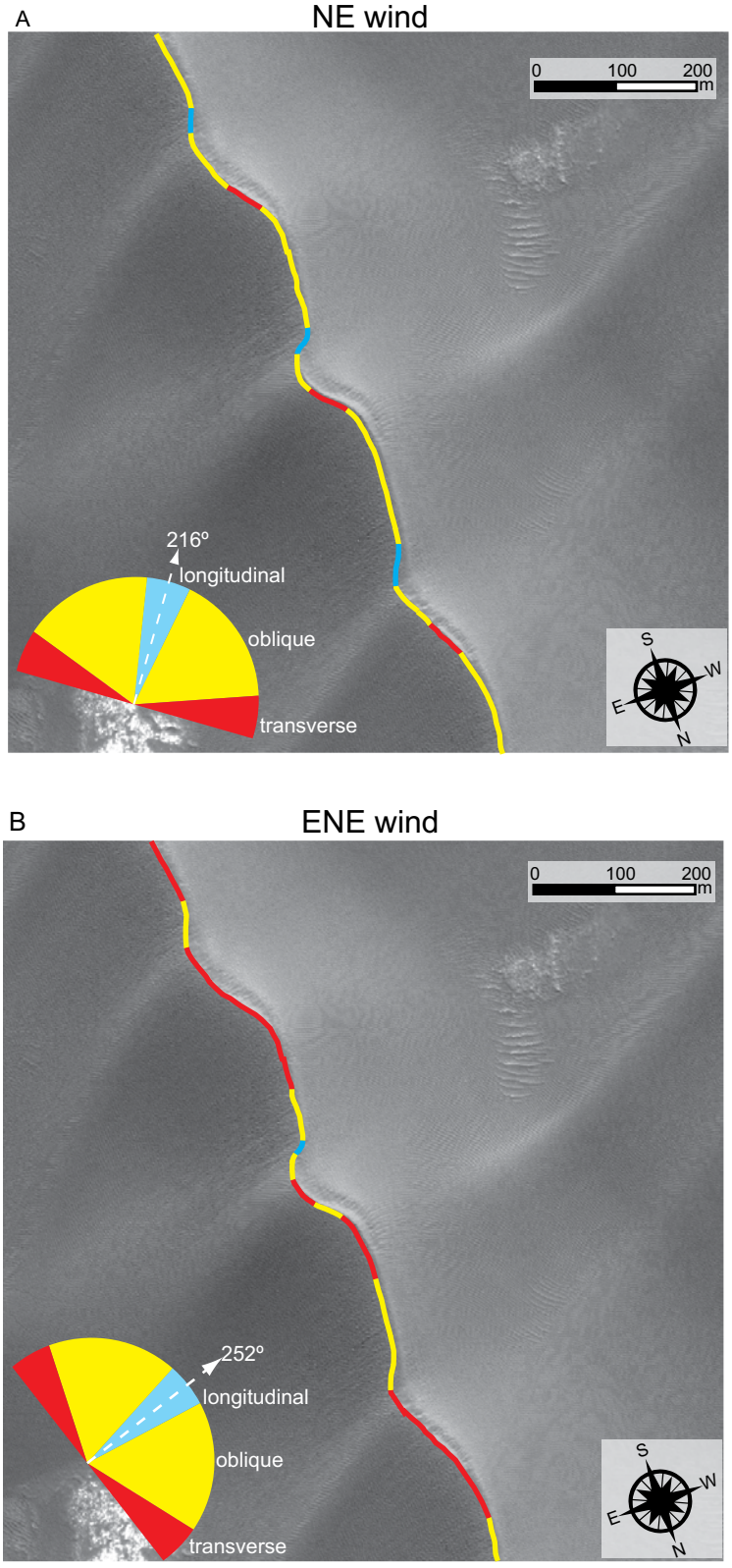

Figure 47. Incident angles shown along a portion of the primary crestlines within the study area for both the NE wind (A) and the ENE wind (B). Colored areas indicate the incident angle, as defined by Sweet and Kocurek (1990), between the primary crestline and the wind. Red areas are transverse (70 º - 90 º), yellow areas are oblique (10 º - 70 º), and blue areas are longitudinal (0 º - 10 º). In both images three slipfaces are shown along the primary crest, the middle of which is also shown in Fig. 42A-B. Under the NE wind (A) the most developed areas of the slipfaces are transverse, whereas the remainder of the crestline is oblique or longitudinal. Under the ENE wind (B) both slipfaces and subdued, wind-rippled portions of the crestline are transverse. Wind-rippled portions of the crestline that are not transverse to the ENE wind are oblique, except one wind-rippled area that is longitudinal and the middle slipface, which has an oblique portion of crest. Note that the only slipface that has a secondary dune developed downwind is also oblique to the ENE wind.

slipfaces consistently occur along areas that are transverse (red) to the NE wind. The flanks of the slipfaces are commonly oblique (yellow) to the NE wind and extend into stretches of subdued, wind-rippled crestal areas that occupy much of the area between the slipfaces. Short pieces of crestline south of the slipfaces are longitudinal to the NE wind. Sediment transported through the secondary flow fields created by the NE wind would move southward along-slope until reaching a region of increasing flow deceleration and deposition, with maximum deposition at the transverse portions of the crestline.

Figure 47B shows the incident angles for the ENE wind. In contrast to the NE wind, nearly all of the crestal areas with slipfaces are transverse to the ENE wind, except in one instance, along the middle slip face, where the center portion of the slipface is oblique. Although the surface features in Fig. 47B reflect the NE winds, it is important to note that transverse portions of the primary crestline are rippled without any evidence that these segments had previously developed slipfaces. Sediment transported under the ENE secondary flow field would move southward along-slope through the oblique and longitudinal areas, except along the oblique portion in the center of the middle slipface where it would be moving NW with deposition occurring at the high-angle oblique and transverse areas.

Figure 48 shows secondary-flow configurations in another area of the dune field. The crestal areas transverse to the NE wind are nearly always coincident with the slipfaces, but overall most of the primary crestline is oblique to this wind. With the ENE wind, most of the crestline is transverse and punctuated by small segments of oblique flow, which commonly occur along the slipfaces. Larger stretches of oblique crestline in ENE wind are longitudinal to the NE wind, and are associated with breaks and offsets in the primary crestline. A side-by-side comparison of the flow configurations for both winds (Fig. 48) shows that secondary crestlines start in the interdune areas downwind of slipfaces that are transverse to the NE wind and oblique to the ENE wind. Secondary crestlines on the stoss

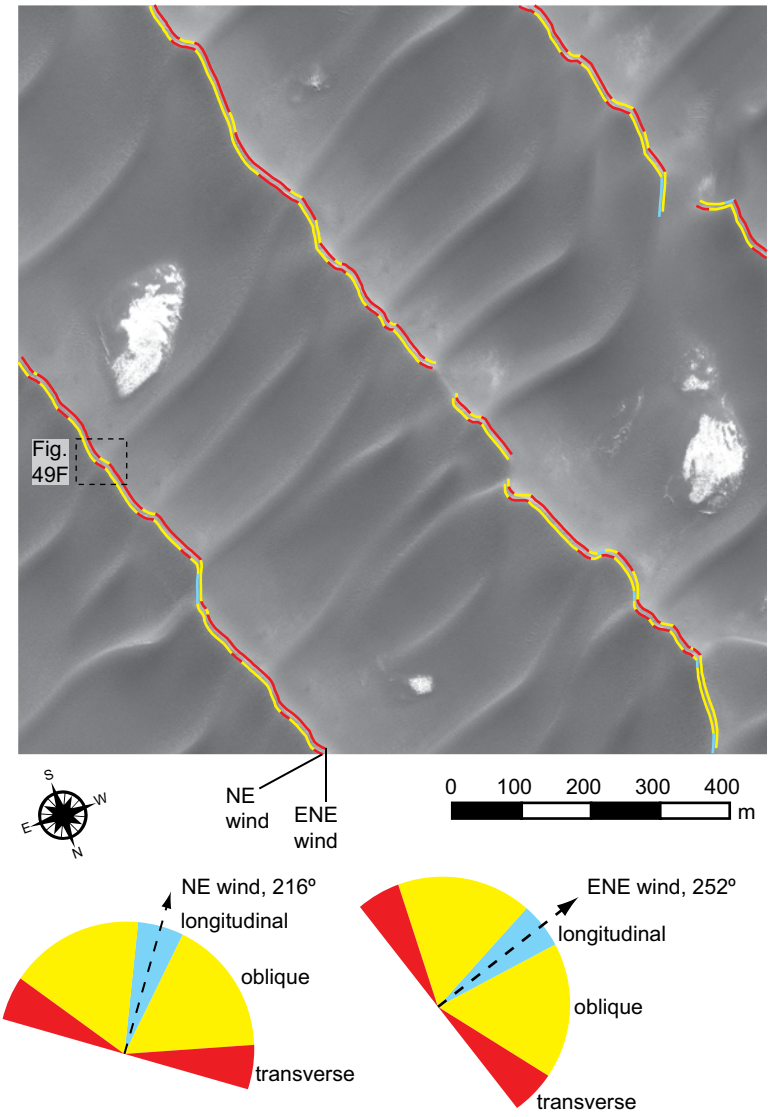

Figure 48. Incident angle map with both the incident angles for the NE and the ENE winds side-by-side along the primary crestlines. Note that the same relationships discussed for Fig. 47 are apparent. Under the NE wind the slipfaces are nearly the only transverse elements, whereas under the ENE wind most of the crestline is transverse except small portions at the middle of the slipfaces, which are oblique. Where a slipface is transverse to the NE wind and oblique to the ENE wind a secondary dune is apparent downwind. The location of Fig. 49F is marked by the dashed box.

slope are nearly always associated with a slipface that is transverse to the NE wind.

The occurrence of the most developed slipfaces transverse to the NE wind, the active-appearing ripples in the lee of the secondary dunes under the NE wind, and the potential sediment influx from the katabatic winds all suggest that the NE wind introduces

more sediment to the dune field than the ENE wind, although both winds are likely highly undersaturated because of frozen dune conditions. If the ENE wind carried a significant amount of sand, well developed slipfaces should appear transverse to these winds, rather both slipfaces and wind-rippled crestlines are transverse to the ENE wind. The secondary flow fields and geomorphic evidence suggest that much of the sediment supply entering the field within the study area likely derives from the NE wind, whereas the ENE wind acts to only move sediment deposited by the NE wind.

Model of pattern construction

The interaction between the primary and secondary dunes within the bimodal wind regime creates a feedback in which the primary crestline is segmented and reoriented, and the secondary crestline is propagated in the resultant flow direction (Fig. 49). First, during the NE winds flow emerges from the hollow on the stoss slope of the primary dunes and is deflected by the secondary crests to intersect the primary crest transversely and give rise to a slipface and flow separation (Fig. 49A). Away from the secondary crests the incidence angle is oblique, and lee flow is deflected to the SE toward the slipface. Combined, the pattern of secondary lee flow causes a focal point of deposition in the form of a prograding convex nose that is transverse to the NE winds (Fig. 49B). Once progradation of the convex nose has reoriented the SW flank of the convexity by about 20°, it becomes oblique to subsequent ENE winds (Fig. 49C). With this change in obliquity, sediment previously deposited on the slipface by the NE wind is now transported along-slope by the ENE wind to the NW until reaching the NW transverse flank of the convex nose (Fig. 49C). Return of the NE wind renews deposition along the SW flank of the convexity (Fig. 49D).

The net effect of the interactions between the primary and secondary crestlines in prograding the convex nose is to cause a segmentation of the primary crestline (Fig. 49 E, F). Geomorphically, this is evident as a dislocation along the primary crestline (Fig. 34A,

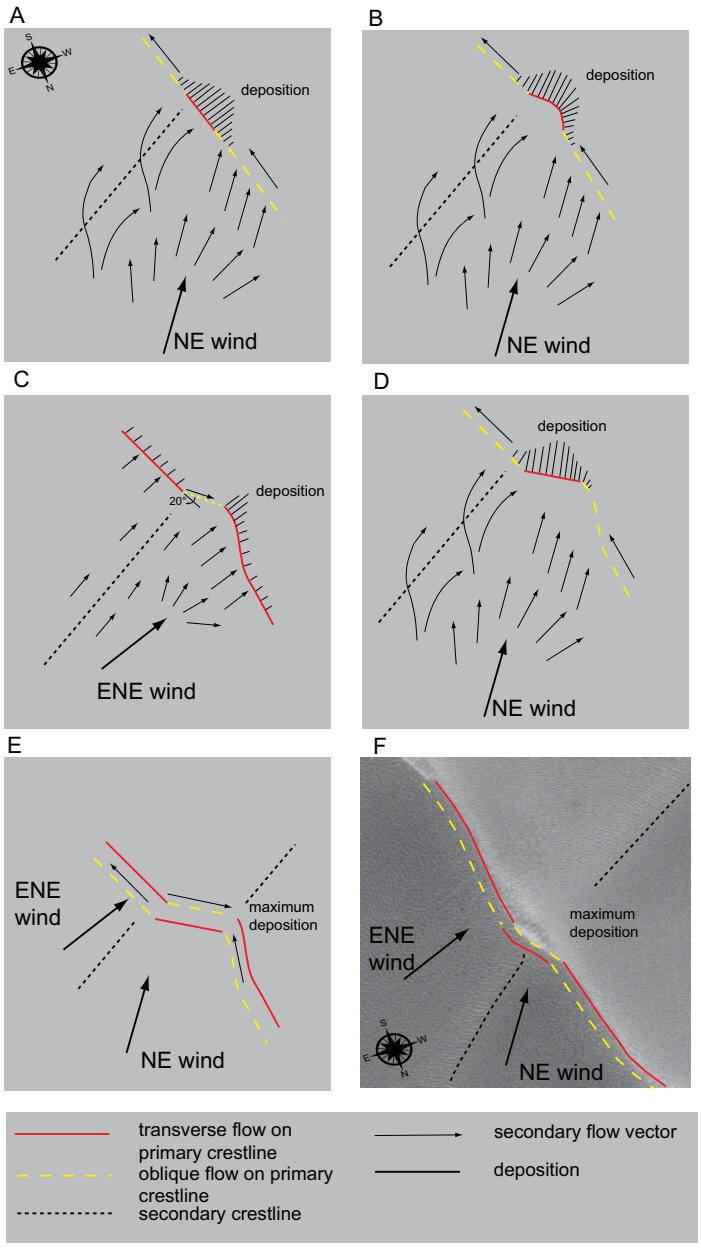

Figure 49. Model of slipface development and primary crestline segmentation based upon the relationship between the primary crestline and secondary crestline within the bimodal wind regime. (A) Development of a slipface on the primary crestline arising from the secondary flow configuration determined by the interaction of the primary and secondary dune topography under the NE wind. Lines indicate relative amount of deposition, with maximum deposition (i.e., longer lines) occurring at the most transverse portions of the crestline and less deposition as flow becomes more oblique. (B) Creation of a convex nose at the focal point of deposition which becomes transverse to the NE wind. (C) Influence of the ENE wind when the SE flank of the convexity becomes oblique (~20º) to this wind. Flow is deflected NW toward the transverse areas at the nose of the convexity. (D) Renewal of the NE wind and continued progradation and segmentation of the primary crestline. (E) Side-by-side flow configurations for both the NE and ENE winds, as in Fig. 48. Note the reciprocal flow configuration along the slipface that creates a point of maximum deposition at the nose of the convexity. As shown in (F), this flow configuration coincides with a downwind secondary dune.

38B, 49F). This segmentation is the process of pattern reformation within the new wind regime and the development of a complex pattern.

In addition, the process that breaks up the primary crestlines also initiates creation of new secondary dunes lee of the primary crestline thus giving rise to the reticulate pattern. Secondary crestline formation occurs in a manner similar to the formation of linear dunes in a bimodal wind regime, but in this case as secondary flow on the plinth of the primary

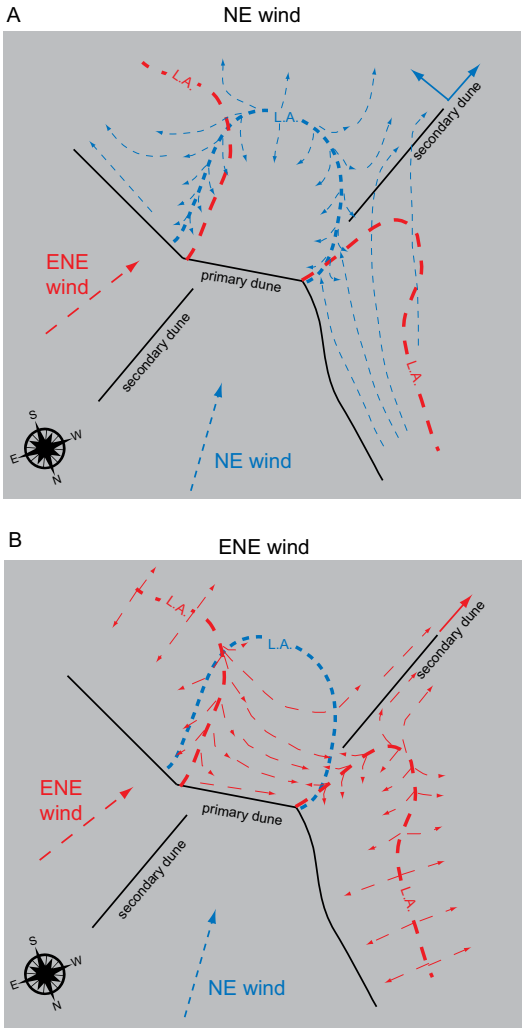

Figure 50. Detail of the secondary flow configuration occurring along the primary dune plinth that gives rise to the initiation, elongation and migration of the secondary dunes. (A) Flow configuration for the NE winds. (B) Flow configuration for the ENE winds. The secondary dune initiates where secondary flow from the bimodal wind regime converges on the dune plinth creating a focal line of deposition. The thick dashed lines are lines of attachment (L.A. in the figure) defining the separation cell in the lee of the transverse portions of the crestline for both the NE (blue) (A) and the ENE (red) (B) winds. This area bound by the attachment line is well defined for the NE wind by the mottled ripples in the lee of the slipface shown in Fig. 42A-B. The dashed arrows represent secondary flow vectors for the NE (blue) and ENE (red) winds. Return flow (i.e. flow inside the attachment line) moves directly back toward the crestline along the most transverse portions of the separation cell and sweeps inward toward the crest along the oblique regions. Outboard of the attachment line, flow returns to the primary flow direction or becomes incorporated into secondary flow along the primary or secondary dune. The solid blue arrows in (A) indicate the WSW elongation and SE migration of the secondary dune under the NE wind. The solid red arrow at the end of the downwind secondary dune in (B) indicates the WSW elongation of the secondary dune under the ENE wind.

crests during the bimodal wind regime. During the NE winds plinth along-slope transport to the SE is blocked where it encounters the line of attachment that occurs in conjunction with the transverse segment of the primary crest, forming a focal line of deposition (Fig. 50A). During the ENE winds oblique flow to the NW on the plinth is similarly blocked by the attachment line as defined with the flow separation along the transverse segments (Fig. 50B). These two focal lines of deposition coincide, initiating a positive topographic feature. Once initiated, any ENE winds are longitudinal to this positive topography and will cause its extension to the WSW (Fig. 50B). Any NE winds will strike the topography oblique and be deflected along the lee SE flank, resulting in both extension to the SW and

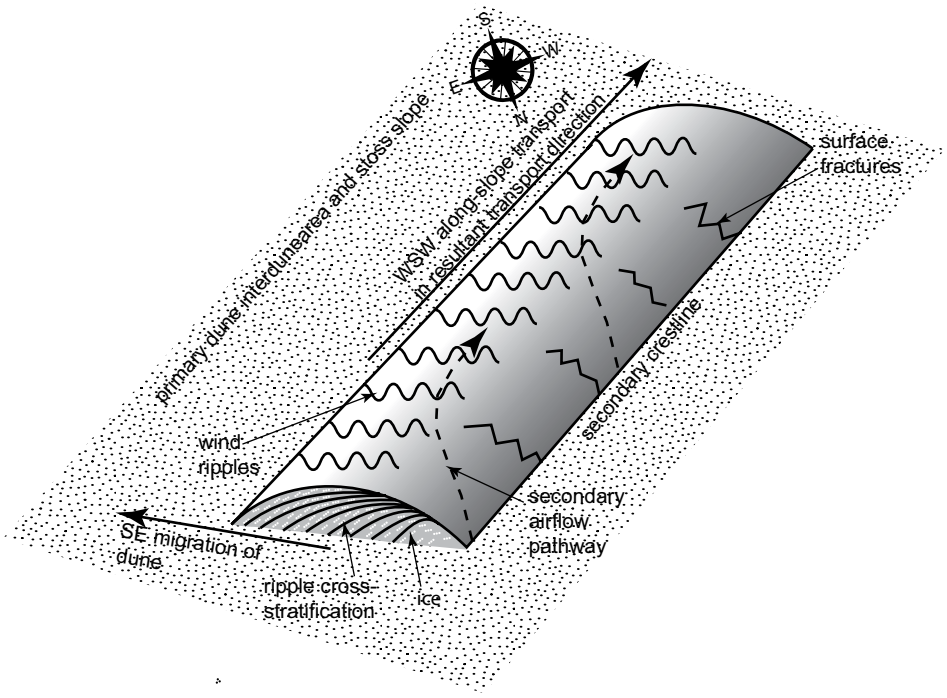

Figure 51. Model of the WSW elongation and SE migration of the secondary dunes by wind-ripple migration along the SE slope of the dune. Wind ripple migration on the SE-facing slope arises from NE flow that becomes deflected to the WSW as it crosses the secondary dune crestline, and from longitudinal flow from the ENE winds. Elongation occurs with WSW along-slope sediment transport. SE migration of the dune occurs through accumulation on the SE-facing slope, which is the depositional side of the dune under the NE winds. In cross-section the SE migration would be apparent by wind-ripple stratification dipping to the SE. Surface fractures exposed on the erosional stoss slope of the secondary dune likely indicate the presence of subsurface ice (Feldman et al., 2008).

migration to the SE because of lee deposition (Figs. 50A, 51). This crestline can then extend to the next dune downwind, with the formative process repeated and position of the next downwind secondary crestline somewhat offset from the first. The upwind (NE) termination of the secondary dune is fixed lee of the slipface of the primary dunes and on the plinth between the separation cells.

Conclusions

The dune-field pattern in one area of the Olympia Undae Dune Field was analyzed via measurements and statistical analysis of the pattern elements, and the flow field was reconstructed based upon wind ripples formed during the most recent transport winds.

Pattern analysis and geomorphic relationships show that the pattern is complex in which older, well organized NNW-oriented dunes are being reworked by younger, NE- oriented dunes. A third, yet older generation of dunes is represented by aeolian dune cross-strata exposed in the deflationary sequence surface that floors the current dune field. Mapped flow fields indicate that the most recent transporting winds were from the NE and are likely related to katabatic winds descending Planum Boreum through the Olympia Cavi re-entrant.

Within the general context of dune-field pattern formation, the scenario of pattern reformation with the onset of a changed wind regime is well illustrated with this Martian example. First, the position and development of the secondary dunes is controlled by the boundary condition of the antecedent primary dune topography. In the absence of this boundary condition the longitudinal secondary dunes would be expected to be unstable under this wind regime and would destabilize into trains of barchans. Rather, they reach a downwind primary crest before destabilization can occur. Second, it shows the development of a complex pattern through dune interactions between pattern generations (i.e., the younger secondary dunes intersecting the older primary dunes), as well as the reformation of the older pattern with their break-up by the secondary dunes. Third, the secondary flow field that allows for the reformation of the field arises because of the interactions between the dune generations.

References

Aharonson, O. and N. Schorghofer (2006), Subsurface ice on Mars with rough topography, J. Geophys. Res., 111, E11007, doi:10.1029/2005JE002636.

Allen, J.R.L. (1973), Features of cross-stratified units due to random and other changes in bedforms, Sedimentology, 20, 189-202.

Allen J.R.L. (1982), Sedimentary Structures: Their Character and Physical Basis. Developments in Sedimentology, 30A, 593 pp., Elsevier, Amsterdam.

Anderson, R.S. (1990), Eolian ripples as examples of self-organization in geomorphological systems, Earth-Science Reviews, 29, 77-96.

Anderson, R.S. and K.L. Bunas (1993), Grain size segregation and stratigraphy in aeolian ripples modeled with a cellular automaton, Nature, 365, 740-743.

Anderson, R.S. and R.R. McDonald (1990), Bifurcations and terminations in eolian ripples, Eos, 71, 1344.

Baas, A.C.W., (2002), Chaos, fractals and self-organization in coastal geomorphology: simulating dune landscapes in vegetated environments, Geomorphology 48, 309-328.

Baas, A.C.W., (2007), Complex systems in aeolian geomorphology, Geomorphology 91, 311-331.

Bagnold, R.A. (1941), The physics of blown sand and desert dunes, 265 pp, Methuen, London.

Ball, P. (1999) The Self-Made Tapestry: Pattern formation in nature. Oxford University Press, Oxford.

Bandfield, J., Hamilton, V., and P. Christensen (2000), A global view of Martian surface compositions from MGS-TES, Science, 287, 1626-1630, doi: 10.1126

Beveridge, C., Kocurek, G., Ewing, R.C. Lancaster, N., Morthekai, P., Singhvi, A.K. and S.A. Mahan (2006), Development of spatially diverse and complex dune-field patterns: Gran Desierto Dune Field, Sonora, Mexico, Sedimentology, 53, 1391-1409, doi:10.1111/j.1365-3091.2006.00814.x

Bishop, S.R., Momiji, H., Carretero-Gonzalez, R., and A. Warren (2002) Modelling desert dune fields based on discrete dynamics, Discrete Dynamics in Nature and Society 7, 7-17.

Bourke, M.C., Balme, M., Beyer, R.A., Williams, K.K., and J. Zimbleman (2006), A comparison of methods used to constrain the height of sand dunes on Mars, Geomorphology, 81, 440-452, doi:10.1016/j.geomorph.2006.04.023.

Bourke, M.C., Bullard, J.E., and O.S. Barnouin-Jha (2004), Aeolian sediment transport pathways and aerodynamics at troughs on Mars, J. Geophys. Res., 109, E07005, doi:10.1029/2003JE002155.

Bourke, M.C., Edgett, K.S., and B.A. Cantor (2008), Recent aeolian dune change on Mars, Geomorphology, 94, 247-255, doi:10.1016/j.geomorph.2007.05.012.

Bourke, M. C., Philippoff, A., and N. Bridges (2009), Studies of dune change on Mars combining MOC and HiRISE images: Lunar Planet Sci. XXXX, abstract 1748.

Breed, C.S., Grolier, M.J., and J.F. McCauley (1979), Morphology and distribution of common 'sand' dunes on Mars: comparison with Earth, J. Geophys. Res., 84(B14), 8183-8204.

Bristow, C.S., Duller, G.A.T., and N. Lancaster (2007), Age and dynamics of linear dunes in the Namib Desert, Geology 35, 555-558.

Byrne, S., and B. Murray (2002), North polar stratigraphy and the paleo-erg of Mars, J. Geophys. Res., 107(E6), 5044, doi:10.1029/2001JE001615.

Coleman, S.E. and B.W. Melville (1994), Bed-form Development. Journal of Hydraulic Engineering, 120, 544-560.

Cross, M.C. and P.C. Hohenberg (1993), Pattern formation outside of equilibrium. Rev. Mod. Phys. 65, 851-1112.

DeMenocal, P., Ortiz, J., Guilderson, T., Adkins, J., Sarnthein, M., Baker, L., and M. Yarusinsky (2000), Abrupt onset and termination of the African Humid Period: rapid climate responses to gradual insolation forcing, Quaternary Science Reviews 9, 347-361.

Derickson, D., Kocurek, G., Ewing, R.C. and C. Bristow (2008), Origin of a complex and spatially diverse dune-field pattern, Algodones, southeastern California, Geomorphology, 99, 186-204, doi:10.1016/j.geomorph.2007.10.016.

Derickson, D., Kocurek, G., Ewing, R.C., and C. Bristow (2008), Origin of a complex and spatially diverse dune-field pattern, Algodones, southeastern California, Geomorphology 99, 186-204.

Diniega, S., Glasner, K., and S. Byrne (in press) Long-time evolution of models of aeolian

sand dune fields: Influence of dune formation and collision, Geomorphology.

Dohmen-Janssen C.M., Lansink J., Paarlberg A.J., Hulscher, S.J.M.H., and A.P.P. Termes (2008), Modelling river dune splitting. In: Marine and River Dune Dynamics (Eds D Parsons, T Garlan, J Best. Third International Workshop: Leeds; 79-86.

Eastwood, E.N., Nield, J.N., Baas, A.C.W., and G. Kocurek (in review) Quantifying controls on aeolian dune-field pattern evolution using a source-to-sink cellular automaton model.

Elbelrhiti, H., Claudin, P., and B. Andreotti (2005), Field evidence for surface-wave-induced instability of sand dunes, Nature, 437, 720-723.

Elbelrhiti, H., Claudin, P., and B. Andreotti (2008), Barchan dune corridors: Field characterization and investigation of control parameters, Journal of Geophysical Research, 113, F02S15.

Endo, N. and K. Taniguchi (2004), Observation of the whole process of interaction between barchans by flume experiments. Geophysical Research Letters, 31, L12503.

Endo, N., Kubo, H. and T. Sunamura (2004), Barchan-shaped ripple marks in a wave flume, Earth Surface Process and Landforms, 29, 31-42.

Ewing, R.C. and G. Kocurek, (in press), Aeolian dune-field pattern boundary conditions. Geomorphology.

Ewing, R.C., and G. Kocurek (in review), Aeolian dune interactions and dune-field pattern formation: White Sands Dune Field, New Mexico, Sedimentology.

Ewing, R.C., Kocurek, G. and L.W. Lake (2006), Pattern analysis of dune-field parameters, Earth Surface Process and Landforms, 31, 1176-1191.

Ewing, R.C., McElroy, B.J., and B.J. Andrews (2007) Point-pattern analysis of star-dune fields. Eos Trans. AGU 88 (52) Fall meet. Suppl., Abstract NG41C-0673, San Francisco, California.

Ewing, R.C., Peyet, A., Kocurek, G., Mohrig, D., and E. Eastwood (2008), Three-dimensional characterization and morphological dynamics of gypsum sand dunes at White Sands National Monument using airborne LiDAR. In Planetary Dunes Workshop: A Record of Climate Change, LPI contribution No. 1403, Lunary and Planetary Institute, Houston.

Feldman, W.C., Bourke, M.C., Elphic, R.C., Maurice, S., Bandfield, J., Prettyman, T.H., Diez, B., and D.J. Lawrence (2008), Hydrogen content of sand dunes within

Olympia Undae, Icarus, 196, 422-432, doi:10.1016/j.icarus.2007.08.044.

Fishbaugh, K., and J. Head III (2005), Origin and characteristics of the Mars north polar basal unit and implications for polar geologic history, Icarus, 174, 444 – 474, doi:10.1016/j.icarus.2004.06.021.

Fishbaugh, K.E., Poulet, F., Chevrier, V., Langevin, Y., and J.P. Bibring (2007), On the origin of gypsum in the Mars north polar region, J. Geophys. Res.,112, E07002, doi:10.1029/2006JE002862.

Forrest, S.B. and P.K. Haff, (1992), Mechanics of wind ripple stratigraphy, Science, 255, 1240-1243.

Fryberger, S. G., P. Hesp, and K. Hastings (1992), Aeolian granule ripple deposits, Namibia, Sedimentology, 39, 319– 331.

Fryberger, S.G. (2000), Geological overview of White Sands National Monument. http://www.nps.gov/whsa/Geology%20of%20White%20Sands/GeoHome.html.

Fryberger, S.G., Krystinik, L.F. and C.J. Schenk (1990), Tidally flodded back-barrier dunefield, Guerrero Negro area, Baja California, Mexico. Sedimentology 37, 23-43.

Greeley, R. and J.D. Iversen (1985), Wind as a geological process on Earth, Mars, Venus and Titan, 333pp, Cambridge University Press, Cambridge.

Hallet, B., (1990) Spatial self-organization in geomorphology: from periodic bedforms and patterned ground to scale-invariant topography, Earth-Science Reviews 29, 57-75.

Hayward, R.K., Fenton, L.K., Tanaka, K.L., Mullins, K.F., Titus, T.N., Bourke, M.C., Hare, T.M., and P.R. Christensen (2008), Mars global digital dune database: Distribution in North Polar region and comparison to equatorial region, LPSC XXXIX, abs. # 1208.

Herkenhoff, K.E., Byrne, S., Russel, P.S., Fishbaugh, K.E., and A.S. McEwen (2007), Meter-scale morphology of the north polar region of Mars, Science, 317, 1711-1715, DOI: 10.1126/science.1143544.

Herrmann, H.J. (2006), Pattern Formation of Dunes. Nonlinear Dynamics, 44, 315-327.

Hersen, P. (2005), Flow effects on the morphology and dynamics of aeolian and subaqueous barchan dunes, Journal of Geophysical Research, 110, F04S07

Hersen, P., S. Douady (2005), Collision of barchan dunes as a mechanism of size regulation. Geophysical Research Letters 32, L21403.

Horgan, B., Bell, J., Bourke, M.C., (2009b) A search for dune induration and activity in the north polar region of Mars, 7th International Conference on Geomorphology Melbourne, Australia.

Horgan, B.H., Bell III, J.F., Dobrea, E.Z.N., Cloutis, E.A., Bailey, D.T., Craig, M.A., Roach, L.H. and J.F. Mustard (2009a), Distribution of hydrated minerals in the north polar region of Mars, J. Geophys. Res., 114, E01005, doi:10.1029/2008JE003187.

Howard, A.D. (1977), Effect of slope on the threshold motion and its application to orientation of wind ripples, Geological Society of America Bulletin, 88, 853-856.

Howard, A.D. (2000), The role of eolian processes in forming surface features of the Martian Polar Layered Deposits, Icarus, 144, 267-288, doi:10.1006/icar.1999.6305.

Hunter, R.E. (1977), Basic types of stratification in small eolian dunes, Sedimentology, 24, 361-387.

Hunter, R.E., Richmond, B.M. and T.R. Alpha (1983), Storm-controlled oblique dunes of the Oregon coast, Geological Society of America Bulletin, 94, 1450-1465.

Jerolmack, D.J., Mohrig, D., Grotzinger, J.P., Fike, D.A., and W.A. Watters (2006), Spatial grain size sorting in eolian ripples and estimation of wind conditions on planetary surfaces: application to Meridiani Planum, Mars, J. Geophys. Res., 111, E12S02, doi:10.1029/2005JE002544

Katsuki, A., Nishimori, H., Endo, N. and Taniguchi, K. (2005), Collision dynamics of two barchan dunes simulated using a simple model, Journal of the Physical Society of Japan, 74, 538-541.

Kocurek, G., Carr, M., Ewing, R.C., Havholm, K.G., Nagar, Y.C. and A.K. Singhvi (2007), White Sands Dune Field, New Mexico: Age, dune dynamics and recent accumulations, Sedimentary Geology, 197, 313-331.

Kocurek, G., Deynoux, M., Blakey, R.C., and K.G. Havholm (1991), Amalgamated accumulations resulting from climatic and eustatic changes, Akchar Erg, Mauritania, Sedimentology 38, 751-772.

Kocurek, G., and R.C. Ewing (2005), Aeolian dune field self-organization – implications for the formation of simple versus complex dune-field patterns, Geomorphology, 72, 94-105, doi:10.1016/j.geomorph.2005.05.005.

Kocurek, G., Ewing, R.C., and D. Mohrig. (in press), How do bedform patterns arise? New views on the role of bedform interactions within a set of boundary conditions, Earth Surf. Process. Landforms.

Kocurek, G. and N. Lancaster (1999), Aeolian system sediment state: theory and Mojave Desert Kelso dune field example, Sedimentology 46, 505-515.

Kocurek, G., Townsley, M., Yeh, E, Havholm, K., and M.L. Sweet (1992), Dune and dune-field development on Padre Island, Texas, with implication for interdune deposition and water-table-controlled accumulation, Journal of Sedimentary Petrology, 62, 622-635.

Lahtela, H., Titus, T.N., Geissler, P.E., Roach, L.H., Verba, C.A., Mustard, J.F., Murchie, S.L., Brown, A.J., Seelos, F., Seelos, K., Calvin, W.M., Parente, M., Cornwall, C., 2009. Coordinated HiRISE/CRISM Observation on Gypsum Signature in Martian Polar Dunes, Lunar and Planetary Institute Science Conference Abstracts, pp. 2254.

Lancaster, N. (1989), The Namib Sand Sea: Dune Forms, Processes and Sediments. A.A. Balkema, Rotterdam.

Lancaster, N. (1995), Geomorphology of Desert Dunes. Routledge, London.

Lancaster, N., and R. Greeley (1990), Sediment volume in the North Polar Sand Seas of Mars, J. Geophys. Res., 95(B7), 10,921-10,927.

Lancaster, N., Kocurek, G., Singhvi, A., Pandey, V., Deynoux, M., Ghienne, J.F., and K. Lo (2002), Late Pleistocene and Holocene dune activity and wind regimes in the western Sahara Desert of Mauritania, Geology 30, 991-994.

Landry, W. and B.T. Werner (1994), Computer simulations of self-organized wind ripple patterns. Physica D, 77, 238-260.

Langevin, Y., Poulet, F., Bibring, J.P., and B. Gondet (2005), Sulfates in the north polar region of Mars detected by OMEGA/Mars Express, Science, 307, 1584-1586, DOI: 10.1126/science.1109091.

Langford, R.P. (2003), The Holocene history of the White Sands Dune Field and influences on eolian deflation and playa lakes, Quaternary International, 104, 31-39.

Langford, R.P., Rose, J.M., and D.E. White (2009), Groundwater salinity as a control on development of eolian landscape: An example from the White Sands of New Mexico. Geomorphology 105, 39-49.

Lee, K.D., 2003, Terrain Analysis of Afghanistan. East View Cartographic, Minneapolis.

Mabutt J.A. and R.A. Wooding (1983), Analysis of longitudinal dune patterns in the northwest Simpson Desert, central Australia. Zeitschrift fur Geomorphologie Suppl. 45, 597–646.

McKee, E.D. (1966), Structures of dunes at White Sands National Monument, New Mexico (and a comparison with structures of dunes from other selected areas). Sedimentology, 7, 1–69.

Momiji, H., Carretero-Gonzales, R., Bishop, S.R., A. Warren (2000), Simulation of the effect of wind speedup in the formation of transverse dune fields. Earth Surface Processes and Landforms 25, 905-18.

Murray, J.D., (1990), Mathematical Biology. Spring, Berlin.

Nishimori, H. and N. Ouchi (1993), Formation of ripple patterns and dunes by wind-blown sand, Physical Review Letters, 71, 197-201.

Rachal, D.M. and D.P. Dugas (2009), Historical dune pattern dynamics: White Sands Dune Field, New Mexico, Physical Geography, 30, 64-78.

Roach, L., et al. (2007), CRISM spectral signatures of the north polar gypsum dunes, Lunar Planet Sci., XXXVII, Abstract 1970.

Rubin, D.M. and H. Ikeda (1990), Flume experiments on the alignment of transverse, oblique, and longitudinal dunes in directionally varying flows, Sedimentology, 37, 673-684.

Rubin, D.M. and R.E. Hunter (1987), Bedform alignment in directionally varying flows, Science, 237(4812), 276-278.

Sarnthein, M., L. Diester-Haass (1977), Eolian-sand turbidites. Journal of Sedimentary Petrology, 47, 868-890.

Schatz, V., Tsoar, H., Edgett, K.S., Parteli, E., and H.J. Herrmann (2006), Evidence for indurated sand dunes in the Martian north polar region, J. Geophys. Res., 111, E04006, doi:10.1029/2005JE002514.

Schenk, C.J. and S.G. Fryberger (1988), Early diagenesis of eolian dune and interdune sands at White Sands, New Mexico. Sedimentary Geology, 55, 109-120.

Schwammle, V. and H.J. Herrmann (2003), Solitary wave behavior of sand dunes. Nature, 426, 619-620.

Sharp, R.P. (1963), Wind Ripples. Journal of Geology, 71,617-636.

Silli, T., R. M. Haberle, and J. R. Murphy, (1997), Sensitivity of martian southern polar cap edge winds and surface stresses to dust optical thickness and the large-scale sublimation flow, Adv. Space Res., 19, 1241–1244.

Sinclair, A.J. (1976), Applications of probability graphs in mineral exploration, Assoc. of Exploration Geochemists, special volume No. 4.

Sun, J., and T. Liu (2006), The age of the Taklimakan Desert. Science 312, 1621.

Sweet, M.L. and G. Kocurek (1990), An empirical model of aeolian dune lee-face airflow, Sedimentology, 37, 1023-1038.

Tanaka, K.L, and R.K. Hayward (2008), Mars' north circum-polar dunes: distribution, sources, and migration history, In Planetary Dunes Workshop: A Record of Climate Change, p. XX. LPI Contribution No. 1403, Lunar and Planetary Institute, Houston.

Tanka, K.L., Rodriguez, J.A.P., Skinner, J.A., Bourke, M.C., Fortezzo, C.M., Herkenhoff, K.E., Kolb, E.J., and C.H. Okubo (2008), North Polar region of Mars: Advances in stratigraphy, structure, and erosional modification, Icarus, 196, 318-358, doi:10.1016/j.icarus.2008.01.021

Tsoar, H. (1978), Dynamic processes acting on a longitudinal (seif) sand dune, Sedimentology, 30, 567-578.

Tsoar, H., R. Greeley, and A. R. Peterfreund (1979), Mars: The North Polar Sand Sea and related wind patterns, J. Geophys. Res., 84(B14), 8167– 8180.

Tufillaro, N.B. (1993), Discrete dynamical models showing pattern formation in subaqueous bedforms, International Journal of Bifurcation and Chaos. 3, 779-784.

Tyler, D. and J.R. Barns, (2005), A mesoscale model study of summertime stmospheric circulations in the north polar region of Mars, J. Geophys. Res., 110, E06007, doi:10.1029/2004JE002356.

Venditti, J.G., Church, M., and S.J. Bennett (2005), On the transition between 2D and 3D dunes. Sedimentology, 53, 1343-1359.

Walker, I.J. and W.G. Nickling (2002), Dynamics of secondary airflow and sediment transport over and in the lee of transverse dunes, Progress in Physical Geography, 26(1), 47-75.

Walker, I.J. and W.G. Nickling (2003), Simulation and measurements of surface shear stress over isolated and closely spaced transverse dunes in a wind tunnel, Earth Surf. Process. Landforms, 28, 111-1124, doi: 10.1002/esp.520

Wang, X., Dong, Z., Yan, P., Zhang, J., and G. Qian (2005), Wind energy environments and dunefield activity in the Chinese deserts, Geomorphology 65, 33-48.

Wang,X., Dong, Z., Zhang, J., G. Chen (2002), Geomorphology of sand dunes in Northeast

Taklimakan Desert, Geomorphology 42, 183-195.

Werner, B.T. (1995), Eolian dunes: computer simulations and attractor interpretation, Geology 23, 1107-1110.

Werner, B.T., (1999), Complexity in natural landform patterns, Science 284, 102-104.

Werner, B.T. (2003), Modeling landforms as self-organized, hierarchical dynamical systems, in. Wilcock, P.R. and Iverson, R.M.,eds, Prediction in Geomorphology: Geophysical Monograph 135, Washington D.C., American Geophysical Union, 133-150.

Werner, B.T. and G. Kocurek (1997), Bedform dynamics: Does the tail wag the dog?, Geology, 25(9), 771-774.

Werner, B.T and G. Kocurek (1999), Bedform spacing from defect dynamics, Geology, 27(8), 727-730.

Werner, B.T., and D.E. McNamara (2007), Dynamics of coupled human-landscape systems. Geomorphology 91, 393-407.

Whitney, J.W., 2006. Geology, Water, and Wind in the Lower Helmand Basin, Southern Afghanistan. USGS Scientific Investigations Report 5182.

Wyatt, M., McSween, H., Tanaka, K., and J. Head (2004), Global geologic context for rock types and surface alteration on Mars, Geology, 32, 645-648.

Zimbelman, J.R. (in press) Transverse aeolian ridges on Mars: First results from HiRise images, Geomorphology.

Zu, R., Xue, X, Qiang, M., Yang, B., Qu, J, and K. Zhang (2008), Characteristics of near-surface wind regimes in the Taklimakan Desert, China, Geomorphology 96, 39-47.

Vita

Ryan Cotter Ewing was born in Arkansas. He attended Rogers High School in Rogers, Arkansas. He matriculated at The Colorado College in Colorado Springs, Colorado in 1994 and in May of 1998 he received a Bachelor of Arts in Geology from The Colorado College. In 2001, after a 3 year sojourn through many worlds, Ryan entered the Graduate School at the University of Texas at Austin. Ryan received his MS in Geological Sciences from the University of Texas at Austin in 2004 and began working toward a PhD in Geological Sciences at the University of Texas at Austin that same year.

Permanent address (or email): ryancewing@gmail.com

This dissertation was typed by the author.